Escuela Politécnica Superior de Jaén

Grado en Ingeniería Geomática y Topográfica

UNIVERSIDAD DE JAÉN
Escuela Politécnica Superior de Jaén

Trabajo Fin de Grado

SPATIO-TEMPORAL ANALYSIS OF THE FLOOD RISK IN LOWER OUED MAJERDA VALLEY (TUNISIA) USING SENTINEL 1&2 IMAGERY

Alumno: Adel Chouk

Tutor: Prof. D. Jorge Delgado García
Prof. D. Tomás Fernández del Castillo
Dpto: Ingeniería Cartográfica, Geodésica y Fotogrametría

Noviembre 2020

Universidad de Jaén

Escuela Politécnica Superior de Jaén

Departamento de Ingeniería Cartográfica, Geodésica y Fotogrametría

Don Jorge Delgado García y Don Tomás Fernández del Castillo, tutores del Proyecto Fin de Carrera titulado: Spatio-temporal Analysis of the Flood Risk in Lower Oueda Valley (Tunisia) using Sentinel 1 and 2 imagery, que presenta Adel Chouk, autoriza su presentación para defensa y evaluación en la Escuela Politécnica Superior de Jaén.

Jaén, Noviembre de 2020

El alumno:

Adel Chouk

Los tutores:

Jorge Delgado

Tomás Fernández

Dédicace

Qu'il me soit permis à travers ce modeste travail d'exprimer ma plus profonde reconnaissance à :

Ma chère mère et mon cher père, que nulle dédicace ne puisse exprimer ce que je leurs dois, pour leurs bienveillances de ma plus jeune enfance et leurs soutiens, en témoignage de mon profond amour « Que Dieu vous garde ».

Ă ma chère sœur et frère, pour tout ce que nous avons vécu ensemble et leur encouragement continue tout au long de mes études.

Ă tous mes amis pour leurs conseils et soutien moral durant l'élaboration de ce travail.

Et à tous ceux et celles qui me sont chers et pour qui je suis cher.

Acknowledgment

First of all, I would like to especially thank Mr Jorge Delgado García and Tomás Fernández ,for allowing me to carry out this document in the best conditions, but also for his rich scientific advice and lessons, for its permanent availability, in particular during the period of health crisis, for its unfailing frankness and for all the enriching discussions that we were able to have.

I would like to deeply thank the president of the jury, for having honored us to accept to chair the jury for my project. I am infinitely indebted to him. May he find my deep gratitude and respect here. I would like to thank the jury member, for having accepted to read our report and to participate in the judgment of the work of our project.

In the end, I cannot close my thanks without being grateful to everyone who has participated directly or indirectly in the development of this work.

Abstract

Satellite images (optic or radar) of river inundations reveal themselves to be very relevant to flood operational management. For example, Copernicus Emergency Management Services that provides useful maps extracted from satellite images few hours after receiving images. These maps are then given to competent rescue services in order to make their operations easier.

In this context the study aims at deploying methods of satellite images analysis in order to show the potential of these images in monitoring floods. To meet this aim, the report has been tackled through two research issues. The first is related to land use and urban area mapping the second, fusion between relevant information resulting from these products with water mask extracted after certain flood day.

The results of the Thesis imply especially great potential benefits for flood operational management and especially damage assessment.

Resumen

Las imágenes satelitales (ópticas o de radar) de las inundaciones fluviales se revelan muy relevantes para la gestión operativa de las inundaciones. Por ejemplo, Copernicus Emergency Management Services que proporciona mapas útiles extraídos de imágenes satelitales pocas horas después de recibir imágenes. Estos mapas se entregan a los servicios de rescate competentes con el fin de facilitar sus operaciones.

En este contexto, el estudio tiene como objetivo desplegar métodos de análisis de imágenes satelitales con el fin de mostrar el potencial de estas imágenes en el seguimiento de inundaciones. Para alcanzar este objetivo, el informe se ha abordado a través de dos cuestiones de investigación. El primero está relacionado con el uso del suelo y el mapeo de área urbana la segunda, fusión entre la información relevante resultante de estos productos con máscara de agua extraída después de cierto día de inundación.

Los resultados de la tesis implican beneficios potenciales especialmente grandes para la gestión operativa de inundaciones y especialmente la evaluación de daños.

General introduction

In the world, floods are ranked as the first natural risk (Berz, 2000). In recent decades, the damage caused by the floods has been particularly significant, with average annual attributable costs estimated at 600 million € for the period 1980-2000 (Gresillon, 2004) and According to world health organization flooding is the most frequent type of disaster between 1998 and 2015, with 3148 events representing 43% of all recorded events. Floods also affected the largest number of people, at more than two billion between the same period, causing 142,088 deaths and 656 billion euro of economic loss. The extent of this damage is mainly attributable to past urbanization and industrialization in a floodplain (Torterotot, 1993), which has resulted in an increase in the vulnerability of goods and people. The very important issues linked to flooding explain the efforts that are being made today to analyze and understand this phenomenon in order to reduce the risk.

Flood risk is defined as the combination of hazard and vulnerability. The hazard represents the physical, natural and uncontrollable phenomenon (Ministry of the Environment and Sustainable Development), regardless of its potential effects on the environment and human activities. Vulnerability expresses the degree of damage of an issue subject to a hazard of given intensity and occurrence (Ancey, 2005). Flood risk management must therefore take place at both the hazard and vulnerability levels. It must meet two main objectives which are to limit the location of goods and people in highly exposed areas and protect the existing one. The combination of these two objectives is the basis of a coherent approach to flood management.

In the 1970s, spatial earth observation data appeared. Derived from satellite Remote Sensing, they provide objective visions of flooding over large areas. In particular, synthetic aperture radar (SAR) and passive optical imaging satellites make it possible to obtain flood maps (Sanders & Tabuchi, 2000; Sassier et al., 2000; Schmugge, 1987), which very useful in an operational context. For example, The European Flood Awareness System (EFAS) is the first operational European system monitoring and forecasting floods across Europe. It provides complementary flood early warning information up to 10 days in advance also provides a variety of different products including flood monitoring, probabilistic flood forecasts, flash flood indicators, flood impact assessments and seasonal flood risk outlooks.

Report plan

The report is structured in six chapters, the first, titled project framework and study area, describes the objectives, problematics and the geolocation of the study area also its topographic and geometric characteristics the second chapter state of Art, aims to place the report in its thematic and scientific context by presenting general concepts concerning the hydraulic flood hazard and the fundamentals of active and passive satellite Remote Sensing. The third chapter sets the heart of our study it presents the process and results of mapping flooded area. the fourth chapter contains the extraction of urban foot print by means of interferometric coherence technique the fifth contains Land Use Mapping of the lower valley of Majerda and finely the last chapter last chapter devoted to the development of the interactive web map for emergency services management and publishing the results of this work.

.

Table of Contents

Figure Index

CHAPTER 1: Project framework and study area

I-1- Introduction

This project is part of the final project of the engineering cycle in Geomatics and Topography at the Higher School of Aeronautics and Technologies (ESAT), constitutes the practical part of the specialty test.

So, this first chapter is devoted to the presentation of the project framework, the study area, the problematics, the objectives which we aim to achieve them.

I-2- Project framework

This work takes place within the framework of the mobility of Erasmus program (European Action Scheme for the Mobility of University Students), at the University of Jaén, Erasmus is a program for the exchange of students and teachers between universities, European High schools and educational establishments around the world. This program is part of the European Higher Education space.

I-3- Problematics

In Tunisia, the flooding phenomenon is old. Throughout history, there are dozens of times regions have been affected. The best-described and best-known events, for the most part still in people's memory, are those recorded since the beginning of the last century and especially after the 1950s. The floods of 1969 (the whole country, and in particular the center and the North), 1973 (medium and low Medjerda), 1982 (Sfax), 1990 (Region of Sidi Bouzid), 1995 (Tataouine), 2003 (Grand-Tunis), 2007 (Sabbalet Ben Ammar), 2009 (Redayef)… are so many episodes which will mark the hydrological chronicles of the country for a long time. In this context we then try to highlight the contribution of satellite remote sensing technology coupled with GIS software in the visualization of floods and the assessment of damage related to this phenomenon.

I-4- Objectives

In order to promote the contribution multi-source satellite Remote Sensing imagery and web mapping to the fight against natural disasters, flooding in particular. We aim to study a flood event in the lower valley of Majerda and create an interactive map that allows the publication of the product realized in this project also to serve as a tool of alert and analysis for the organizations responsible for the management of natural disasters in Tunisia.

The main objectives:

- Develop a multi-temporal approach to the quantitative assessment and cartography the urban footprints through interferometric coherence technique.

- Study the land use in the catchment area of the lower valley of Majerda using Remote sensing.
- Contribute to the broadening of the applications of remote sensing from space and to a wider use of multi-source satellite data for monitoring and assessment of floods impact.
- develop an interactive map for the publication of the result product on the one hand and it acts as a means of warning of natural disasters.

I-5- Methodology of work

The main objective of this project is to highlight the power of remote sensing in cartography and monitoring flooding, we have developed a multi-source approach we worked with Sentinel 1 RADAR imagery to extract the flooded part in the study area in Mars 2015 and mapping the footprints of urban area the lower valley of Majerda also we used optical images to map the Land Use in the same area , finely we developed an emergency management application were we published the results of this study .

I-6- Software used

Software	*Version*	*Description*
QGIS	3.10.8	QGIS est un logiciel SIG libre multiplate-forme publié sous licence GPL. It Manages the PostgreSQL spatial extension, PostGIS and supports a large number of vector data formats (Shapefile, ArcInfo coverages, Mapinfo, GRASS GIS, etc.). Also supports a large number of raster layer formats (GRASS GIS, GeoTIFF, TIFF, JPG, etc.). One of the characteristics of QGIS is to use it as a graphical interface for GIS GRASS and SAGA extension for terrain analyses.
SNAP	8.0.0	SNAP architecture is ideal for Earth Observation processing and analysis due to the following technological innovations: Extensibility, Portability, Modular Rich Client Platform, Generic EO Data

SNAP		Abstraction, Tiled Memory Management, and a Graph Processing Framework.
PostgreSQL	13.0	PostgreSQL is a relational and object database management system (RDBMS). It is a free tool available under the terms of a BSD-type license. This RDBMS uses modern types of data, known as composed or enriched according to the terminologies used in the usual computer term. This means that PostgreSQL can store more data types than traditional integer, character simple types. PostGIS is an extension of the PostgreSQL DBMS, which enables manipulation of geographic information in the form of geometries, in accordance with standards established by the Open Geospatial Consortium. It allows PostgreSQL to be a spatial DBMS to be able to be used by geographic information systems.

I-7- Geographical context of the study area

Majerda, also spelled Majerdah is a valley its source is located in Algeria and whose bed is mainly on the territory of Tunisia (Figure 1). It is characterized by a permanent flow over the whole of its course, which gives it the profile of a river. This river was called Bagrada in Antiquity (Beschaouch, 1986).

Characterized by a permanent flow over the whole of its course, the Majerda is the only Tunisian river. It rises near Souk-Ahras (in Algerian Constantine) then flows east before flowing into the Mediterranean (Gulf of Tunis). Its watershed covers 22,000 km², of which 6,000 are in Algeria. Its diet is typically Mediterranean and presents a strong irregularity. In Medjez el Bab, the low water flows (low water in July) are 5 to 10 m3/s they sometimes go down to 1m3/s those of floods reach 500 to 700, and even torrential downpours, 1000 m3/s. Interannual contrasts are also very marked, the average annual debits can vary from 1 to 4 m3/s 1950-1951, 404Hm3; 1953-1954, 1,620Hm3. Before construction dams on its tributaries (river el-Lil, Mellègue), an estimated 13 million t were mass of materials transported per year to the delta,and growing very rapidly.

Under the French protectorate, the creation of the Office for the development of the Valley of Majerda was to be the starting point in order to use the Majerda for the irrigation of 50,000 hectares of land in the lower valley. From 1956, the Mellègue dam in Nebeul retained 150 million cubic meters to mitigate floods and maintain low flow rates 15 cubic meters per second in the lower course; the El Aroussia “run-of-river” dam - raises the water level 10 meters above the low water levels and supplies two canals main irrigation. In the low plain, the intersection of two large meanders aims to facilitate the flow of floods, and systematic drainage of marshy areas ensures its sanitation. The reforestation and the development of benches on the slopes of the mountain limit soil erosion and slow the clogging of dams.

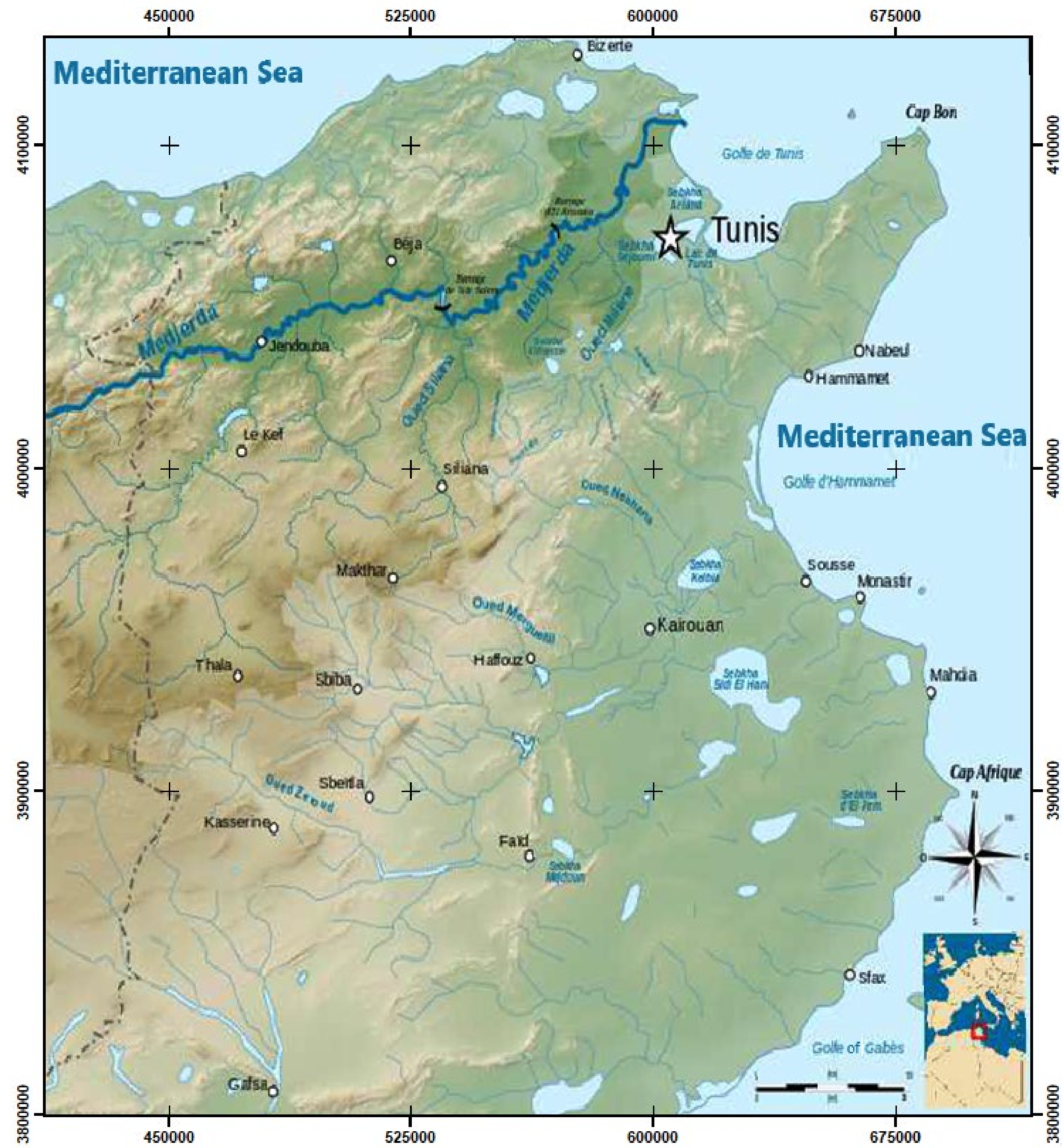

Figure 1:Part of the Majerda flowing into Tunisia.

In the downstream part, the River experiences an average annual flow of 29 m^3/s even if it experiences very marked seasonal contrasts (Oueslati et al., 2006), in particular due to the influx of river's with irregular flows. Thus, the low flow can be reduced to less of 1 m^3/s whereas, for floods with a ten-year periodicity (Oueslati et al., 2006), it can reach 1000 to 1200 m^3/s. The exceptional rains of March 1973 (Oueslati et al., 2006) even led to flow rate of 3,500 m3/s. La Majadra carries around 800 Hm^3year of water. Because it crosses land subject to sometimes intense erosion (Poncet, 1956), the river also carries large quantities of alluvium: between 10 and 30 g/l, even 100 g/l during very heavy rains such as those of March 1973, i.e. an annual sediment input in the Gulf of Tunis estimated at 22.106 million tones before the construction of dams (Oueslati et al., 2006). The average size of the particles transported is less than 0.2 mm (Oueslati et al., 2006).

The materials are deposited when the river reaches the low and flat regions of its lower valley. We then witness a general raising of the bed, the banks of which end up dominating the plain, and its lengthening by a delta which progressively advances over the sea instability, resulting from the valley flowing between its banks, leading to frequent bed changes (five known to date) and increasing difficulty in the flow of water in an area more and more flat.

Thanks to this phenomenon, the Majadra valley is one of the most fertile in Tunisia and represents a twelfth of its water resources. This is why the river is equipped with several hydroelectric dams. La Majerda is also a waterway crucial for irrigation and therefore plays an important role for regional agriculture

I-7-1- Geometric characteristics of the watershed

a. Watershed delimitation

Watershed represents, in principle, the geographical unit on which is based analysis of the hydrological cycle and its effects. More precisely, the watershed which can be considered as a "system" is an elementary surface hydrologically closed, that is to say that no flow penetrates there from outside and all excess precipitation evaporates or drains through a single section at the outlet.

The catchment area of a river considered, at a given point in its course, is the area bounded by the contour within which the precipitated water flows to this point in the river. The outlet of a basin is the most downstream point of the hydrographic network through which pass all runoff water drained by the basin. The crest line of a watershed is the watershed line. The line thus defined, limits the topographic watersheds adjacent. However, the watercourse of a given watershed may be fed by water precipitated over a topographically adjacent basin. This is the case caused by the presence of an impermeable horizon or complex underground flows such as in land karstic. In the event of heavy rainfall, the runoff could join the adjacent basin as seepage water would flow into the main basin.

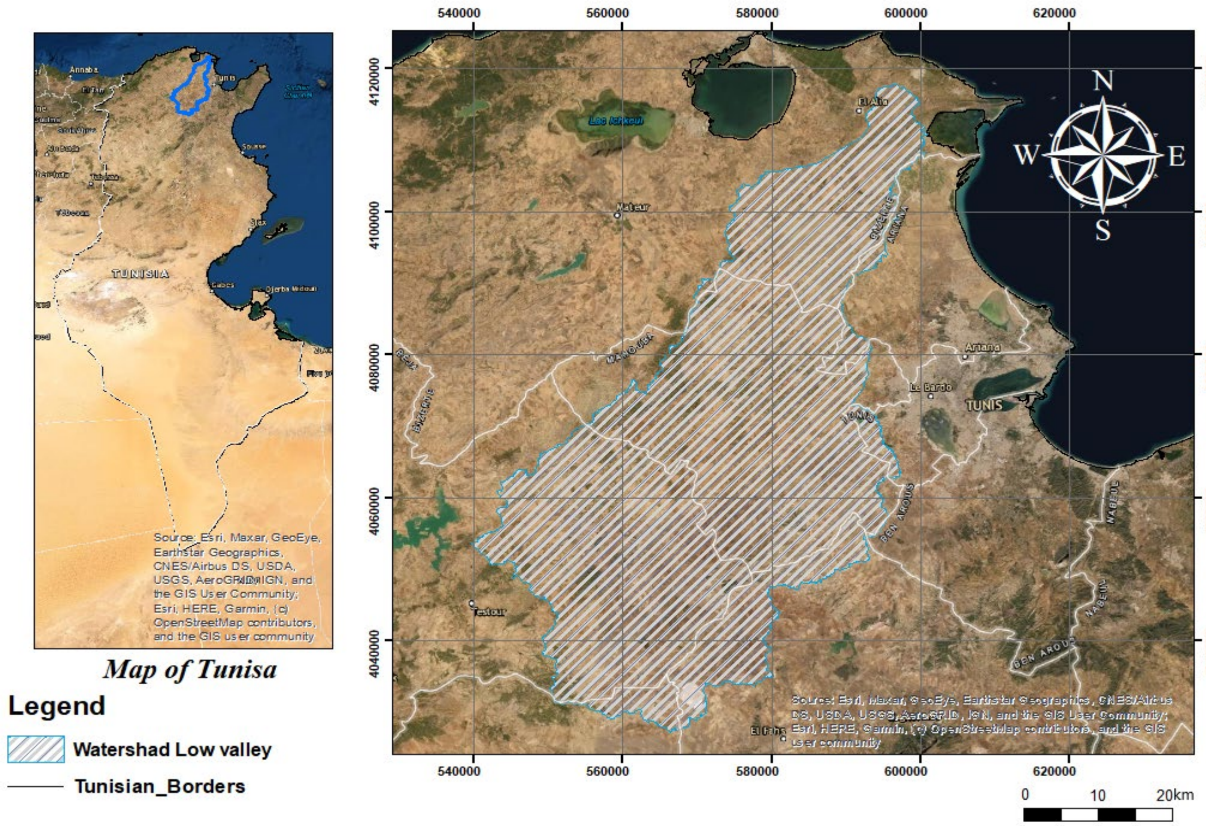

Figure 2:figure shows the limits of the low valley basin of majerda extracted from Shuttle Radar Topography Mission SRTM high resolution digital elevation model with Qgis using the tool watershed in Grass GIS extension.

b. Compactness Index

The index accepted by hydrologists to characterize the shape of a watershed is the GRAVELIUS compactness index which is the ratio of the perimeter of the basin to that of a circle with the same area.

If A is the area of the basin in km² and P its perimeter in km, the coefficient Kc is equal to:

$$K_c = \frac{P}{2\sqrt{\pi A}} = 0.28\frac{P}{\sqrt{A}}$$

The coefficient Kc is greater than 1 and all the closer to this value as the basin is compact.

In our case:

P=250km; A=2500km²

Then kc = 1.4

c. Equivalent rectangle

This notion was introduced in order to be able to compare basins between them from the point of view the influence of their geometric characteristics on the flow.

$$K = 0,28\frac{P}{\sqrt{A}} \qquad 2(L+I) = P \quad = \quad \frac{K\sqrt{A}}{0,28} \qquad L \cdot I = A$$

$$\text{Then} : L = \quad \frac{K\sqrt{A}}{1,12}\left[1+\sqrt{1-\left(\frac{1,12}{K}\right)^2}\,\right]$$

L = length of the rectangle; I = the and the width of the rectangle; P = the perimeter of the watershed; A = the area of the watershed.

A=2500km²; P=250km²; k=1.4 Then L=112km and I= 13km

I-7-2- Topographic characteristics of the watershed

The watershed in a straight section of a watercourse is therefore defined as the totality the topographic surface drained by this watercourse and its tributaries downstream of this section. He is entirely characterized by its outlet, from which we can trace the point of departure and arrival of the watershed that delimits it.

Usually, the watershed line is the ridge line. We speak then topographic catchment area. The relief of a basin is often characterized by the curve of its distribution hypsometric. The hypsometric distribution is given by the percentage of the surface between the different contour lines at the total surface.

However, the topographical delimitation necessary for the determination of the surface natural watershed is not sufficient. When a permeable soil covers a substratum impermeable, the division of water according to topography does not always correspond to the line of effective sharing of groundwater. The watershed is then different from the watershed strictly delimited by topography. It is called in this case the real watershed.

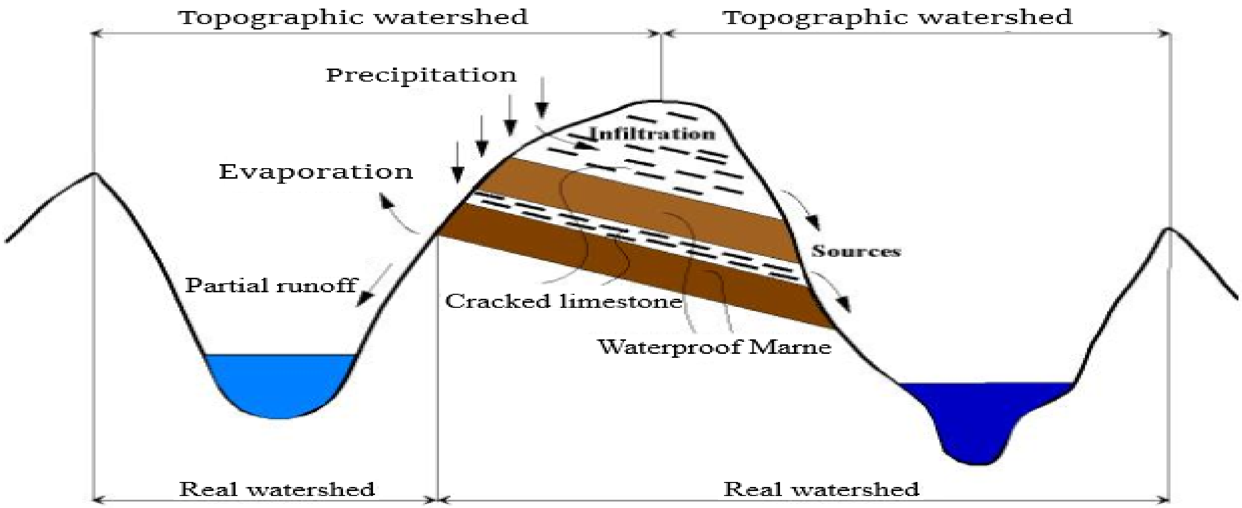

Figure 3:Distinction between real watershed and topography watershed (Roche, 1963).

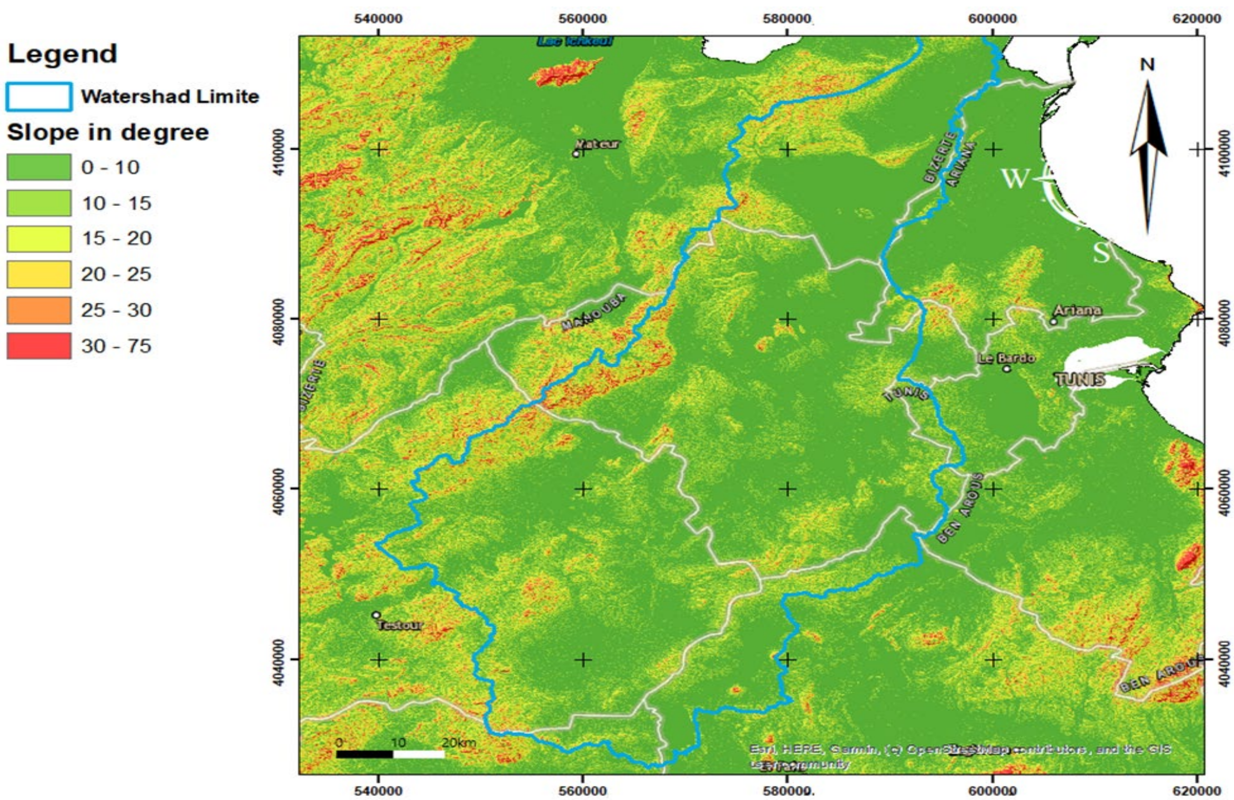

Figure 4:Slope map of Majrda's lower valley The it was extracted from the SRTM-30m digital elevation data using Qgis software (Raster→Analyses →Slope).

The map shows that the majorty oh the area as plain where most of the zone characterized with low slop less then15° which favorize the occurrence of floods during heavy rainfall or river overflow.

I-8 Conclusion

In this chapter we have presented the general context of the project by exposing the problematic, the objectives that we aim to achieve and a global view of the study area. In what follows we will define technical terms, concepts related to flooding and the fundamental aspects of active and passive remote sensing before moving on to the application for the rest of the report.

CHAPTER 2: State of the Art

II-1-Introduction

This chapter aims to place the report in its thematic and scientific context, the first section defined general concepts concerning the hydraulic flood hazard, vulnerability and the risk of flooding, the second presents State of the Art of the fundamental aspects behind active and passive Remote Sensing sensors.

II-2-Flood Hazard

II-2-1-Floods: magnitude, definitions and concept of risk

Based on the definition given in the "Flood" information folder (MEDD-PRIM@): « Flooding is a rapid or slow submersion of an area usually out of water ». According to the same file: « In the broad sense, floods include the overflows of a watercourse, rising water tables, runoff resulting from heavy rainstorms, floods by rupture of protective works, estuarine floods resulting from the conjunction of high tides, low pressure situations and the flooding of rivers ».

The major factor causing a plain flood is the fall of significant precipitation in the catchment with many other contributing factors. When rain falls on a catchment, the amount of rainwater that reaches the waterways depends on the characteristics of the catchment, particularly its size, shape, land use and soil characteristics. (Figure5).

Schematically, during heavy precipitation, part of the water infiltrates into the ground depending on the soil permeability, the rest trickles down the slopes and is thus routed to the rivers (Figure 5). When a very large quantity of water reaches the stream, it overflows from its "usual" bed (or minor bed) and thus gives rise to the flooding phenomenon.

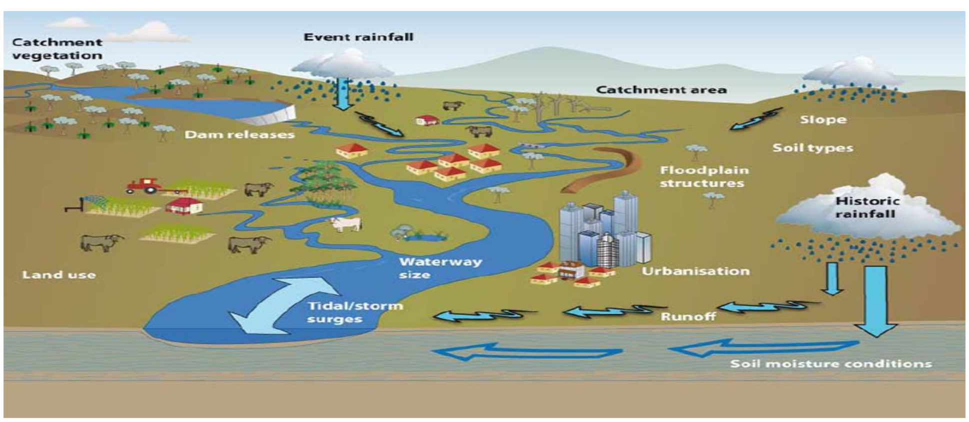

Figure 5: An illustration of the factors that contribute to floods.

II-2-2- The alluvial plain

The term "alluvial plain" usually designates the valley bottom areas, with a slight drop, consisting of alluvium deposited during the flooding of the river. In terms of flow, the alluvial plain is often broken down into three zones: the minor bed, the middle bed and the major river bed (**Figure 6**). The minor bed corresponds to the flow area of the watercourse without overflow. The average bed corresponds to the flow zone for floods of relatively low occurrences. The major bed contains all the areas of the plain in which the watercourse is likely to flow and overflow.

The alluvial plain is made up of alluvium (generally old sediments, including various debris and materials) deposited during flooding of the watercourse, theoretically it belongs to the flood zone of a watercourse; but it is common for bank improvements (embankments) to reduce the possibilities of flooding. The soils here are generally rich and well supplied with water and therefore biologically very productive this explains why they have attracted many populations of pastoralists and farmers in fact most of the human activities is developed in these areas to take advantage of the water availability most of the biggest cities around the world are located near of the rivers (Paris, London, Madrid, Lisbon, Rome…) have been built there despite the risk of flooding.

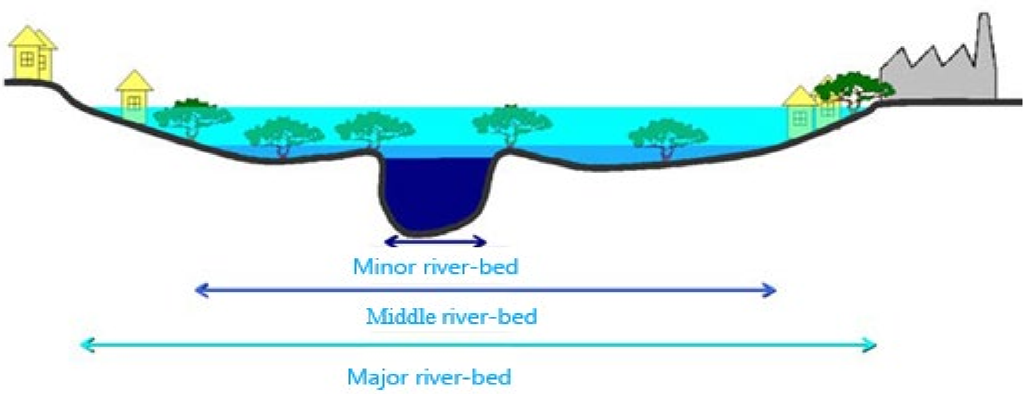

Figure 6 : Schematic representation of the minor, middle and major beds in the alluvial plain.

II-2-3- Risk: hazard and vulnerability

The concept of risk is commonly defined as the combination of two components which are hazard and vulnerability (Ancey, 2005; Gilard & Gendreau, 1998; Oberlin et al., 1993). Indeed, according to (Torterotot, 1993): "There is no risk without natural hazards, there is no risk without a vulnerable element exposed."

II-2-3-1 The hazard

The hazard is a physical, natural and uncontrollable phenomenon, of given occurrence and intensity (Ministry of the Environment and Sustainable Development). It can be characterized according to two components, one frequency (occurrence), the other spatio-temporal (intensity).

The frequency component of the hazard expresses the probability of a location being exposed to a given occurrence of a flood. The occurrence of a flood is most of the time characterized statistically by a return time T. The return time is defined as the mathematical inverse of the probability F that a flood has an amplitude given to occur in a given year:

$$T=1/F$$

Particular attention should be paid to considering the return time of a flood from a statistical point of view. Indeed, a return time of a 100-year flood does not mean that this flood occurs every 100 years, but that it has a 1% probability of occurring in a given year.

II-2-3-2- The vulnerability

Vulnerability expresses the importance of the damage potentially suffered by issues subject to a hazard of given intensity. The concept of stake includes the people, goods and activities likely to be affected by the hazard.

The consequences of the hazard on issues can be beneficial (recharge of groundwater, supply of agricultural land with silt ...) or harmful (destruction of habitats, death of people, cut of communication routes ...). The notion of vulnerability relates to harmful consequences, i.e., damage. The latter can be of several types (Torterotot, 1993):

- loss of life and effects on human health,

- damage,

- impacts linked to operating, exchange and communication difficulties (qualified as indirect impacts).

For example, a maximum vulnerability, for a hazard of intensity I, means the ruin of the development or the death of the people concerned if a flood of intensity greater than or equal to I occurs (Ancey, 2005) which implies that vulnerability is closely linked to the intensity of the phenomenon.

II-2-3-3- The risk of flooding

Risk represents the probability of material and economic damage, injury, and / or death linked to the occurrence of a natural hazard (Ancey, 2005). It integrates the hazard and the vulnerability, that is to say that it depends on a natural phenomenon obeying a law of probability, and on the stakes exposed in connection with the resources available to face it (Torterotot, 1993).

Risk characterization is a delicate issue. To arrive at an objective quantification of risk, the Flooding method (Gilard & Gendreau, 1998) aims to measure in the same unit and compare the two independent factors that are hazard and vulnerability. Its implementation on a watershed consists of hydrological modeling (Flow-duration-Frequency), coupled with hydraulic modeling and land use to result in a cartographic representation of the risk.

In addition, the quantification of the risk is estimated using a difference (Risk = Δ (hazard, vulnerability)) unlike traditional approaches which often favor a product (Risk = Cost × probability), thus allowing the definition of an acceptable risk (Δ negative).

An increased risk of flooding in an alluvial plain may be due to an increase in the stakes or an increase in the hazard. For example, urbanization is frequently responsible for increased risk for two reasons:

- The construction of houses in the alluvial plain increases the stakes.

- The establishment of buildings, parking lots, roads, etc. waterproofs part of the watershed and leads to an increase in runoff, an increase in peak flow and a reduction in concentration time, resulting in an increase in the hazard and a reduction of the time available to cope (Figure 7).

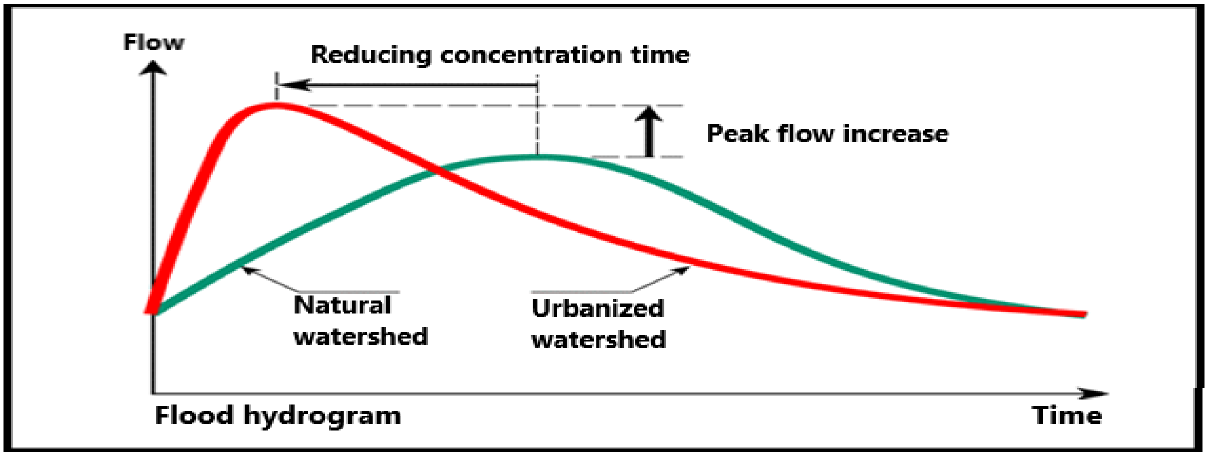

Figure 7: Illustration of the increase in peak flood flow due to the urbanization of watersheds (MEDD-PRIM @).

The devastating effect that natural and manmade hazards have on societies around the world is particularly relevant in developing regions, where countries are experiencing rapid population growth and intense urbanization but where, for many areas at risk, hazard, vulnerability and exposure maps are often inadequate, unavailable or inaccessible. The lack of adequate information for disaster response was so profound that it triggered a global collaborative effort to develop exposure information via the worldwide web using remotely sensed imagery.

II-3-Passive optical satellite Remote Sensing

This third part of chapter 2 presents the principles of passive optical satellite Remote Sensing. For any further information, it is possible to refer in particular to the work by (Girard & Girard, 1999).

II-3-1- Reflection, transmission and absorption phenomena

When electromagnetic radiation reaches the surface of an object, a part ρ of it is reflected (reflectance), a second part α (absorbance) is absorbed and a last part τ is transmitted (ie: passes through the object without being altered) (Figure 8).

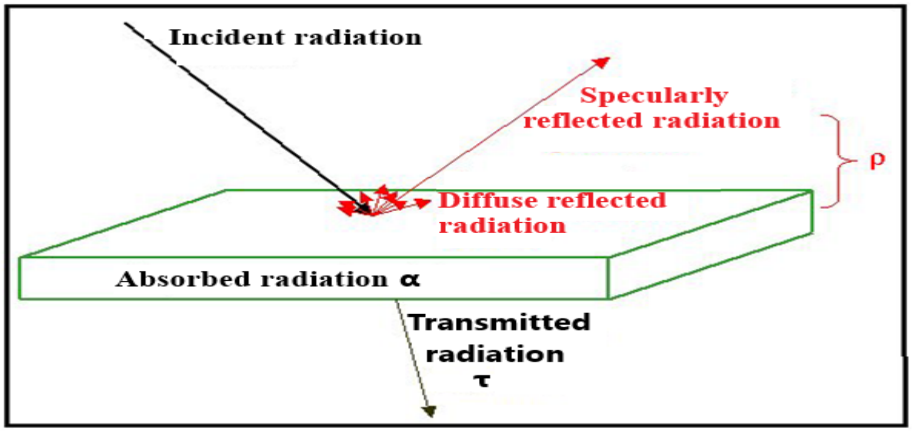

Figure 8:Reflection, absorption and transmission of radiation on an object.

Optical satellites record the intensity of radiation (or luminance) that comes from the surface of the earth over given frequency bands (spectral bands) of the electromagnetic spectrum.

II-3-2-The electromagnetic spectrum

The spectral bands are delimited by two wavelengths (or frequencies). They are shown diagrammatically in (Figure 9). Not all electromagnetic radiation spectral bands are used in satellite Remote Sensing for Earth observation (e.g.: Ultraviolet). This is in particular due to the fact that part of the electromagnetic spectrum is absorbed by the atmosphere (Figure 10)

As a result, for the corresponding wavelengths, no radiation reaches the Earth observation satellites. On the other hand, due to the absorption of part of the radiation by the Earth's atmosphere, the characteristic measured by a satellite is not the reflectance of objects on the surface of the Earth. To find the latter, it is necessary to quantify the share of radiation absorbed by the atmosphere.

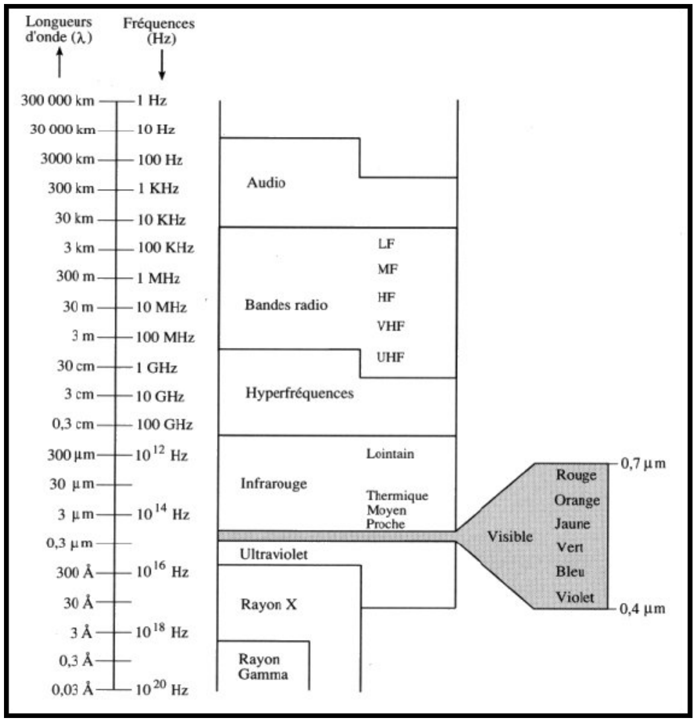

Figure 9:Electromagnetic spectrum and spectral bands (Bonn & Rochon, 1993).

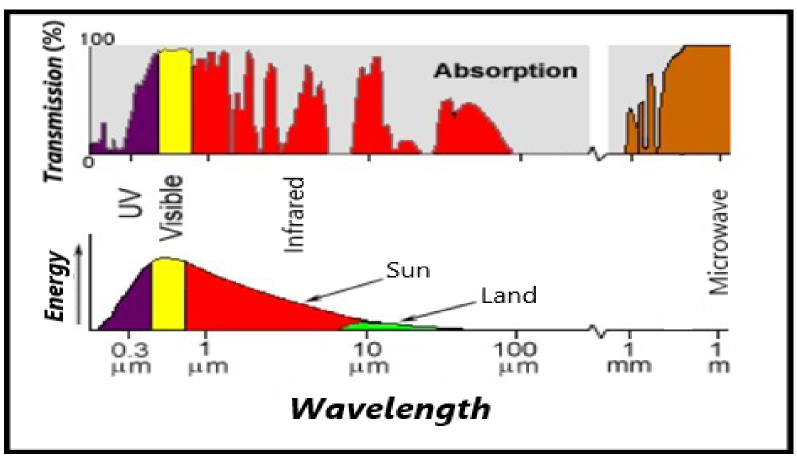

Figure 10: Absorption phenomenon in the atmosphere and emission spectrum of the sun and the Earth (CCT @).

II-3-3- Image acquisition method

Passive satellites acquire images by measuring the intensity of the radiation reaching them from the Earth, this radiation coming partly from the Earth's own radiation - in particular in Thermal Infrared (IRT) - and reflected solar radiation. by the Earth - in particular in the visible and the infrared (near and medium).

II-3-4-Optical image acquisition geometry, and distortions due to relief

All images obtained by Remote Sensing are subject to geometric distortions. In particular, the geometric distortions due to the reliefs arise from the fact that Remote Sensing techniques generally try to represent data taken on the surface of the Earth (in three dimensions) on a two-dimensional image (Figure 11). Consequently, depending on the local viewing angle of the satellite, slopes and objects have different shapes on the images.

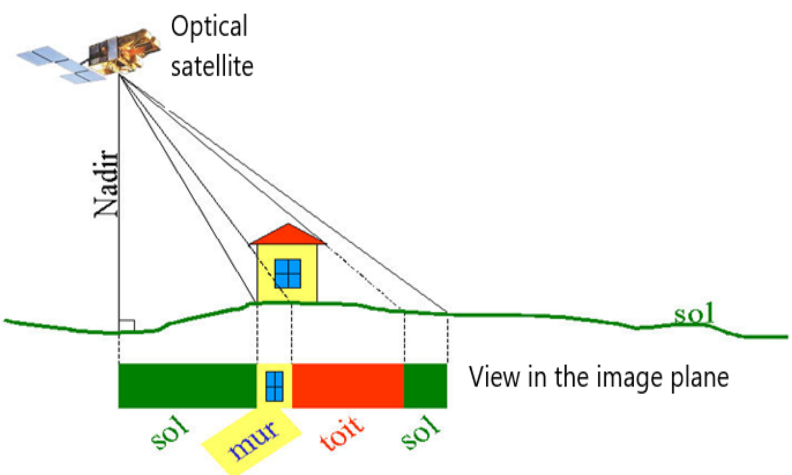

Figure 11: Geometric distortions in relief on optical images

II-3-5-Image specifications

Optical satellite images can be characterized by four resolutions (Henry, 2004; Raclot, 2003a):

- **The spatial resolution** characterizes the ability of the sensor to separate two objects close to the ground. In addition, the smallest element represented in the image is called a pixel. The pixel is closer to the grain on the film in analog photography.

- **The spectral resolution** designates the separating power of the sensor in the electromagnetic spectrum. It is related to the number and the width of the spectral bands measured by the satellite. In particular, a distinction is made between multi-spectral sensors - measurements along several spectral bands (for example 13 for the sentinel 2 satellite) -, hyper-spectral sensors - measurements of radiation on much more spectral bands (for example 220 for the Hyperion sensor of the EO-1 satellite) and most of the time thinner (CCT @).

- **The radiometric resolution** characterizes the power of the sensor to measure two values of intensity of the electromagnetic field that are not very different.

- Temporal resolution, also called revisit period which characterizes the temporal delay between two overflights of the same area of the Earth.

II-4-Active sensors Remote Sensing

Most imaging radar satellites have the ability to acquire the same quality flood imagery regardless of cloud conditions. Floods are mostly accompanied by significant cloud cover. As a result, radar satellite systems have a higher potential for image acquisition during active phases of a flood than passive optical satellite systems. This is why, in view of the objective of using satellite images for the study of floods, it was chosen to present the radar systems in more detail.

II-4-1-Radar measurement and backscatter coefficient

Radar satellite sensors (Radio Detection and Ranging) are said to be active because they acquire images of the earth's surface by emitting microwave pulses and then by measuring the characteristics of the back-broadcast signal - intensity and date of reception of the retro-signal. disseminated - (CNES @, 2000; Polidori, 1997). The characteristics of the backscattered signal are then compared with those of the transmitted signal.

The fundamental relationship between the characteristics of the radar, the target and the received signal is called the radar equation. It is broken down as follows (Ulaby et al., 1981):

$$P_r = \frac{G^2 \lambda^2 \sigma}{(4\Pi)^3 R^4} P_e \qquad (3.1.)$$

In equation (3.1), Pe and Pr respectively designate the powers transmitted and received by the antenna, G the gain of the antenna, λ the wavelength of the signal, and σ the equivalent backscattering section of target. The latter is complex in the mathematical sense of the term:

$$\sigma = Ae^{i\varphi} \text{ (with A the amplitude and } \varphi \text{ the phase) } (3.2)$$

In equation (3.2), σ is a function of the directions of the incident wave and the wave reflected towards the antenna, but also of the shape and dielectric characteristics of the target. The amplitude of σ corresponds to the surface of a perfect flat reflector, oriented in front of the antenna, which would reflect a signal of the same power Pr as the real target. Its phase corresponds to the phase shift between the transmitted wave and the wave received by the antenna.

Usually, the equivalent backscattering surface is converted into a backscattering coefficient σ0 of the target, defined as the logarithm of the ratio between σ and a reference surface S

$$\sigma^0 = \log\left(\frac{\sigma}{S}\right) \qquad (3.3)$$

II-4-2- The principle of lateral radar acquisition

The pulses are emitted by the antenna perpendicular to the carrier's trajectory, in oblique aiming, at an angle θ called the aiming angle. The reflectors on the surface of the earth are located by their distance to the antenna which is calculated from the time of return of the radar wave and the speed of propagation of the radar waves in the atmosphere. The repetition of the pulses ensures the azimuth scanning, i.e. in the direction of movement of the antenna.

II-4-3-Spatial resolution and aperture synthesis

Radar systems, like all imaging satellites, have limited spatial discrimination. To characterize the discriminating power of radar on objects on the surface of the Earth, two resolutions are defined (Henry, 2004). The azimuthal resolution δ_{az}(Cf. Figure 12) characterizes the power of discrimination in the direction of movement of the antenna, and the radial resolution (Cf. Figure 12) in the plane perpendicular to the direction of movement of l 'antenna (Polidori, 1997). Thus, two objects located on a parallel to the direction of movement of the antenna can only be discriminated if the distance between them is greater than the azimuthal resolution. Similarly, two objects located in a plane perpendicular to the direction of movement of the antenna can only be discriminated if the distance between them, in the horizontal plane, is greater than the radial resolution.

The azimuthal resolution is proportional to the angular opening of the antenna lobe (ratio of the wavelength λ of the signal emitted by the length D of the antenna) along its trajectory (Figure 12). Therefore, fine azimuth resolution requires a large antenna size.

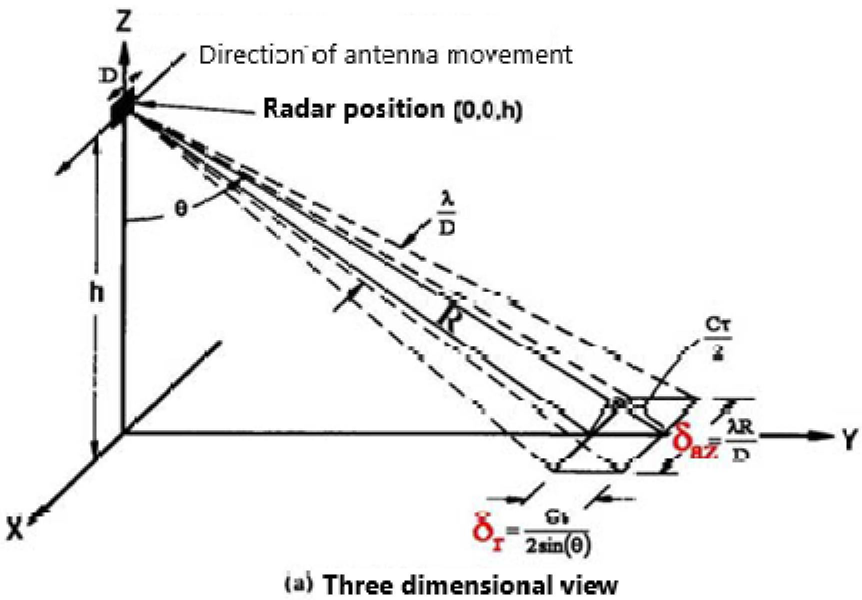

Figure 12: Lateral radar and spatial resolution (adapted from Ulaby et al., 1982)

The radial resolution is imposed by the duration of the pulses. Indeed, so that two close reflectors can be discerned, it is necessary that the signals which they reflect towards the satellites are temporally separated. Consequently, a fine radial resolution imposes a very short pulse duration, which implies the use of a large transmitting power.

To avoid the use of very large and powerful antennas, two methods are used in current radar satellite techniques: aperture synthesis and pulse compression.

a. Improved spatial resolution

To improve the radial resolution, the solution adopted in the pulse compression is the emission of a wave strongly modulated in frequency. This modulation makes it possible to simultaneously light two neighboring reflectors with signals of different frequencies, and therefore to discriminate them.

The received signal is correlated with a reference signal called a replica, identical to the transmitted signal but shifted in time (Polidori, 1997). The auto-correlation peak is obtained at time $t_0$corresponding to the round-trip propagation time. The radial resolution is then determined from the width of the autocorrelation peak at -3dB. This processing, called "matched filter" has the particularity of increasing the intensity of the signal compared to noise.

To improve the azimuthal resolution, the aperture synthesis is possible thanks to the Doppler effect, ie the variation of the frequency of the signal returned by a point element during the movement of the radar: when the point is in front of the satellite, the frequency of the backscattered signal is greater thanf_0, and conversely when the point is behind the radar, it is less than f_0. This implies that the Doppler frequency is responsible for frequency modulation of the radar signal. Pulse compression can therefore be applied in the same way as for radial resolution.

b. Spatial sampling of radar images

The information present on each pixel of a radar image results from an integration of the backscattering on the pixel surface. After this integration, a complex image (in the mathematical sense of the term) is obtained: amplitude and phase information are known for each pixel. The transition to an image in amplitude (real value, in the mathematical sense of the term) is called detection (Polidori, 1997). According to the Shannon-Nyquist sampling theorem, this operation requires doubling the sampling frequency on the image in amplitude compared to the complex image. As a result, on an amplitude image, the pixel size is equal to half the spatial resolution of the complex image.

II-4-4- Radiometry on radar images

a. Radiation sampling and calibration of radar images

On radar satellite images, the information present for each pixel is not directly the radar backscatter σ0, but discrete information called a digital count. To estimate the backscattering coefficients from the digital counts, several relationships can be used. These relationships, specific to each sensor, use calibration constants of the radar system (Small et al., 1997). Usually these are provided in the image header file.

b. Speckle

Radar images are subject to the effects of speckle (Fellah, 1997). The latter is a noise inherent in all systems that emit coherent waves and is reflected on images by a granular appearance (Henry, 2004). It is due to the random interference of coherent waves emitted by the radar on a rough surface.

Indeed, each signal received at a given point on the antenna is the sum of the backscattering from a large number of elementary reflectors (Saad & El Assad, 1985). The waves reflected by these elementary reflectors interfere with each other, which reduces the spatial coherence of the signal (Comblet, 2005) and is responsible for a radiometric degradation on the images.

The effects of speckle can be detrimental for the thematic analysis of radar images. Indeed, they add a radiometric variability on the images which disturbs the identification of the objects present on the surface of the Earth, in particular by the presence of atypical backscattering values within homogeneous zones. To characterize the level of speckle on a radar image, an equivalent number of views is defined (ENL) which translates an average number of illuminations of ground targets by radar. The higher the value of ENL, the more the shimmer is reduced. Assuming that each pixel of a homogeneous area (vis-à-vis the radar signal) is affected by a realization independent of the speckle, the ENL can be estimated, on a homogeneous area of the image, by the following formula (Ulaby et al., 1982):

$$\mathrm{ENL} \sim \frac{1}{\mathrm{CV}^2\left(\mathrm{I}_{\mathrm{surf\_homog\grave{e}ne}}\right)} \qquad (3.4)$$

(With the coefficient cv($I_{surf\_homogenous}$) of variation of the intensity over a homogeneous area of the image)

To limit the effects due to speckle, two methods of processing radar images are frequently used: temporal filtering and spatial filtering.

c. Spatial filtering

Spatial filtering is applied to a single radar image. Spatial filters are numerous and more or less complex. The simplest filters - median or average - consist in replacing the backscattering value of a pixel by the median or the average of the backscattering in a given neighborhood. The size of the neighborhood is defined by the size of the sliding window - in pixels - used for filtering. More advanced filters, called adaptive filters, modify the calculation method according to local backscattering statistics in a given neighborhood - sliding window - of the pixel considered (Jingfeng et al., 2003). Among these, it is possible to cite the adaptive filters of Lee (Lee, 1980), Frost (Frost et al., 1982), and Gamma MAP - Maximum A Posteriori - (Lopes et al., 1993; Lopes et al ., 1990). Some publications offer comparative studies of these different types of adaptive filters, for example (Mansourpour et al., 2006; Zhiyong et al., 2004).

Spatial filters, although effective in reducing the effects of speckle, are responsible for a deterioration in the spatial resolution of images, directly linked to the size of the sliding window used. Also, in the case where image analysis requires the finest spatial resolution possible, the use of this type of filter may prove to be irrelevant.

II-4-5-Parameters that influence backscatter

This section of the document presents the different parameters that influence radar backscatter. These include on the one hand the morphological and physical characteristics of the objects observed, and on the other hand the characteristics of the signal emitted (Ulaby et al., 1986). For clarity, each of these parameters will be presented in a separate paragraph, with the implicit assumption that the other parameters are invariant. It therefore seems important to keep in mind that their effects on backscatter are combined in reality.

a. Surface roughness

Generically, three main classes of radar signal reflectors can be defined on the surface of the Earth: specular (smooth) reflectors, rough (diffuse) reflectors, and corner reflectors.

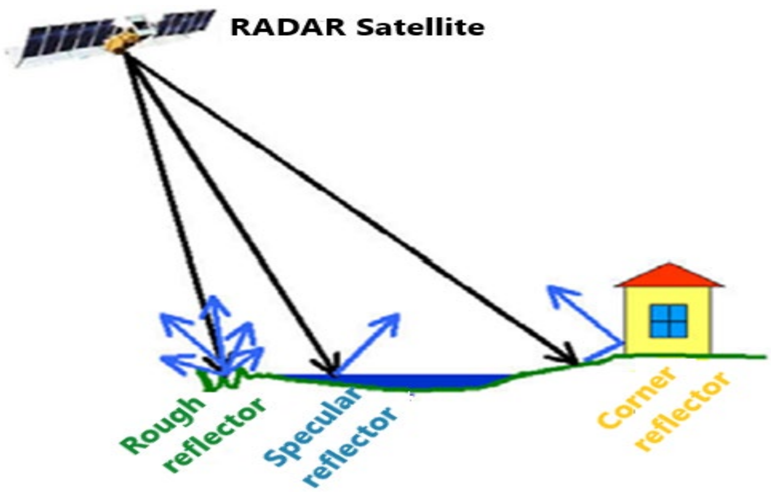

Figure 13: Illustration of the influence of roughness on radar backscatter

When viewed from the side, on a smooth surface, a specular effect occurs: the entire signal is reflected in a divergent direction from the antenna (Figure13). This implies a theoretically zero backscatter for smooth open water bodies.

In the case of a rough reflector (Figure 13), a more or less significant part of the signal emitted by the antenna is reflected towards it. The rougher the surface of the reflector, the greater the backscattered signal. The roughness or smoothness of a surface is in particular defined by the Rayleigh and Fraunhofer criteria in relation to the wavelength of the incident signal. According to these criteria, a surface is smooth with respect to the incident signal if:

$$\sigma_h < \frac{\lambda}{32\cos\theta} \quad \text{Rayleigh criterion} \quad (3.6)$$

$$\sigma_h < \frac{\lambda}{8\cos\theta} \quad \text{Fraunhofer criterion} \quad (3.7)$$

In relations (3.6) and (3.7), σ_h is the standard deviation of height of the target, λ the wavelength of the signal and θ the angle of incidence) The more restrictive Fraunhofer's criterion sometimes proves to be more consistent with experimental tests and more appropriate for modeling diffusion on a natural surface (Ulaby et al., 1982). As part of the detection of flooded areas on radar images, wind, currents or heavy precipitation can cause the roughness of open water surfaces which tends to bring their radiometric response closer to that of rough reflectors and make them more difficult to detect in images. Ripples will have different effects on images depending on their size and the wavelength of the radar signal.

In the case of corner reflectors, for example buildings, effects of multiple reflections between the ground and these reflectors generate strong backscattering values (Figure 13). In the presence of flooding under vegetation cover, multiple reflections between the surface of the water and the trunks can take place if the wavelength of the radar signal allows it to cross the vegetation cover. The result is a signal backscattered by vegetation that is greater than in the absence of the flood.

b. The dielectric characteristics of the target

The backscattering coefficient is linked to the dielectric characteristics of the target (Aires et al., 2005; CNES @, 2000). These dielectric characteristics are often expressed by the complex dielectric constant, which translates the conductive and reflective character of a medium, in a given domain of the electromagnetic spectrum. The higher the dielectric constant of the observed target in the microwave range, the more it will be reflective to the radar signal. It follows that with invariant acquisition characteristics and roughness, an increase in the dielectric constant of a target leads to an increase in its backscattering.

In the microwave field, for most dry natural environments, the dielectric constants encountered are of the order of 3 to 8, while that of water is of the order of 80. Consequently, an increase of the water content of a target, for example of a soil, causes an increase in backscattering.

c. The wavelength

Radar systems emit signals into microwaves, which include wavelengths between 1mm and 1m. In the microwave field, the electromagnetic spectrum is divided into several spectral bands designated by capital letters (Table 2). Most imaging radar satellites use X, C or L band signals.

Band	Frequency (GHz)	Wavelength (cm)
P	0.255 - 0.390	133 - 76.9
L	0.390 - 1.550	76.9 - 19.3
S	1.550 - 4.20	19.3 - 7.1
C	4.20 - 5.75	7.1 - 5.2
X	5.75 - 10.90	5.2 - 2.7
K	10.90 - 36.0	2.7 - 0.83
K_u	10.90 - 22.0	2.7 - 1.36
K_a	22.0 - 36.0	1.36 - 0.83
Q	36.0 - 46.0	0.83 - 0.65
V	46.0 - 56.0	0.65 - 0.53
W	56.0 - 100.0	0.53 - 0.30

Table 2: Radar spectral bands - frequencies and associated wavelengths

Depending on the wavelength of the transmitted signal, the transparency of the atmosphere vis-à-vis the radar signal is more or less marked (Henry, 2004). In the case of imaging radar satellites, for the X, C and L bands, the transparency to the atmosphere is fairly well marked.

The sensitivity of the radar to surface roughness varies with the wavelength of the signal (Figure 14).

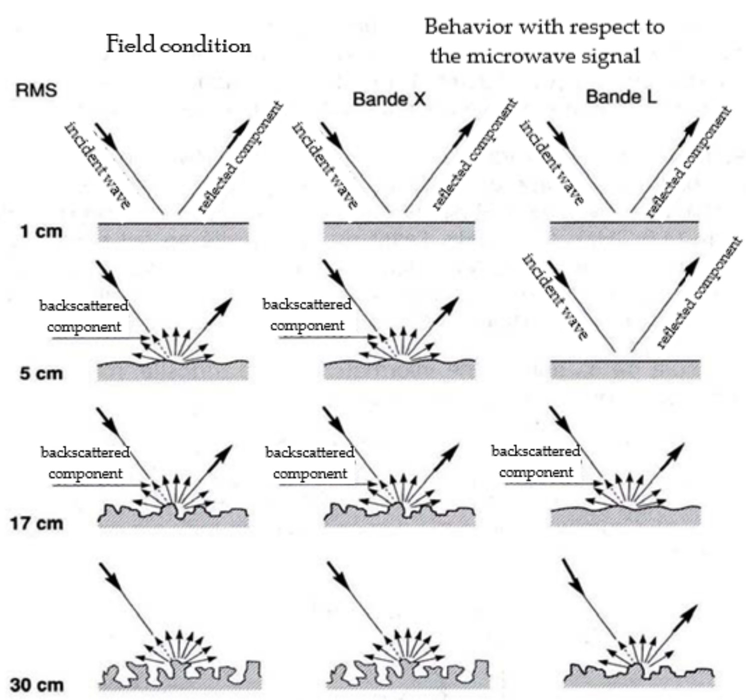

Figure 14: Illustration of the influence of the wavelength on the sensitivity of the radar to surface roughness for the X and L bands (Girard & Girard, 1999).

Indeed, the roughness of a surface depends on the spectral band with which it is illuminated. This is directly linked to the notion of surface roughness as defined by the Rayleigh or Fraunhofer criteria - relations (3.6) and (3.7). Consequently, for an invariant rough surface, illuminated from a given point in space, the backscattered signal is all the more important the smaller the wavelength of the signal.,

d. Polarization

For radar satellites, polarization is characterized by two letters. The first indicates the polarization according to which the wave is emitted, and the second the direction in which the antenna measures the backscattered wave. For transmission or reception, the letter H indicates a horizontal polarization and the letter V a vertical polarization (e.g.: HH, transmitted wave horizontally polarized, and measurement of the reflected wave in the horizontal direction). VV polarization implies a higher sensitivity of the radar to vertical objects (ESA, 2000). On the contrary in HH polarization, vertical objects are more transparent with respect to the radar signal (Figure 15)

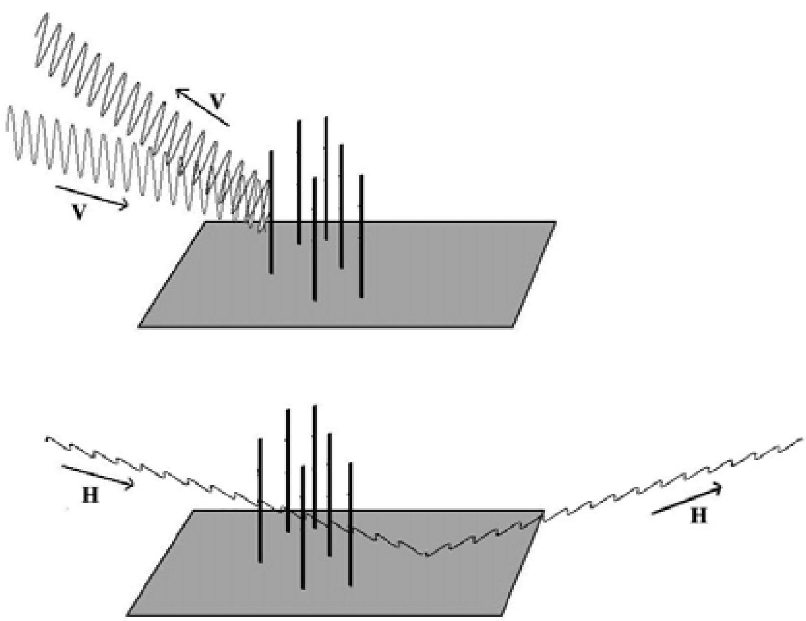

Figure 15:Influence of vertical objects on the radar signal according to polarization

In addition, the most recent radar satellites have been obtained with several simultaneous polarizations, particularly in cross-polarization (HV and VH): multi-polarization sensors.

e. The angle of incidence

In the acquisition geometry of the imaging satellites, a viewing angle and an angle of incidence are defined. The viewing angle corresponds to the angle between the vertical to the right of the antenna (Nadir) and the antenna-target direction. The angle of incidence corresponds to the angle between the antenna-target direction and the ground normal at the target level. The normal is the vector perpendicular to the ground. It depends on the local slope and the azimuth of the natural terrain. The slope represents the inclination of the natural terrain in a vertical plane. The azimuth translates the orientation of the natural terrain in the horizontal plane.

The backscatter phenomenon is generally not isotropic (Polidori, 1997). Consequently, depending on the angle of incidence of the radar wave, the backscattering of the same object will not be identical. In Figure 16, (Ulaby & Dobson, 1989) propose general behavior curves for the backscattering of a fairly smooth coating as a function of the angle of incidence and according to the polarization.

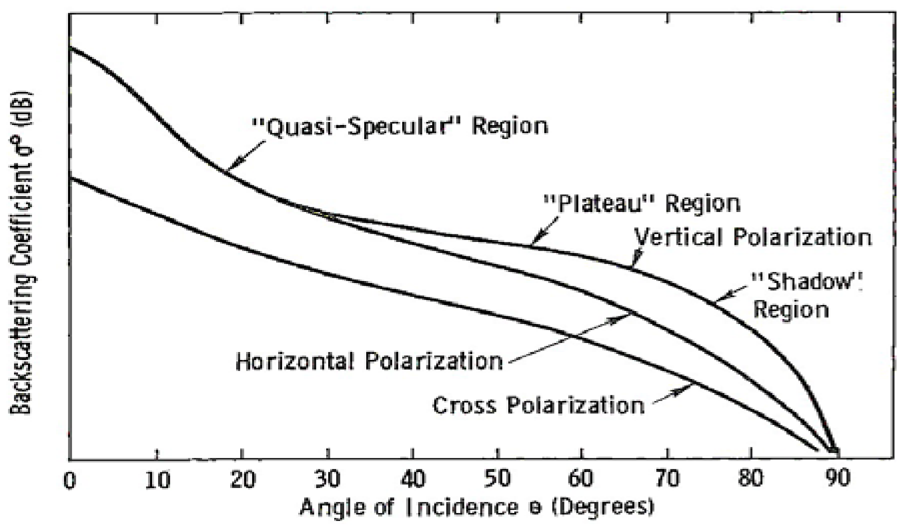

Figure 16:General behavior of the radar backscatter as a function of the angle of incidence (Ulaby & Dobson, 1989)

II-4-6-Terrain morphology and radar image: geometric distortions

Due to the acquisition in oblique geometry, the radar imagers are subjected to geometrical distortions and an erroneous vision of the relief, mainly due to the fact that the radar measures distances between the targets relatively to its position in space and not horizontal distances to the ground (Holah, 2005). Since the subject of study of the thesis concerns the flooded areas in the plain, the distortions on the studied images will be relatively limited. As a result, the presentation of image distortions in this section is relatively succinct. For more details, reference may be made to the work by (Polidori, 1997).

a. Distortions due to oblique aiming

In oblique vision, in the radar image plane, the same target is seen smaller if it is closer to the nadir due to a smaller angle of incidence (Figure17). In the same way, the distances between objects are "shortened" in the image plane by approaching the nadir.

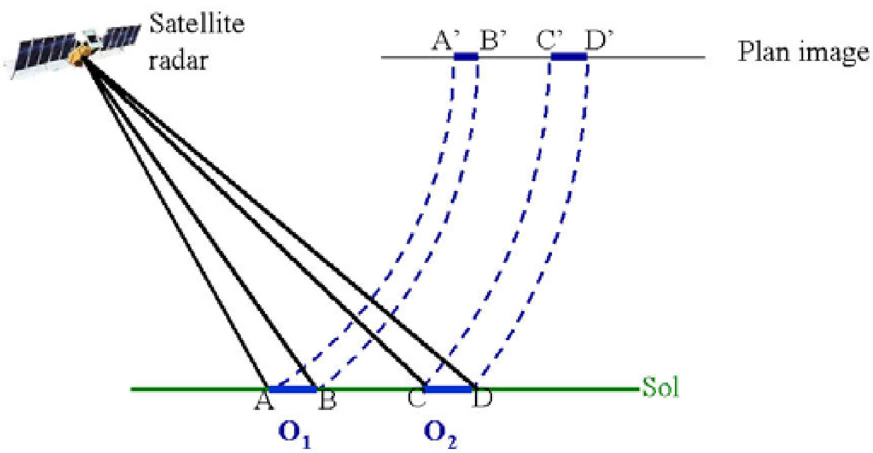

Figure 17: Visée oblique et distorsion géométrique.

b. Folding of the relief

In addition, oblique aiming implies an erroneous vision of the slopes of the natural terrain. Indeed, the same slope of natural terrain is seen shorter if it is oriented towards the antenna than if it is oriented in a direction opposite to the antenna (Figure 18A). This phenomenon is called approximation of the relief ("forshortening" in English). In addition, in Figure 18A, slope B-C is less "lit" by the incident radar signal than slope A-B and therefore appears darker in the image. This phenomenon is called pseudo-shading

When the slope of the slope is greater than the viewing angle, the vertex B of the slope is reached by the incident radar wave before base A. There is therefore an inversion of the positions of vertex B 'and of the base A 'of the slope AB in the image plane. In addition, point C is not illuminated by the incident wave and is therefore not represented in the image plane. We then speak of overlap for slope A-B ("layover" in English) and shading for slope B-C (Figure 18B).

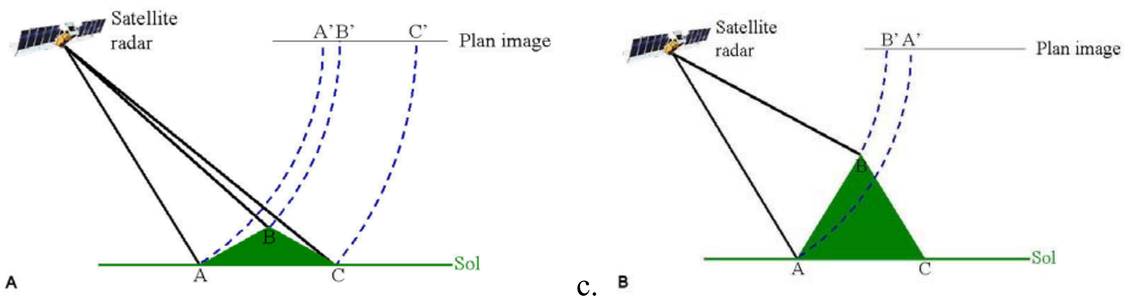

Figure 18: A. Reconciliation of relief and pseudo-shading, B. Recovery and shading

Given the geometric distortions presented above, to find the initial geometry of the terrain from the positions of objects in the image plane, it is necessary to have recourse to certain pre-treatments.

c. Correction of geometric distortions on images

The process of correcting geometric effects due to relief and oblique aiming is called orthorectification. The orthorectification of a radar image requires knowledge on the one hand of the sensor acquisition parameters (antenna displacement speed, aiming angle, geometry of the emitted beam) and on the other hand the local geometry of the terrain (slope and azimuth).

The acquisition characteristics are mostly present in the header files supplied with the images. The local geometry of the terrain can be known thanks to topographic data such as a Digital Terrain Model (DTM). Knowledge of the acquisition characteristics and morphology of the natural terrain thus makes it possible to determine the correspondence between geographic coordinates and image coordinates.

In addition, the orthorectification process can be replaced, in a limited relief area, by a georeferencing process by entering amper points (Small et al., 1997). The latter consists in calculating the position of the pixels of the radar image, in a given projection system. Amber dots are ground surface objects that can be identified both on the radar image and on another georeferenced data source, such as an IGN map. After entering these points, by geometrical transformation of the image, it is possible to recalculate geographic coordinates for all the objects in the radar image.

II-5- Conclusion

Synthetic Aperture Radar (SAR) and passive optical imaging satellites are very useful for the spatial characterization of the flood hazard (Sanders & Tabuchi, 2000; Sassier et al., 2000; Schmugge, 1987). Indeed, they offer spatialized observations of floods with high spatial resolution that it would be very difficult if not impossible to acquire without the help of Remote Sensing. Moreover, as we could see in the first part of the document, satellite images of floods can prove to be very useful in an operational context of crisis management. In general, studies based on the analysis of satellite images acquired during a flood period provide a fine two-dimensional characterization of the hazard, but without consideration for water levels and flood dynamics.

Chapiter 3: Flooded area mapping

III-1-Introduction

Remote sensing techniques are an efficient source of knowledge to discriminate bodies of water over large areas, and thus, they will be accustomed map flooded areas with sufficient temporal and spatial resolution (Bioresita 2019). within the case of multispectral images, water bodies may be easily discriminated thanks to their spectral behavior within the visible and spectrum because it's different from other land covers (McFeeters 1996, Zhang 2009, but they only. operate in natural daylight conditions and cloudless skies. Since severe flooding usually occurs as a result of heavy rainfall, they're not always useful for this purpose. In Tunisia, because of the physiographic characteristics of the basins and also the Mediterranean climate, most floods are related to periods of heavy rainfall. The validity of multispectral observations for this purpose is proscribed by clouds because unclear whether are common during floods. events (Shen, X.; Wang, D 2019). However, the Synthetic Aperture Radar (SAR) may be a style of radar that's accustomed create more useful images over a target region to produce fine spatial resolution (Tomer 2015, Paniconi, C 2015), which may operate day and night and is unaffected. by bad weather, smoke, atmospheric water, or hydrometeors. Moreover, the signal can penetrate through foliage (wavelength dependent), and so can provide more complete information about the inundation state (Ulaby 1983, Kelly, R 2003). SAR based flood mapping methods are usually more complex than those supported optical sensors because. of the method added to mitigate the error. propagated from one or more of the error sources [Shen, X.; Wang, D 2019, Smith, L 1997].

Accordingly, in the present study, we investigated the potential use of the Sentinel-1 SAR images as a powerful and complete tool for flood mapping, and as a crucial element of flood management (European Exchange Circle 2019). This methodology was applied in the case of extraordinary floods that occurred during the month of March 2015 in the Majerda river due to heavy rainfall. The specific goals were: (1) Analysis of the affected area and hydraulic parameters characteristic of the Majerda flood case; (2) selection of the optimal processing and correction options (orbital parameters, radiometric, noise reduction—speckle, and geometric geometric) to perform an accurate and thorough treatment of Sentinel-1 SAR images, in order to optimize the detection and analysis of flooded areas; (3) application of two detection algorithm approaches (RGB—Red, Green, Blue color model - composition and calibration threshold technique) of free water surfaces to derive flood cartography from SAR images, which permits the delimitation of non-permanent water surfaces;

III-2-Data used

In this study, it is been used Sentinel-1 SAR images because of their features, configuration, and the free data set available online from Earth Observation (EO) data resources. Sentinel-1 SAR datasets, coming before and after the event, were downloaded via the Copernicus Open Access Hub platform. The Sentinel-1 sensor is part of an ESA (European Space Agency) satellite constellation. It is composed of Sentinel-1A, launched on 3 April 2014, and Sentinel-1B, on 22 April 2016. Both satellites have a useful life of 7 years and a 12-day orbital repetition cycle (6 days between them). These temporal limitations of image capture mean that we did not have images of the day of the highest level of the Ebro at the study points. The available image that was closest to the moment of maximum flood was from 13 April 2018 and it was the one used for the development of the study.

Table 3 shows the characteristics of the two images used in the study. Usually, depending on the methodology used, the pre-event image serves as a reference and record of permanently flooded areas, while the post-event image serves to establish the differences with the initial image (Klemas 2015).

Image	Mission Identifier	Date of Capture	Hour of Capture
Crises Image	Sentinel 1 A	2015-03-04	17:20
Archive Image	Sentinel 1 B	2015-02-27	14:35

Table 3. Characteristics of the Sentinel-1 SAR images used in the study.

Each image has a coverage range of 250 km with a 5 × 20 m resolution. The images are Level-1 Ground Range Detected (GRD) products; this means that they were detected, multi-looked, and projected to the ground range using an Earth ellipsoid model . The acquisition mode is Interferometric Wide Swath, and the images have a high resolution; the sensor pass is ascending, with incidence angles between 29° and 46°, and dual polarization, VV (Vertical-Vertical) and VH (Vertical-Horizontal). The study area is covered by VV and VH only according to the observation scenarios shown in Earth Observation Data Center for Water Resources Monitoring (EODC). In the free modes of IW (Interferometric Wide) Sentinel-1, only VV + VH polarization over land is available.

III-3-Preprocessing

For quantitative analysis, SAR images need to be radiometrically calibrated, geometrically corrected and filtered so that the pixel value of the images directly represents the radar backscatter of the reflecting surface (Meenakshi and Punitham, 2011). The images were processed with the free software SNAP (Sentinel Application Platform) Tool version 8.0.0.], created specifically by ESA for the analysis of the data captured by Sentinel satellites. It is a very powerful program that has the right tools, Sentinel Toolboxes, to perform an accurate and thorough treatment of the images and subsequently run the analysis. In Figure 19, the sequence of the steps followed for the pre-treatment of the images is shown.

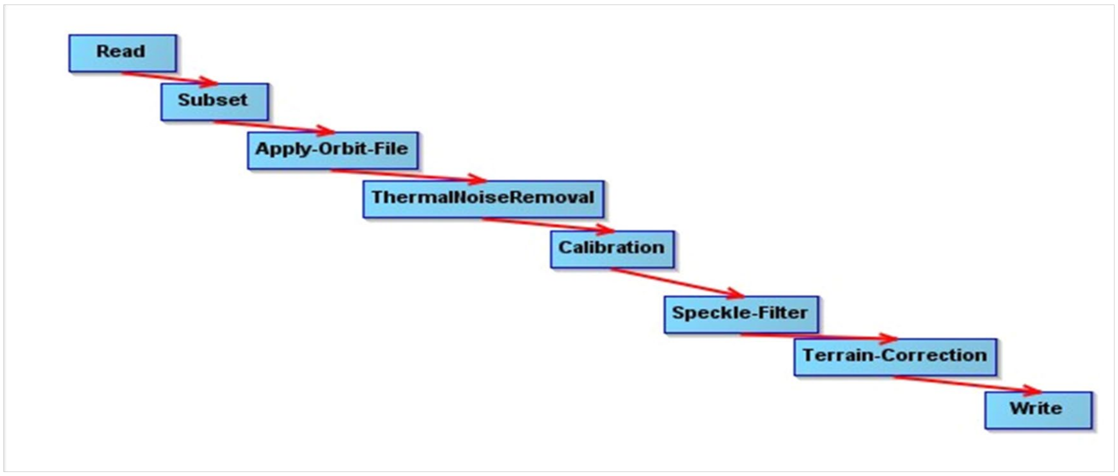

Figure 19:Flowchart showing the preprocessing chain used in RADAR SAR Sentinel-1 GRD images.

The first step in the processing chain was spatial subset as shows **(**Figure 20) the image covers a very large area where we only need a small portion of the image this also contribute to correct manipulation of images, and reduce the processing time. The next thing was updating the orbit state file this step is necessary because the orbit state vector provided in the metadata is generally not accurate and can be refined with accurate satellite position and velocity information improving the analysis that requires satellite information to be as precise as possible. Then we applied **Thermal Noise Removal** function to reduce the background energy that is generated by the receiver itself which excuse the radar reflectivity toward higher values and hampers the position of radar reflectivity estimates.

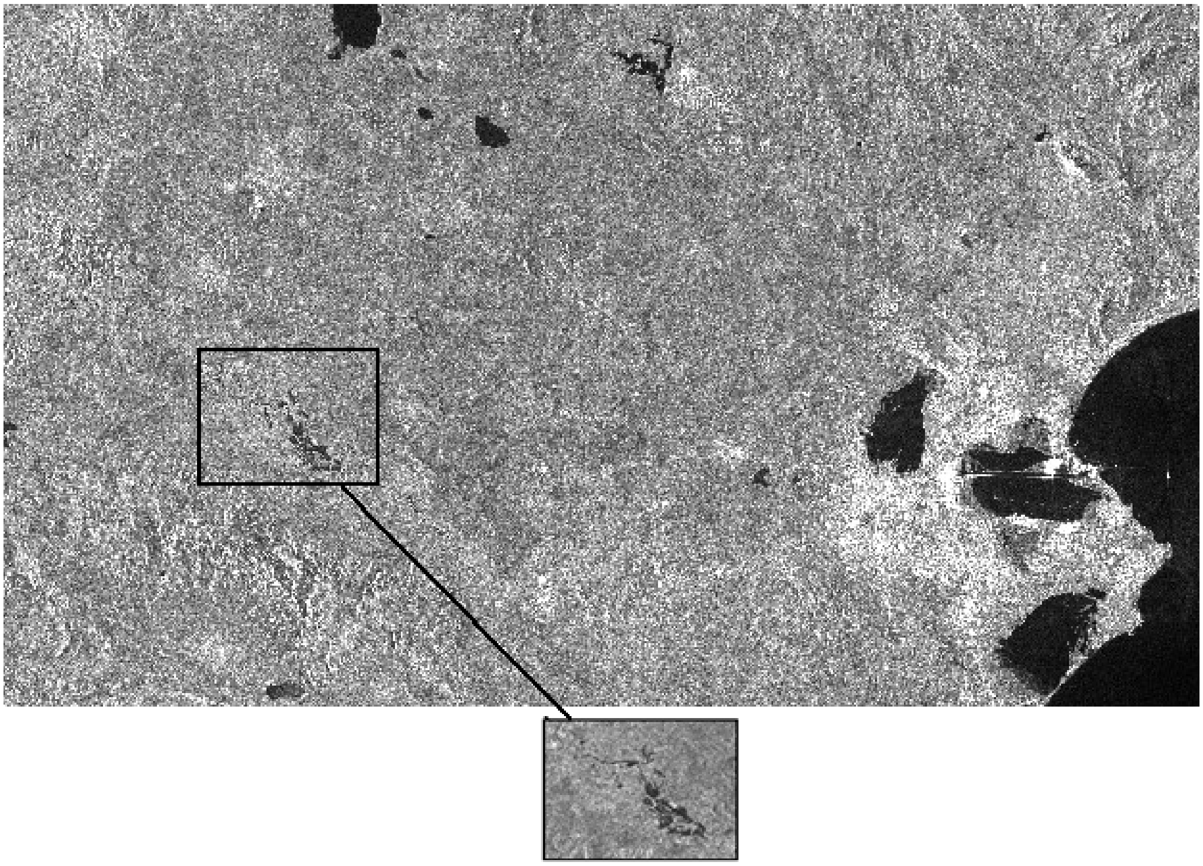

Figure 20:Illustration for the flooded part for Subset

Furthermore, we applied radiometric calibration that aims to provide imagery in which pixel values can be directly associated with the radar backscatter of the scene. While uncalibrated SAR imagery is sufficient in terms of quality, calibrated SAR images are essential to the quantitative use of SAR data. Standard SAR data processing, which produces level 1 images, does not include radiometric corrections and there remains significant radiometric distortion. It is therefore necessary to apply radiometric correction to the SAR images so that the pixel values actually represent the radar backscatter from the reflecting surface. Radiometric correction is also necessary to compare SAR images acquired with different sensors, or acquired from the same sensor but at different times, in different modes or processed by different sensors.

Radiometric calibration function in SNAP performs three different calibrations for the Sentinel-1 datasets, including Sigma naught, Beta naught and Gamma naught and generates the calibrated dataset. We will calibrate the image to **Sigma naught** which calibrates the backscatter returned to the antenna from a floor area unit; it is linked to the range on the ground. Scientists tend to use σ0-band because is the one that provides the best separation between terrestrial soil areas and those with water (Bioresita 2018) So σ0-bands were generated in both polarization VV and VH.

In addition, we performed a speckle filter, speckle is represented in the images as mottled or granular noise. This causes degradation of the image quality and hinders its interpretation (Kudahetty 2012). Mainly, noise is due to random oscillations of the signal returned to the sensor due to the interaction of the emitted wave with the rough terrain surfaces. There is no fixed procedure to suppress the speckle of RADAR images in flood extent mapping. The characteristics and configuration of each RADAR system, together with the conditions of the acquisition and characteristics of the land, establish the type and sequence of filters to be applied.

The SNAP program has numerous filters, all of a statistical nature, to reduce this problem. A visual comparison was made with the filters Gamma Map, Lee, Refined Lee, and Lee Sigma, with different window sizes (Figure 21) in a small area, within the study area, which brings together flood areas, urban areas, and crop areas where the texture variability produced by the application of the different filters can be appreciated. The speckle filtering application does not modify the spatial detail and it is mostly used to achieve smoothing of the limits of the different forms represented, avoiding the loss of image details. The Gamma Map filter is based on the Bayes statistical analysis of the image and it works best for extensive areas, such as oceans, forests, or extensive fields (Senthilnath 2013). The Lee filter uses statistical parameters, such as the mean and standard deviation, with a predetermined window size assessing different factors for smoothing. In homogeneous regions, such as flooded areas, the final pixel value is the linear average of neighboring pixels (Pearlman 1999) .The Refined Lee filter provides a smoother texture in the image, minimizing radiometric and textural loss in the images (Ezzine, A 2018).The Lee Sigma filter uses a statistical distribution of the digital levels of a given area window chosen by the operator and estimates what pixel should be considered (García, R.2003) .Taking into account mainly the topography, the geometry of the urban areas, the polarization, and the need to delimit those areas with smaller intensity values, the Lee filter with a window size 7 × 7 (m) was chosen as being most appropriate for the study.

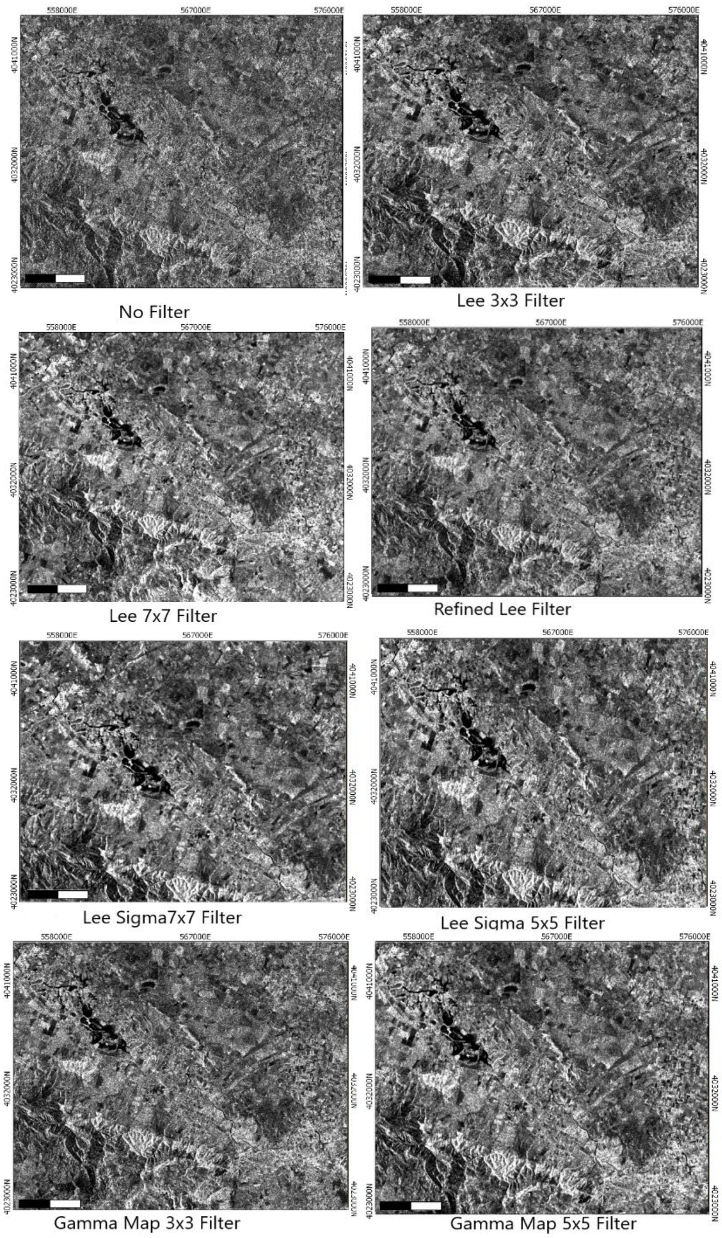

Figure 21: Detailed images of the study (Majaz Al Bab), 04 Mars 2015, after the flood event, with VH polarization in which the comparison is shown between the unfiltered image and the result of the application of different filters of different window sizes.

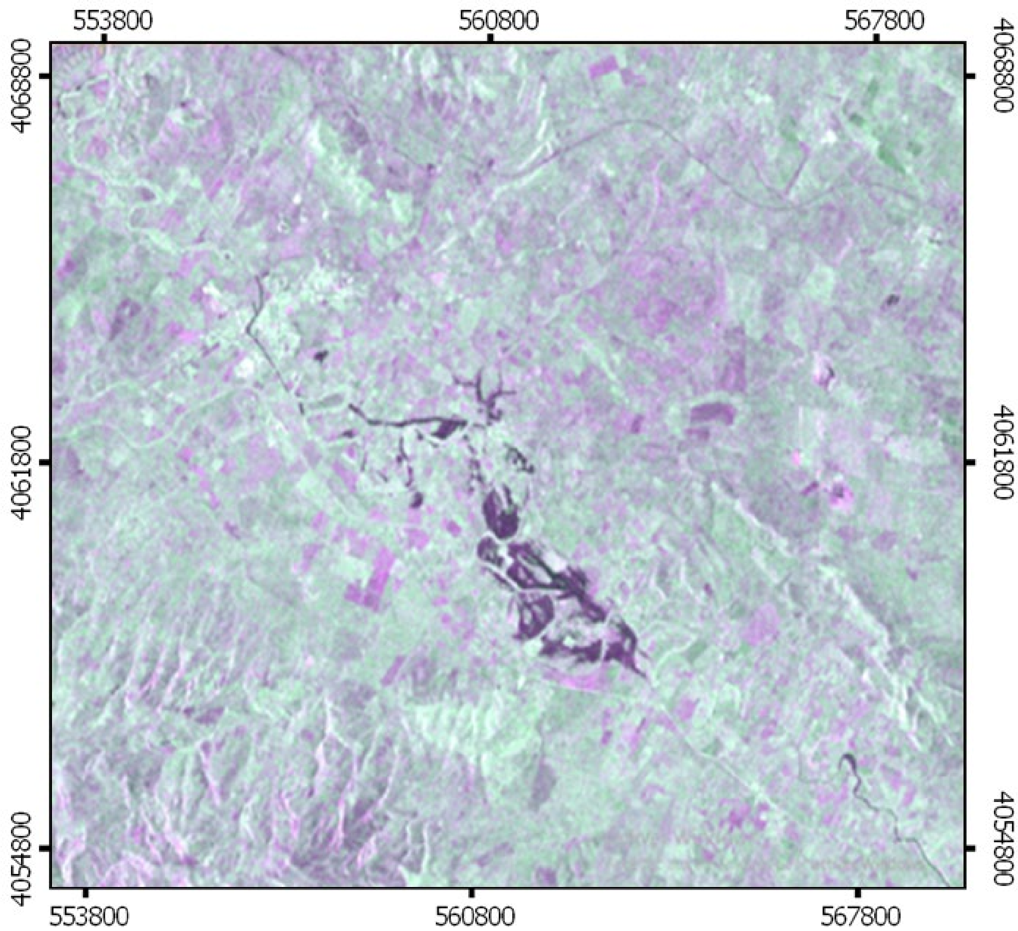

Figure 22: Dual pole Ratio Sigma0 VV+VH RGB composite

Figure 22 shows RGB color-composite of Sigma0_VV, Sigma0_VH and Sigma0_VV polarization after the calibration for flooded area , we can see magenta dominates which corresponds to VV backscatter and we see other area where green dominates corresponds to VH backscatter , the green area likely to be areas of vegetation causing volume scattering such as forest or dense vegetation over the water bodies on the other hand we have very dark response because we have specular reflection in both VV and VH polarization.

The last common step in the pre-treatment of images is to perform a correction of the terrain and orthorectification. This mainly eliminates distortions due to changes in the topography and the angle of incidence with the ground with respect to the nadir. The geometric calibration used in this study was range doppler terrain correction and the digital elevation model (DEM)–SRTM-3Sec.

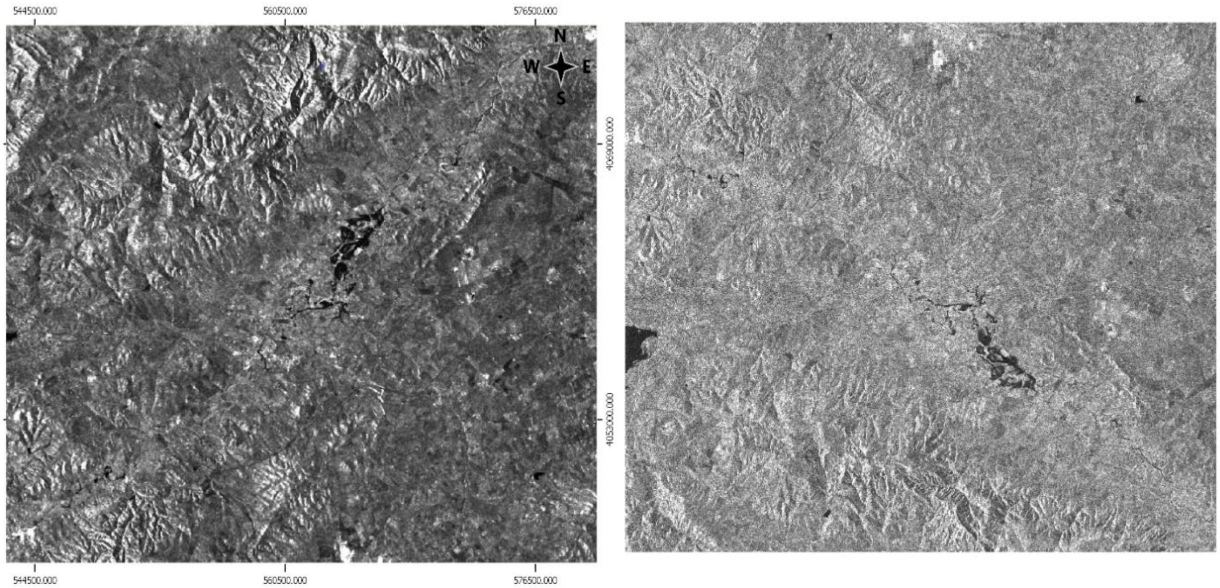

Figure 23: Results showing the effect of Range Doppler terrain correction

III-4-Processing and results

Many authors have used various algorithms for the detection of non-permanent water surfaces. Among these approaches, we can highlight the supervised classification, automatic non-supervised classification (Borah, S.B 2018, Martinis 2011), RGB combination (Tavus, B 2018; Martinis 2011), or the detection or calibration threshold technique (Psomiadis 2013 ; Martinis 2009 ; Dumitrascu, 2017; Pham-Duc 2017 ; Zhang2018) . In this study, the methodologies used were RGB composition and the calibrated thresholds technique. Before the application of any techniques and to perform a multitemporal analysis, it is necessary to unify in a single file the different bands of σ0 of the images before and after the event using a stack.

III-4-1-RGB composition

The RGB composition is an appropriate method to visualize multi-temporal modifications and facilitates the detection of changes on the terrain surface through a temporal color image (Amitrano, D 2019). It is a method based on the differences between the pre- and post-event images, and in which a combination of bands is set for these differences to become visually remarkable. These differences are defined by the change in the intensity value for the same pixel on different dates. The result is a multitemporal image to which a band is assigned to each of the primary colors to form an image of RGB composition (Tavus, 2018).

The combination of bands used for the application of the method was the image before the event for the R-band and the image after the event for the G- and B-band. Different results were obtained for the two polarizations, VV and VH, as can be seen in (Figure 24) There are many possible combinations, but the chosen combination favors the visualization of the flooded areas.

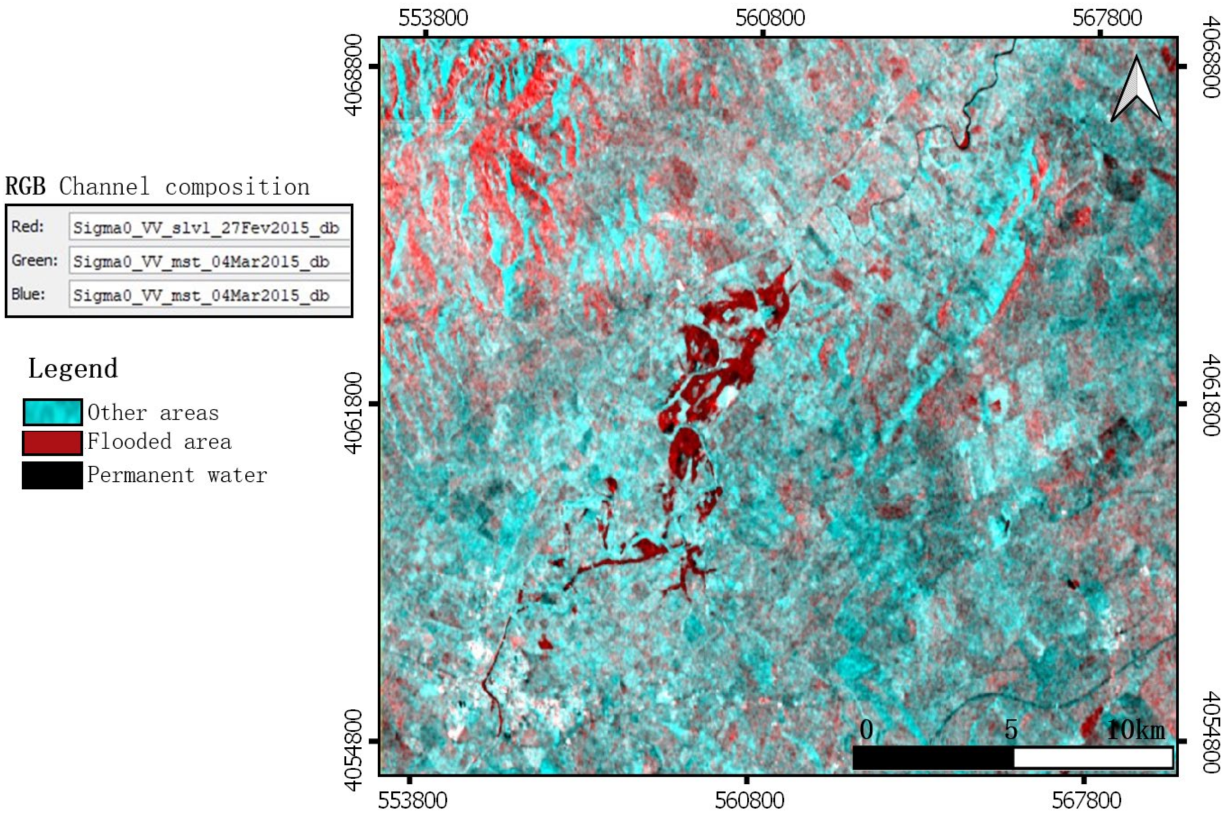

Figure 24: General flood map of Zone 1 using RGB composition created from the RADAR images of 04 Mars 2015 and 27 February 2015 in VV with a Lee 7 × 7 window size filter.

Water surfaces that are stable on both dates, such as the Majerda river or reservoirs, are represented in black. The populations, urban and industrial areas with very high intensity values, are observed in white. Those areas, with intermediate intensity values and in which there have been hardly any variations, are consolidated in blue tones. The light pink tones are characteristic of areas with high humidity while the red ones represent the flood surfaces in which the water has completely flooded.

A correct choice of polarization optimizes the discrimination of flooded areas (Klemas, V 2015). The results obtained in our polarization configurations and the contributions of (Rieke 2015, Schumann, G 2007) in the comparative studies of polarizations to monitor flood areas reaffirm that the VH polarization is more suitable for delimiting flooded areas. It generates well-defined and correctly defined surfaces, results that VV polarization cannot offer. VV polarization is clearly influenced by the roughness and heterogeneity of the terrain .We can see this fact in the floodplains, where the roughness of the soil of the crops fields becomes more evident in the VV polarization.

III-4-2- Calibration Threshold Technique Results

The calibration threshold methodology separated the dry zones from areas with the presence of a water sheet through the interpretation of histograms. In Figure 25, the relationship between polarizations and characteristic histograms for each of them is observed for the zone 1 The histogram of the VV polarization shows a very large curve representative of the intensity values ranging between −1.0 and −22 dB, a very wide spectrum characteristic of areas that range between very rough and moderately rough. While there is no clear projection of low backscatter values, the histogram of the VH polarization itself shows two clear populations where the specific intensity values of the image oscillate. This was chosen for further analysis. On the one hand, there is the curve that provides a greater number of pixels and that represents the areas without water, and on the other hand, a curve of smaller size and with smaller intensity values that represents the areas with water is shown. It is between both areas that the calibration limit can be set. Analyzing the histograms in greater depth, we observe that the cross polarization provides a wider range of backscatter values on surfaces with vegetation than the simple polarization, VV, which results in the latter omitting flooded areas.

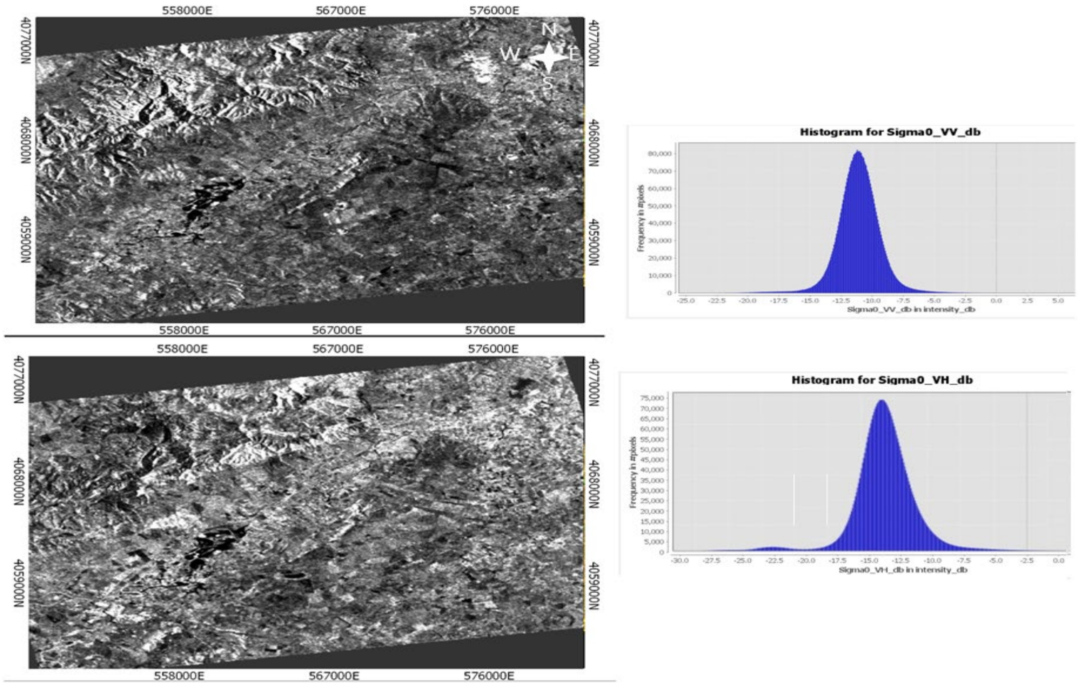

Figure 25: Representation of the characteristic histograms of zone Mdjaze el beb for VV polarization (up) and for the VH (down) in the radar image of 04 Mars 2015 filtered with the Lee 7 × 7 window size filter.

To further specify the boundary point between the areas with water and without water, a water mask was generated on the VH polarization image. This layer was created by randomly capturing some flooded areas and subsequently generating a histogram. In this way, intensity values were obtained in which only areas with water or flooded areas are shown, independent of the frequency or number of pixels taken. It should be noted that this layer serves only to confirm and verify the suitability of the threshold taken with the total histogram of the zone. The comparison of the histogram of the water mask obtained and the polarization VH histogram is shown in (Figure26). A significant spatial linear correlation between both histograms is shown, something that does not happen with VV polarization. After studying the results, we conclude that the most representative values of the presence of the water range mostly between −20.5 and −29.5 dB, so −20.5 dB was considered. The threshold taken was therefore set to −20.5dB.

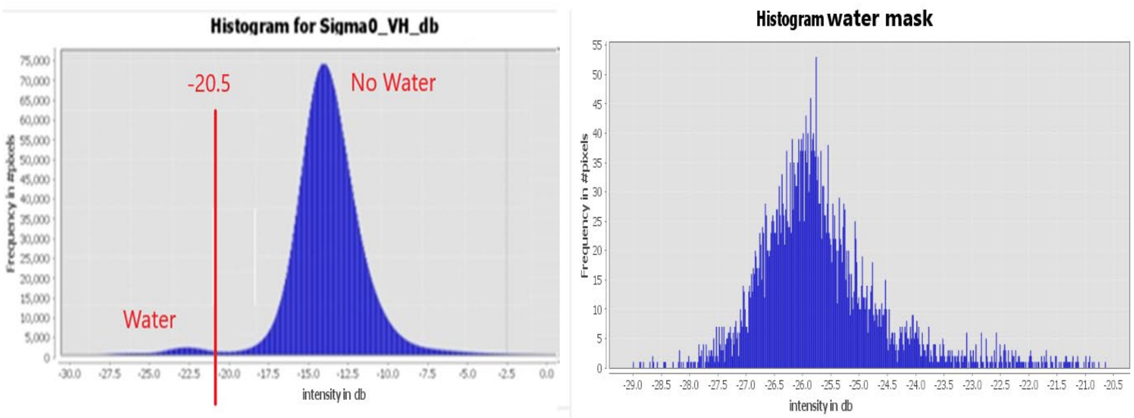

Figure 26:(a) Characteristic histogram of study area with VH polarization. (b) Representative histogram only for the water zones.

With the **Raster-Band Math** tool of the SNAP program, a binary layer was generated in which, on the one hand, below −20.5dB values are represented, representative of the water and flooded areas, and on the other, those above it that would show the dry zones. (Figure 27) shows the areas with the presence of water that are observed in part of the study area for a radar image in which no filter was used and another for which the process of Lee 7×7 filtering was used. The unfiltered image has a large number of random pixels distributed by the image that give "false positives". All of them are points outside the flood area and the course of the river that have backscatter intensity values below −20.5dB. On the other hand, the use of a filter minimizes this effect, favoring less overrepresentation errors.

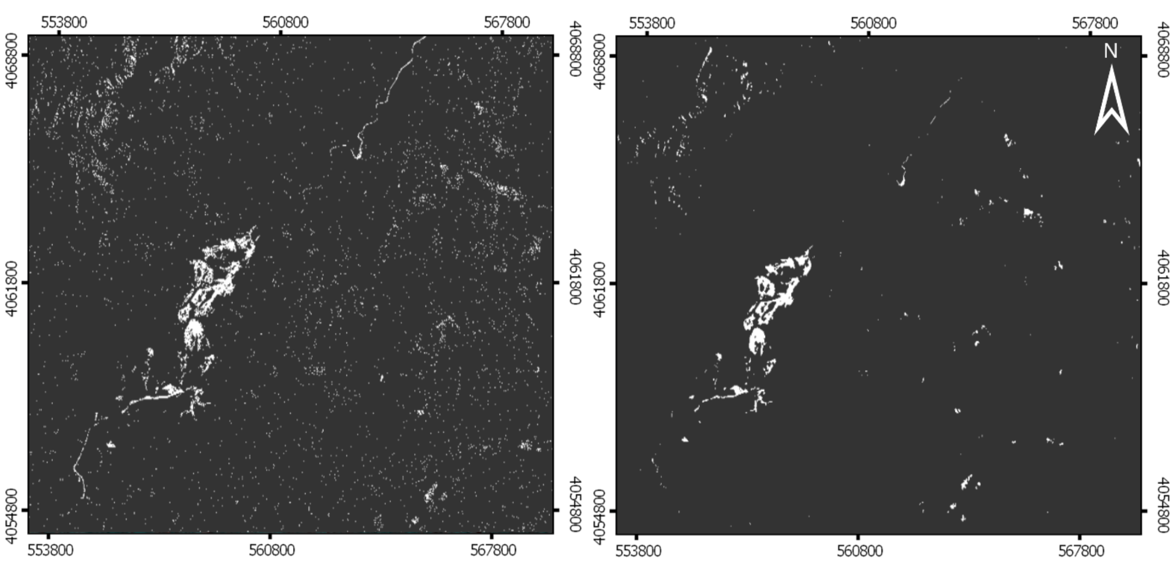

Figure 27: Representation of the areas that were captured as water in the unfiltered radar image and another with the Lee 7 × 7 filter.

The indicative layers of water presence, for the same specific area, were also generated for the other filters and different window sizes that were considered in the study (Refined Lee, Lee Sigma, and Gamma Map) and through which numerical data of the surfaces that show the presence of a water sheet were extracted (Table below). It is quite significant that the use of one filter or another provides notable variations in the areas represented as water. Obviously, the unfiltered image is the one that generates more surface compared to any of the others that were filtered.

Filter	Total Area in (Ha)
No filter	856.2
Lee 3 x 3	743.03
Lee 7 x 7	450.53
Refined Lee Filter	870.64
Lee sigma 7 x 7 Filter	681
Lee sigma 5 x 5 Filter	576
Gamma Map 3 x 3	789.32
Gamma Map 5 x 5	540.52

Table 4: Water covered area

It is quite significant that the use of one filter or another provides notable variations in the areas represented as water. Obviously, the unfiltered image is the one that generates more surface compared to any of the others that were filtered. In comparison, the unfiltered image could provide even more than twice the area flooded than, for example, the image filtered with Lee 7 × 7. Therefore, the application of filtering is necessary not only for speckle reduction but to avoid errors when making quantitative calculations with images. The choice of the Lee 7 × 7 filter, which generates the least area, minimizes the presence of individual pixels outside the flood area and thus prevents overrepresentation in these areas.

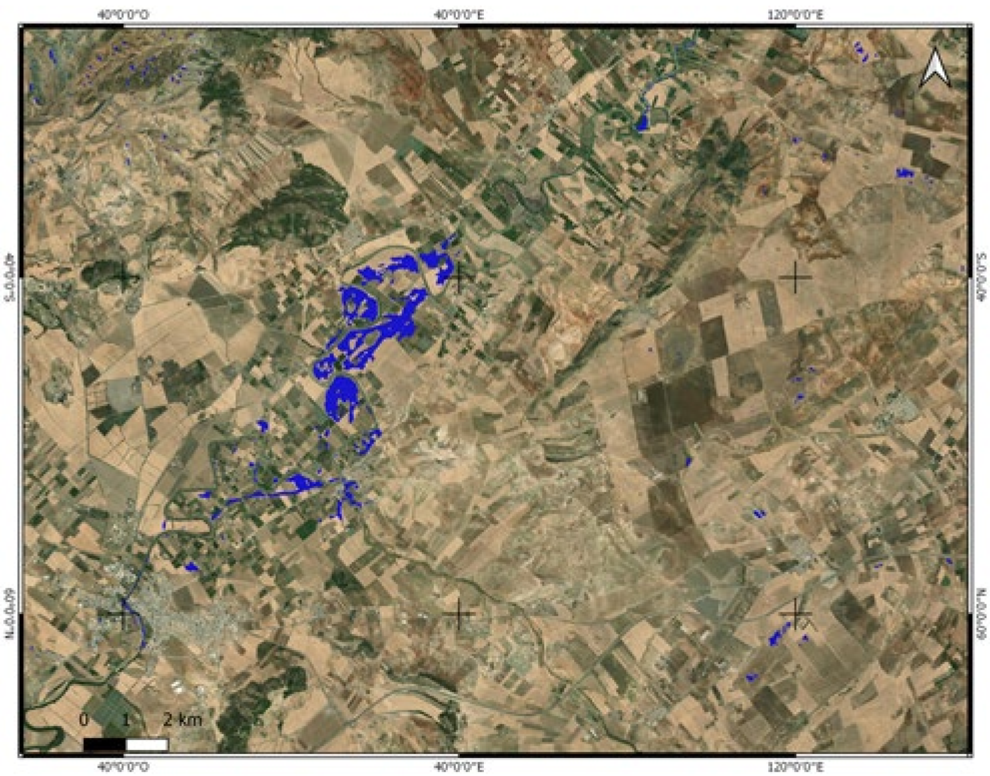

Figure 28:General flood map of the entire study area by calibration thresholds created from the RADAR image of 3 Mars 2015 and a scrubber with the permanently flooded water layer (Source: ESRI base map),

III-5-Conclusion

In SAR images, continental waters have strong contrast in the backscatter values due to their low or null roughness in the absence of waves, behaving like a specular surface that reflects the radar return signal in a direction opposed to the sensor position. However, they need a correction and filtering process (orbital parameters, radiometric, noise reduction speckle, and geometric geometric). Evaluating the different Sentinel-1 parameters, our analysis showed that the best results were obtained using VH polarization configuration. Concerning the need to apply numerous filters to reduce speckle, which also reduces the resolution quality of the images and has an effect on the final flood mapping, Lee filtering with a 7 × 7 window was the most appropriate option and it was proven that it favors the elimination of "false positives".

Two methods were applied to detect and delimitate non-permanent water surfaces from Sentinel-1 SAR images. Method 1 RGB composition is based on differences between the pre- and post-event images, in which a combination of bands is set for identifying these differences as visually remarkable. The calibration threshold technique or binarization is based on a simple and quick process that differentiates flooded areas from those that are not from the characteristic polarization histogram using backscatter values in permanent waters and in flooded areas. The advantages of using the RGB composition methodology is that it guarantees clear differentiation between the areas of permanent flooding and the temporarily flooded ones, while achieving distinction through the technique of calibration thresholds requires other processes. Another advantage of the RGB methodology is that it detects the presence of massive riparian vegetation and vertical growth that can hide the presence of water, and it is essential to get a complete map of the flooded areas. In the calibration threshold technique, the most representative values of the presence of water were mainly between −29.5 dB, so −20.5 dB; therefore, a central value of −20.5 dB was considered.

CHAPTER 4: Urban Footprint Mapping

IV-1- Introduction

Considering the extreme impact of urban areas on the surrounding environments in terms of mass, energy, and resource fluxes (Lambin 2001), combined with the overall growth of the world's population and the its impact on floods behavior, the constant monitoring of urban environments is a key for both sustainable urban development and disaster management.

In this regard, the role of Earth Observation and space technology is recognized by the United Nations as a significant support for the achievement of the SDGs . As such, remotely sensed data constitute a significant resource for mapping anthropized areas (Donnay, J 2001). In fact, the built environment can be identified and studied with different sensors, by analyzing its reflectance, thermal and microwave properties, and night light (Small, C 2018)

The most common approaches for urban monitoring applications involve the use of imagery data originated from multispectral sensors (from the visible to the near and short-wave infrared wavelengths). Such approaches include, for example, pixel- and object-based classifications (Xu, H 2001) and the use of spectral indices (Badlani, B 2014 ; Zha, Y 2003). On the other hand, some authors have used the imagery data of SAR (synthetic-aperture radar) satellite systems, by considering the microwave properties of urban environments (Gamba, P 2011; Valdiviezo-N 2018), whereas some others have explored the thermal infrared properties of urban areas (and land surface temperature) (Weng, Q 2009, Zhan, W 2013), and nighttime light satellite images (Yu, B.; Shu, S 2014).

Nonetheless, the accurate mapping of urban areas still remains challenging, due to limitations in the spatial, spectral, and temporal resolution of remote sensing systems that often fail to obtain a univocal response (Small, C 2018).An additional challenge is represented by the wide heterogeneity of anthropic structures in terms of size, shape, material composition, and fragmentation which might result in strong spectral similarities with other land cover surfaces, such as bare soil and non-vegetated areas (Wu, C 2004 ; Zhou, J 2013).

The general contest of this section focuses on the analysis of a semi-automatic process for the extraction of urban features over non-urban areas, to study impact of flooding on certain areas taking into account the use of machine-learning algorithms.

In this work, we refer to "urban footprint" as the percentage of pixels classified as "urban" over the total number of pixels on a specified study area. In order to perform accuracy assessments, the results will be compared with the land cover map of majadra lower valley produced in this present work.

IV-2-Sentinel-1 SAR Imagery

.In particular, in this work we made use of the Interferometric Wide swath (IW) mode products at Level-1 Single Look Complex (SLC). The IW swath mode acquires data with a 250 km swath at 5 × 20 m spatial resolution (for SLC products). The wide-swath coverage is achieved by employing the Terrain Observation by Progressive Scans (TOPS) acquisition mode, which acquires images by recording different subsets of echoes of the SAR aperture, which are called “bursts” (De Zan, F 2007). Sentinel-1 IW SLC products contain a total of three (single polarization) or six (dual polarization) sub-swath images. For example, the images we examined consist of three sub-swaths (named IW1, IW2, and IW3), each including both polarization (VV and VH). Furthermore, each sub-swath image consists of a series of bursts.

SLC products consist of focused SAR data, geo-referenced using orbit and attitude data from the satellite, and provided in slant-range geometry. Slant range is the natural radar range observation coordinate, defined as the line-of-sight from the radar to each reflecting object. The products are in zero-Doppler orientation where each row of pixels represents points along a line perpendicular to the sub-satellite track. SLC products include a single look in each dimension using the full available signal bandwidth and complex samples (real and imaginary) preserving the phase information.

Within this work, we perform multi-temporal analysis, collecting a series of images from 2020 that are displayed in (Table 5). In particular, in order to achieve interferometry with exact repeated coverage, we took into account only images derived from the same satellite sensor (Sentinel-1A), therefore within a bi-weekly revisit time.

Table 5: All the Sentinel-1 images used in this work. Downloaded from the Sentinel Open Access Hub

Image	**Mission Identifier**	Type	Date of capture	**Hour of capture**
Image 1	Sentinel 1A	SLC	2020-05-01	05:21
Image 2	Sentinel 1A	SLC	2020-05-13	05:21
Image 3	Sentinel 1A	SLC	2020-05-25	05:22
Image 4	Sentinel 1A	SLC	2020-06-06	05:22
Image 5	Sentinel 1A	SLC	2020-06-18	05:22
Image 6	Sentinel 1A	SLC	202-06-30	05:22

IV-2-Preprocessing Interferometric Coherence

The use and interpretation of SAR imagery require a series of complex pre-processing procedures, which we ran on ESA's SNAP software. Such procedures refer to standard preprocessing commonly applied to Sentinel-1 products to derive interferometric coherence. In particular, we followed the approach described by RUS guidelines available online , which we summarize in (Figure29).

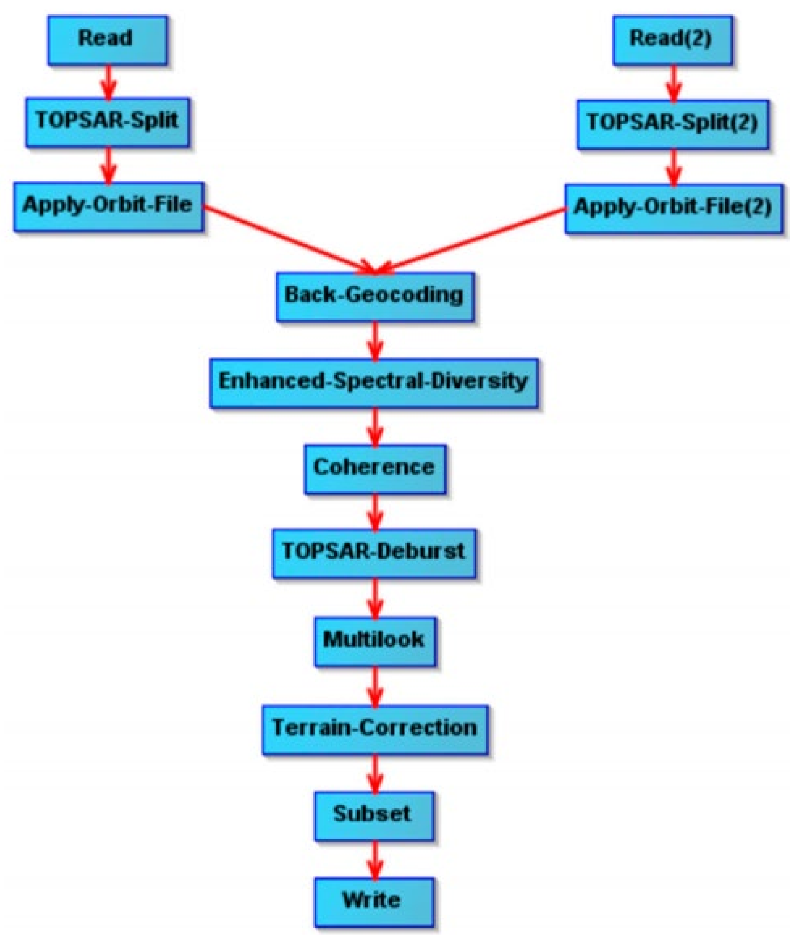

Figure 29:Preprocessing workflow used to produce Sentinel-1 interferometric coherence images in SNAP.

The "Read" and "Read (2)" commands represent the two Sentinel-1 input files, while "Write" represents the output file.

On all SAR input images we took into account both polarizations (VH and VV), which make the output coherence image composed by two different raster files, related to the different polarizations. As for the processing workflow, we identified two of the three sub-swaths from the original product, subsequently selecting only the bursts that cover our study areas, then we updated the orbit state vectors provided in the metadata of a SAR product which are generally not accurate and can be refined with the precise orbit files that provides accurate satellite position and velocity information.

In order to study the coherence between the two image we coregistrated the image using the operator **S-1 Back Geocoding** operator that uses the geolocation of the products, the orbit information and a digital elevation model to create a stack of the tow products where the pixel alignment is good and accurate enough so we can study the difference in the scatter response and to achieve more accuracy we have applied the **Enhanced Spectral Diversity** operator that performs range and azimuth corrections for every burst after estimating their offset.

When we work with complex data where we have phase information, the phase noise can be estimated from the interferogram by means of the local coherence. The coherence values range from 0 where the interferometric phase is just noise, to 1 where complete absence of the noise, where no phase noise, coherence is the fixe relationship between waves in a beam of the electromagnetic radiation, and tow waves of electromagnetic radiation are coherent when they are in phase that means they oscillate in the same way. According to this principle we computed the coherence estimation setting the range window size to the default value of 20 pixels. Furthermore, we have applied **TOPSAR-Deburst** function in order to remove gaps in the image followed by **Multilooking** function that averages different pixels that are together into a single one and reduce the speckle effect. Lastly, for the terrain correction we used the Range-Doppler terrain correction, which involves the use of a digital elevation mode (DTM) automatically downloaded from the Sentinel-1 repository, choosing WGS84-UTM 32N as projected coordinate system and selecting an average output resolution of ≈15 m. An example of output interferometric coherence image is displayed in (Figure 30).

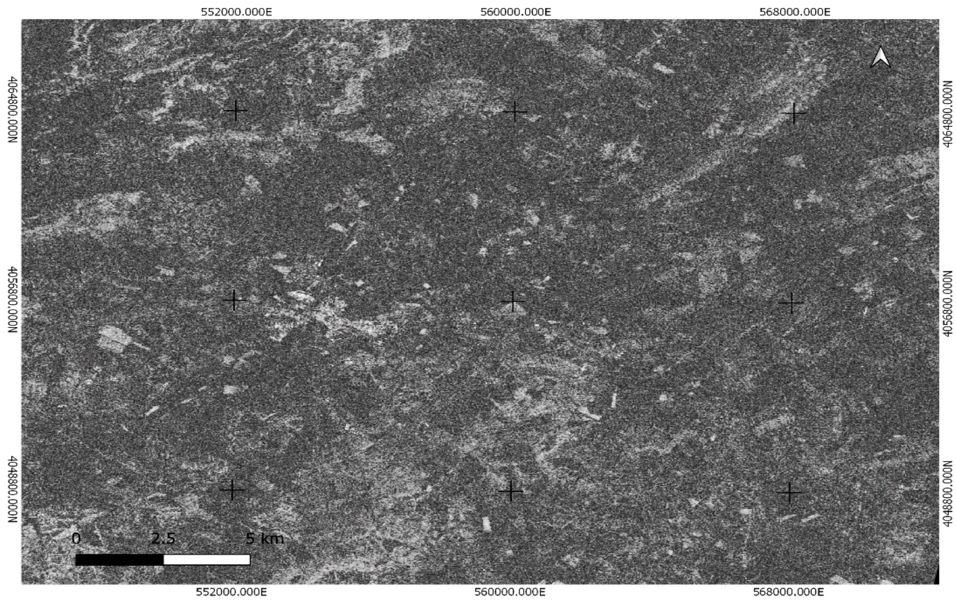

Figure 30:Coherence image of the area. We produced this image from two Sentinel-1A images acquired on 01 May and 13 May 2020(VH polarization only).

In this sample area, we selected sub-swath number 3 (IW3) and bursts 2–7. Urban areas appear distinctively brighter than all other land cover types, with coherence value generally greater than 0.7.

IV-3-Multitemporal Analysis of Interferometric Coherence

Following the tutorial available within the RUS web material, we repeated the processing workflow of interferometric coherence, described within the previous section, to a series of Sentinel-1 images taken from 1 May to 28 June (Table 5), always associated with low valley of Majerda and its surroundings. Subsequently, we produced a series of interferometric coherence images, every time processing two IW SLC images (taking into consideration both polarizations—VH and VV). Then, we stacked all coherence images into one raster file using the Stack tool in SNAP. A sample result's displayed in Figure 32. By doing so, urban areas are likely to be identified more rigorously, progressively reducing the error and noise within the images and increasing the accuracy. Lastly, we applied the identical classification algorithms described within the previous section.

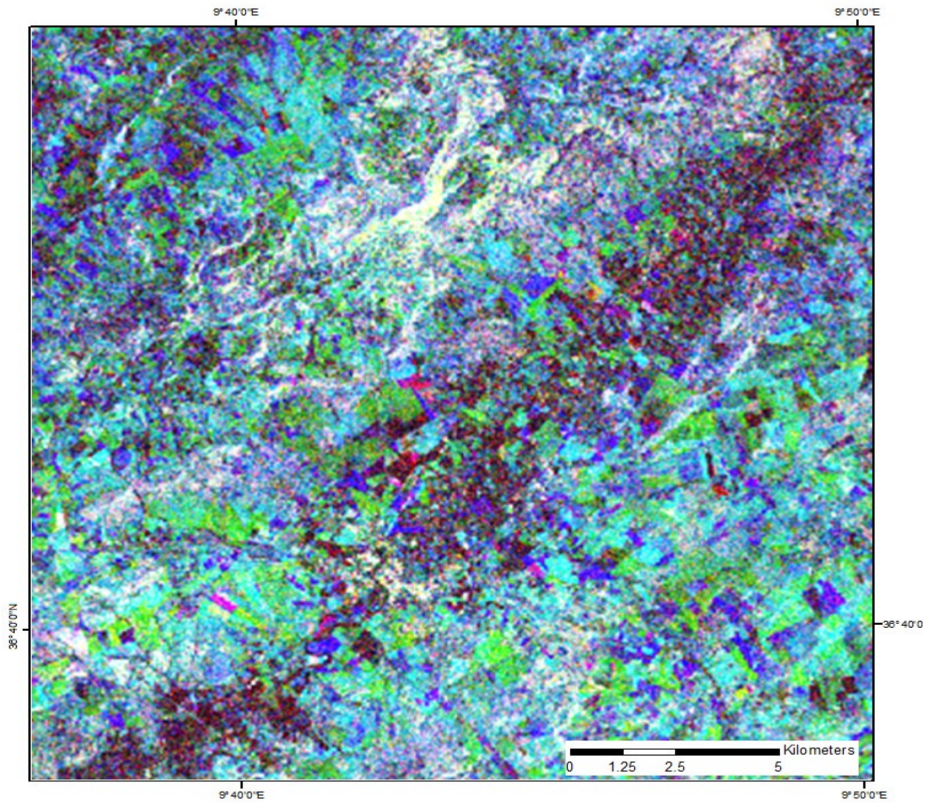

Figure 31:RGB Raster image related to a stack of interferometric coherence images, produced from Sentinel-1A images from 1 May to 28 June.

This image displays in a band composition three coherence images from [01 may, 13 June], [25 May ,6 June] and [18 June, 30 June] respectively, in the red, green, and blue channel. Urban areas are recognizable by their distinctively brighter color compared to all other land cover types.

IV-4-Classification of the Interferometric Coherence

The output coherence image consists of two different bands, reporting interferometric coherence values (from 0 to 1) for 2 polarizations (VH and VV). Within this kind of raster, it's possible to extract urban footprint by applying supervised classification algorithm. In the supervised classification, for training inputs we digitized the ROIs (regions of interest) over a Sentinel-2 image covering the identical place in IW2 and IW3 bursts. Since we were interested in distinguishing only two different classes, i.e., urban and non-urban areas, when digitizing the ROIs, we aggregated all non-urban land cover types into the identical class (such as sparse vegetation, forest, bare soil, and cultivated soil). We then used ROIs as input training sites for the classification algorithms applied to the SAR images. These Sentinel-2 images were processed in SNAP by extracting the bands on the visible wavelength range (bands 2, 3, and 4) and exporting the chosen spatial subset into a GeoTIFF.

Foe the supervised classification algorithm, we made use of the Maximum likelihood (ML) available in SNAP. The ML classifier in SNAP doesn't require setting of a threshold value for classifying pixels, thus no pixel will remain unclassified. Subsequently, we considered the utilization of multiple coherence images, taken within an extended period of the. In fact, the distinct backscattered intensity and interferometric coherence values of urban environments allow their sharp distinction from all other land cover types, no matter the extent of enthronization, atmospheric condition, or environmental parameters.

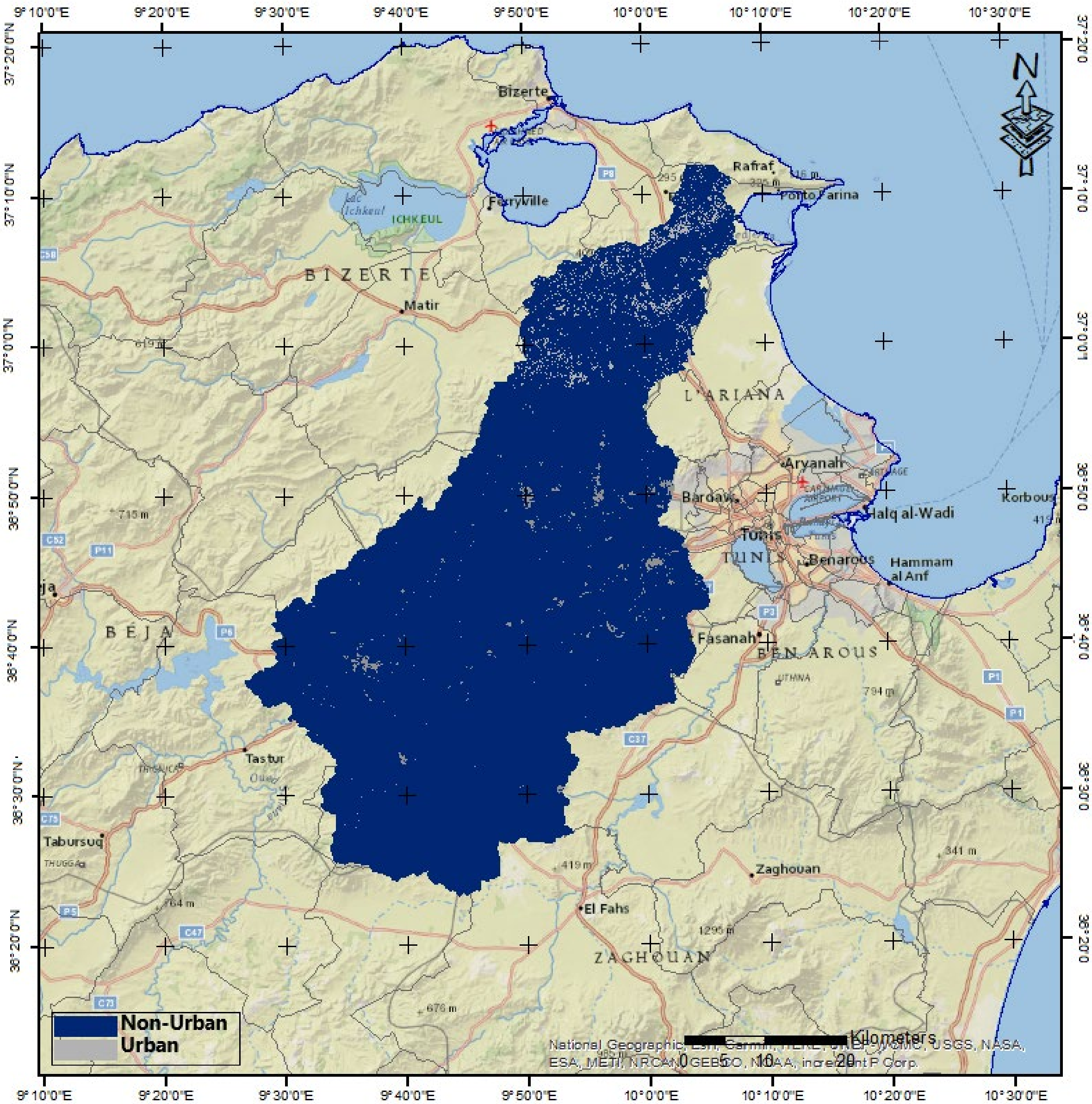

Figure 32:Map of urban area in the lower valley of Majerda

This map is the product of the supervised classification of interferometric coherence layer created from series of sentinel 1 SLC products .As shows the map the study area characterized by a low urban density despite this the radar has great potential to distinguish between urban and non-urban areas , but as we can see in norther side of image we have some false classification of hills without vegetation cover and looks as bright as the urban areas in the coherence layer because it does not change over time and this is the factor we rely on in our study.

IV-5- Conclusion

When dealing with urban mapping, different data sources can be exploited in several different ways. In this work, we investigated the use of Sentinel-1 SAR imagery and in particular IW Level-1 SLC products. The high backscattered intensity of urban areas, acting as corner reflectors, proved to be highly effective when mapping urban environments. In particular, interferometric coherence highlights all surfaces with constantly high backscattered intensity, fixed shape, and constant physical parameters through time. Such surfaces are indeed urban areas.

That being said, some limitations concerning Sentinel data still remain, mostly related to the limited geometric resolution of the Sentinel satellites with respect to other commercial satellites. Moreover, the first Copernicus Sentinel mission (Sentinel-1A) was launched in 2014, limiting so far, the possibility of performing multitemporal analysis in the previous decades (using Sentinel data only). Nonetheless, the ever-increasing availability of high-resolution optical and radar satellite sensor, along with the growing awareness of open data policies, will definitely encourage the use of satellite images to tackle environmental changes and will promote new applications and technologies, in all fields, including urban applications.

CHAPTER 5: Land Use Classification

V-1-Introduction

Land Use Classification (LUC) is a classification providing information on land cover, and the types of human activity involved in land use. It may also facilitate the assessment of flood impacts on, and potential or alternative uses of land for this purpose we will study the land use in the study area use sentinel 2 optical image .

To do that we downloaded tow sentinel 2 Level 1C products, described in the next section, then we applied atmospheric correction to convert radiance to reflectance image furthermore w processed unsupervised and supervised Land Use Classification Finely we overlapped the land use map with the results of CHAPTER 3 to evaluate the damage caused by the floods ,the processing chain in described in **figure**

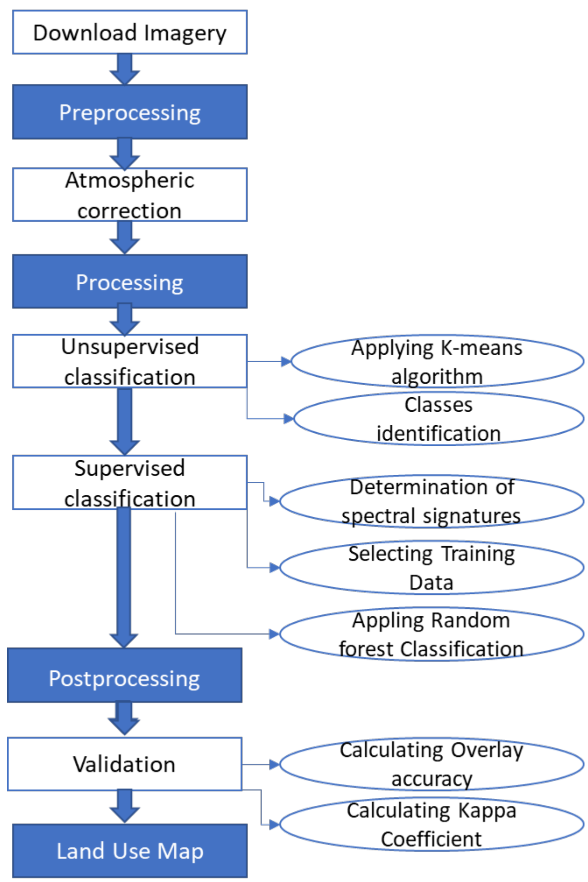

Figure 33:Chart describing the LUC processing chain

V-2- Sentinel-2 Imagery

Sentinel-2 consists of two identical Sentinel-2 satellites (Sentinel-2A was launched on June 22, 2015 and Sentinel-2B on March 06, 2017) operate together. The satellites are phased 180 degrees from each other on the same orbit to achieve frequent revisits and high mission availability. This allows for what would be a 10-day revisit cycle to be completed in 5 days. The 290km swath is created by the VNIR and SWIR, which are each made of 12 detectors that are lined in two offset rows.

Sentinel 2 satellite provides multi-spectral data with 13 bands (Figure35) in the visible, near infrared, and short wave infrared part of the spectrum , with spatial resolution of 10 m, 20 m and 60 m. The radiometric resolution of the imagery makes it great tool for land use mapping where we can take advantage of different band combination to visualize the image also efficient way to classify the image based on the spectral signature of various land use types

Sentinel-2 bands	Sentinel-2A		Sentinel-2B		
	Central wavelength (nm)	Bandwidth (nm)	Central wavelength (nm)	Bandwidth (nm)	Spatial resolution (m)
Band 1 – Coastal aerosol	442.7	21	442.2	21	60
Band 2 – Blue	492.4	66	492.1	66	10
Band 3 – Green	559.8	36	559.0	36	10
Band 4 – Red	664.6	31	664.9	31	10
Band 5 – Vegetation red edge	704.1	15	703.8	16	20
Band 6 – Vegetation red edge	740.5	15	739.1	15	20
Band 7 – Vegetation red edge	782.8	20	779.7	20	20
Band 8 – NIR	832.8	106	832.9	106	10
Band 8A – Narrow NIR	864.7	21	864.0	22	20
Band 9 – Water vapour	945.1	20	943.2	21	60
Band 10 – SWIR – Cirrus	1373.5	31	1376.9	30	60
Band 11 – SWIR	1613.7	91	1610.4	94	20
Band 12 – SWIR	2202.4	175	2185.7	185	20

Figure 34:Spectral bands for the Sentinel-2 sensors

V-3-Preprocessing

In this study we used Level-1C products. These products are radiometrically and geometrically corrected (including orthorectification) with an error around 5-7m also includes an atmospheric correction applied to Top-Of-Atmosphere (TOA) we have upgraded them using SEN2COR280 plugin in SNAP which take as input level-1C products in safe format and applies Bottom-Of-Atmosphere (BOA) correction .The result is Level-2A image of apparent surface reflectance, which can be used to extract accurate spectral information from the characteristics of the Earth's surface.

Image	Mission Identifier	Date of Capture	Hour of Capture
Image 1	Sentinel 2A	28/02/2020	10:10:21
Image 2	Sentinel 2A	28/02/2020	10 :12 :21

V-4-Processing

Classifying an image is about grouping all the pixels in the image into a limited number of classes corresponding to the large structural elements of the image, so it is to map the image based on the radiometric values of the pixels. The most common classification methods can be separated into two broad categories, **unsupervised classification** and **supervised classification**.

V-4-1- Unsupervised classification

In this step we have process unsupervised classification to get an initial analysis about the imagery and make prevision of the classes that may have interference due to similarity in spectral signature or close spectral distance. In unsupervised classification, image processing software classifies an image based on natural groupings of the spectral properties of the pixels, without the user specifying how to classify any portion of the image.

We have used K-means clustering technique which one of the popular methods in unsupervised classification no prior knowledge is required for classifying the features of the image we only choose the K values which we set to 13 and that represents the number of classes that we expect to the image to be segmented in and the number of iterations we set at 30 to get more precise classification and we used all the spectral bands.

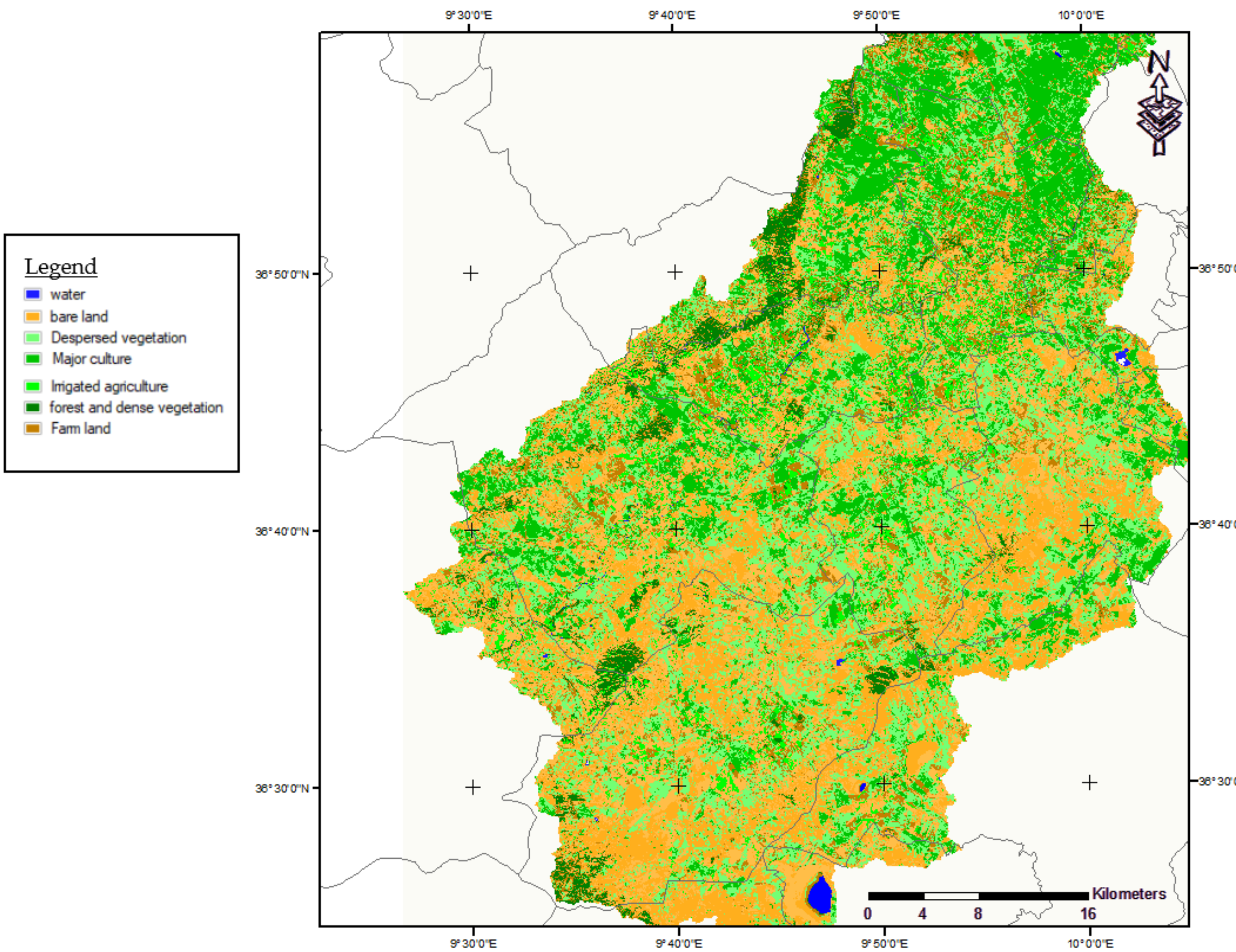

Figure 35: Land Use Classification Map of the study area using K-means algorithm

As the map shows, although we have defined the k value to 13, we are not able to conclude only 8 classes we tried to set the legend so it describe the majority of pixels that it represents but without the required accuracy, as many of the land use types interfere with each other due to similarity in reflectance values, we have noticed the urban areas are interfering with bare land also the vegetation classes are overlapping with each other , also we have noticed that there are some land types maybe represented in more than one class so that we needed to merge them.

V-4-2- Supervised classification

Supervised classification makes use of training samples. Training samples are areas on the ground for which there is Ground truth, that is, what is there is known. The spectral signatures of the training areas are used to search for similar signatures in the remaining pixels of the image, and we will classify accordingly. This use of training samples for classification is called supervised classification. On the opposite hand, for the

RF classifier we specified the utmost number of decision trees, which we set to 500 as best value so as to get a good noise removal and an identical response .

V-4-2-1- Determination of the legend

Before proceeding with the supervised classification, we need to determine the legend of the map in order to be able to take the regions of interest afterwards. Class selection is a very important step, it must be studied carefully in the study area, and this according to several methods, we have used Google Earth pro software , the unsupervised classification which gave us an initial guess for the classes that may appear and prevision of the classes that may have interference due to similarity in spectral signature or close spectral distance. Also, we made use of band combinations to better understand the features in imagery. The way we do this is by rearranging the available channels in creative ways, we can extract specific information from an image. In this regard we used different band combination among them:

- false color Infrared (B8, B4, B3)

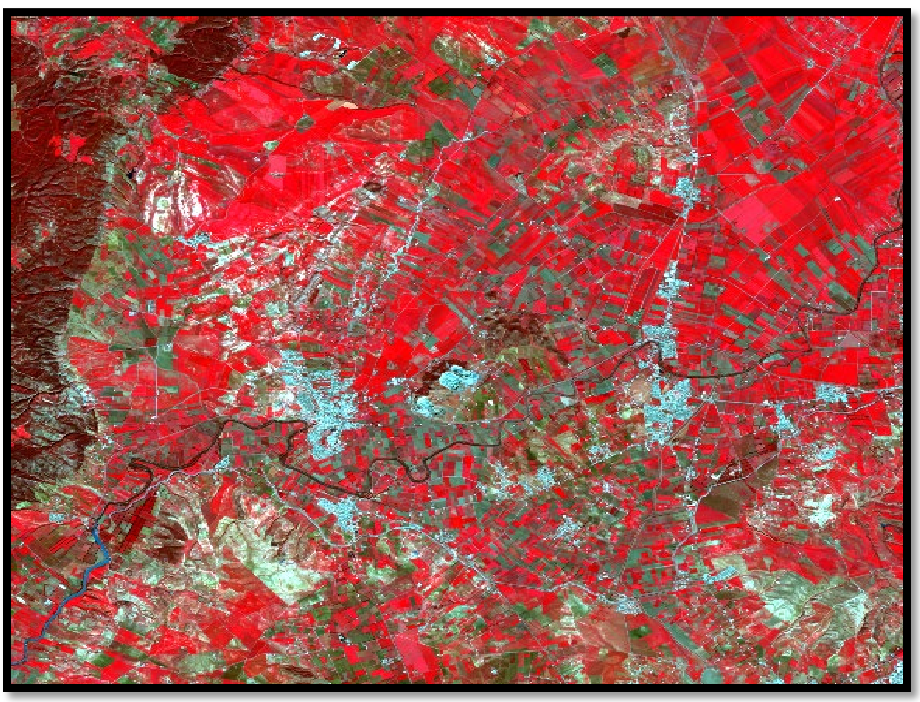

Figure 36:Color combination Infrared (B8, B4, B3)

The color infrared band combination is meant to emphasize healthy and unhealthy vegetation. By using the near-infrared (B8) band, it’s especially good at reflecting chlorophyll. This is why in a color infrared image, denser vegetation is red. But urban areas are white.

- Agriculture (B11, B8, B2)

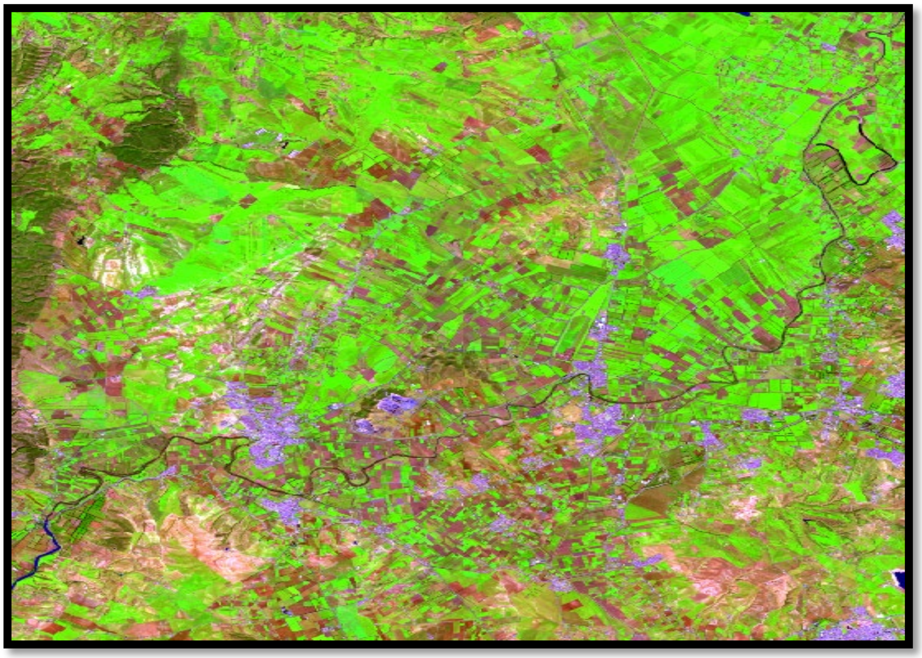

Figure 37:agriculture band combination

The agriculture band combination uses SWIR-1 (B11), near-infrared (B8) and blue (B2). We have used it to monitor the health of crops because how it uses short-wave and near infrared. Both these bands are particularly good at highlighting dense vegetation which appear as dark green.

Also, we have used the famous vegetation index NDVI because near-infrared (which vegetation strongly reflects) and red light (which vegetation absorbs), the vegetation index is good for quantifying the amount of vegetation. The formula for normalized difference vegetation index is (B8-B4)/(B8+B4). While high values suggest dense canopy, low or negative values indicate urban and water features.

Different types of surfaces, such as water, bare ground or vegetation, reflect radiation differently in different channels. Radiation reflected as a function of wavelength is called the spectral signature of the surface. Vegetation has an extremely high degree of reflection in the near infrared channel 8, and a low degree of reflection in the visible red channel 4. It is therefore possible to distinguish the vegetation zones from the bare ground. The difference in reflection in channels 8 and 3 is large for areas of vegetation and almost zero for bare land.The spectral signature of green plants is very characteristic. The chlorophyll of a developing plant absorbs visible light, especially red, for use in photosynthesis, while near infrared light is reflected very efficiently because the plant has no use for it (see Figure). Thus, plants avoid unnecessary heating or loss of sap through evaporation. Consequently, the reflection of vegetation in the near infrared and in the visual ranges of the spectrum varies considerably.

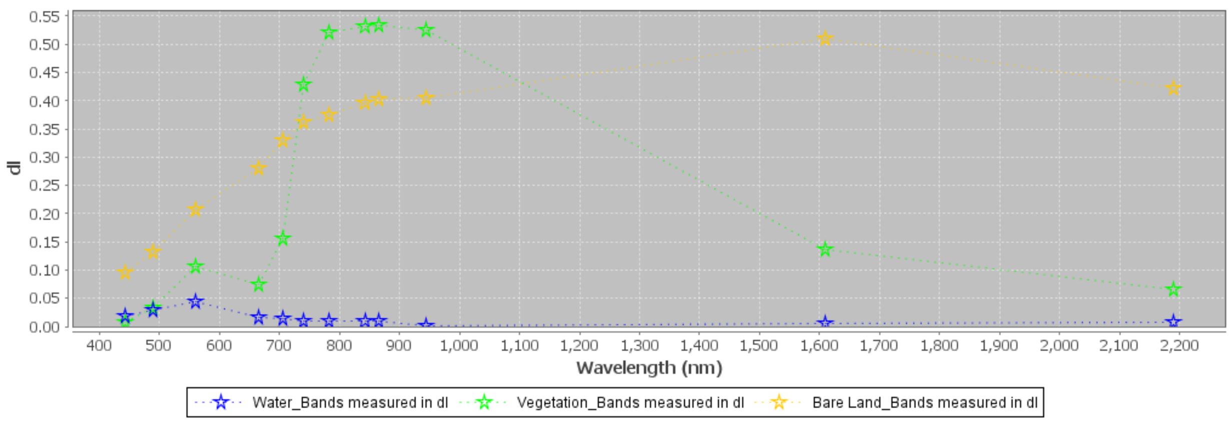

Figure 38:Graphs of spectral signatures of water, soil and vegetation.

Vegetation has a remarkably high reflection in the near infrared channel 8, and a low reflection in the visible red channel 4. This makes it possible to distinguish vegetation areas from bare ground. The difference of reflection in channels 3 and 4 is great for vegetation areas and insignificant for bare ground.

We have managed to distinguish between 9 different classes

a- Forest and dense vegetation:

Forests are determined both by the presence of trees and the absence of other predominant land uses it can be identified throw false color combination.

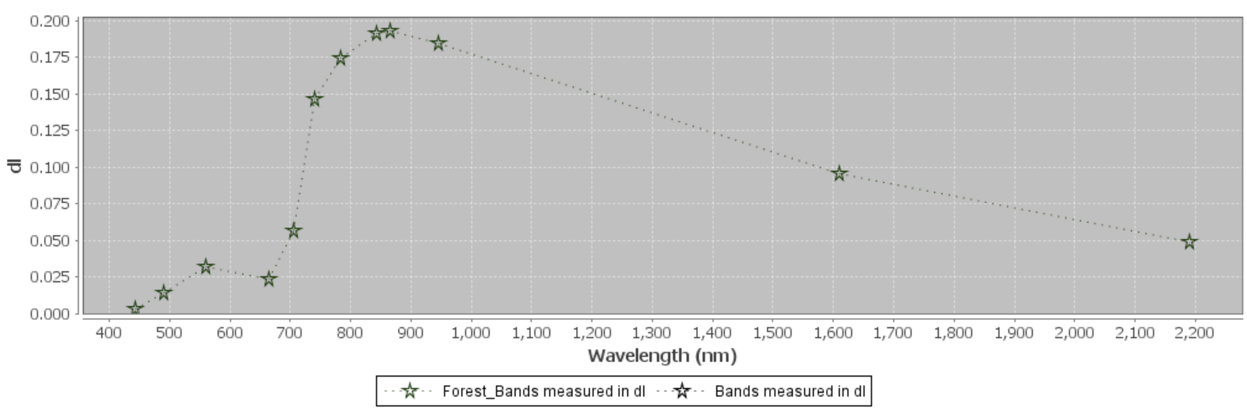

b- Agricultural land

This class presents the land that our made for agriculture but they are out of season when the image was taken, we can distinguish these lands throw its form generally it appears rectangular.

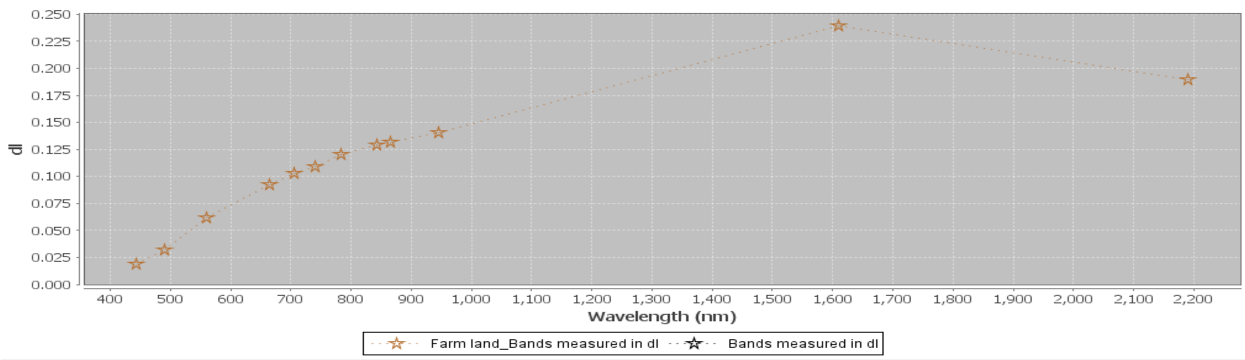

c- Urban areas

Urban areas or artificial land are easy to identify they appears in white in infra-red combination or we can simply see it in true color image thanks to unsupervised classification we find out that this areas may interfere with other classes that represent land with low or no vegetation in the training data selection we focused on this point so we get a precise mapping .

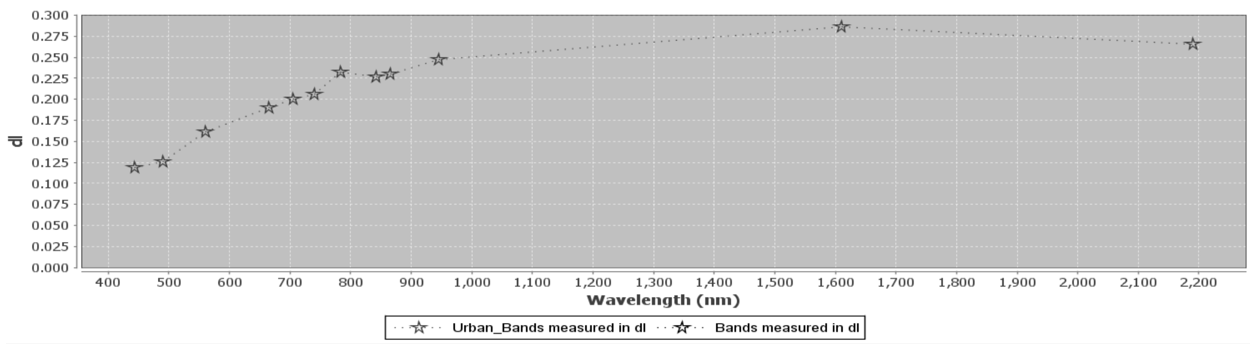

d- Wetlands

Wetlands refer to land covered or saturated with water for all or part of the year. The differences between types of soil, depending on whether it is dry or wet, can be significant.

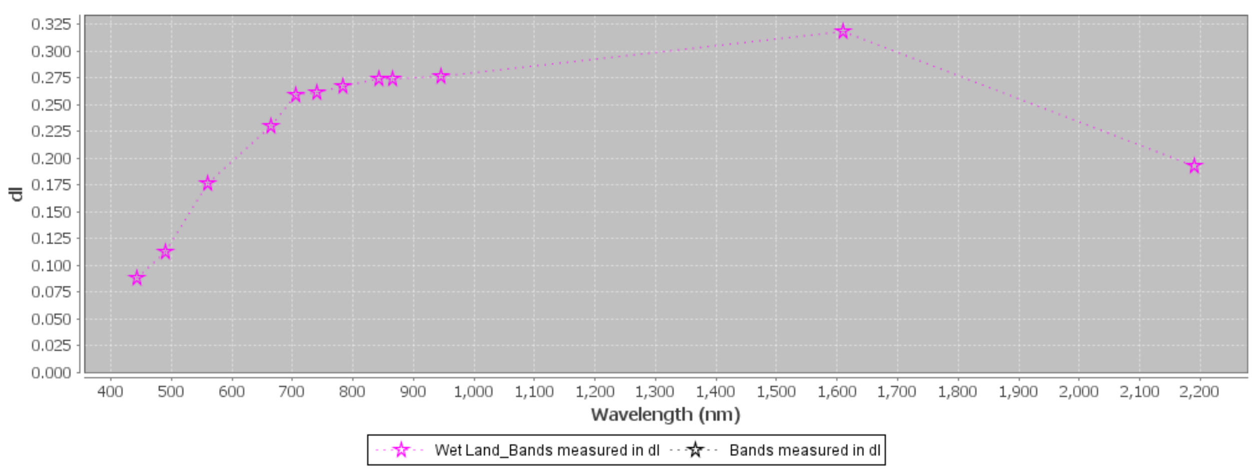

e- Major cultivation

The study area is known for its massive production of large agricultural crops, so this type of vegetation dominates the region in general.

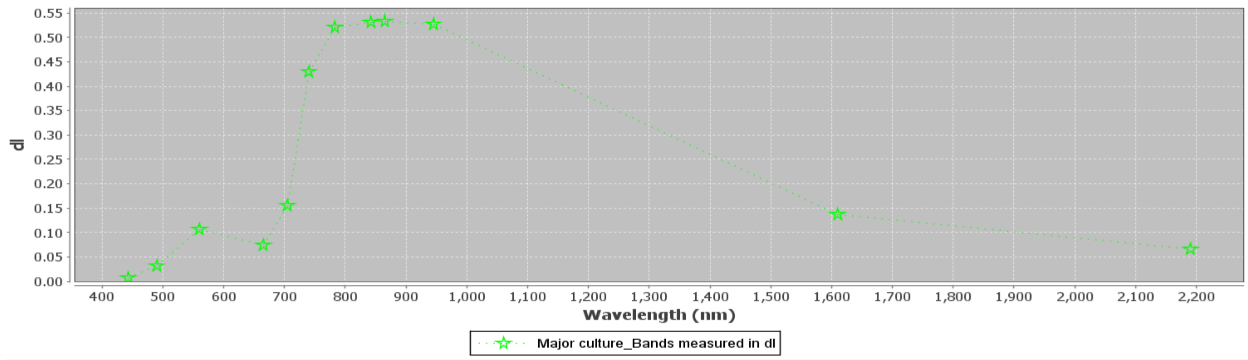

f- Bare land

Bare land class represent the land where no vegetation at all and it's totally empty Rays reflected from bare ground increase slightly from the visible range to the infrared range of the spectrum.

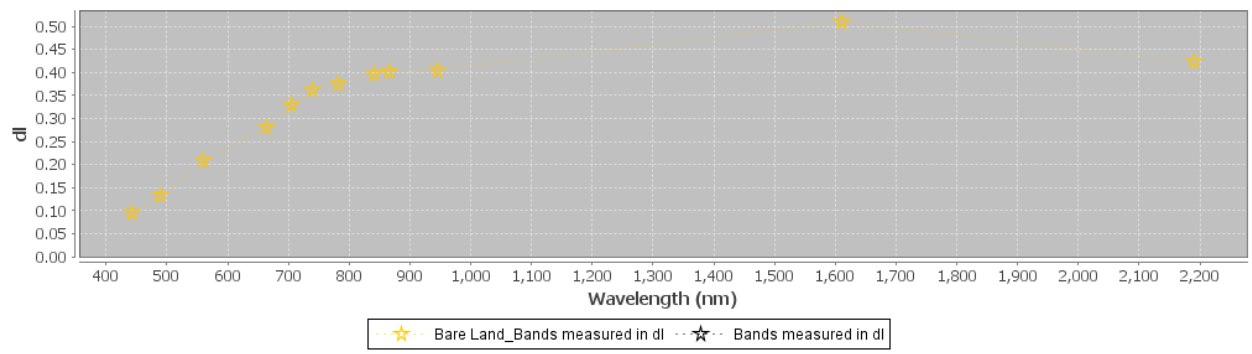

g- Water

Typically, water only reflects in the visible light range. Since water hardly reflects in the near infrared range, it is very different from other surfaces. Thus, water surfaces will be clearly delineated as dark areas (low pixel values) on images recorded in the near infrared.

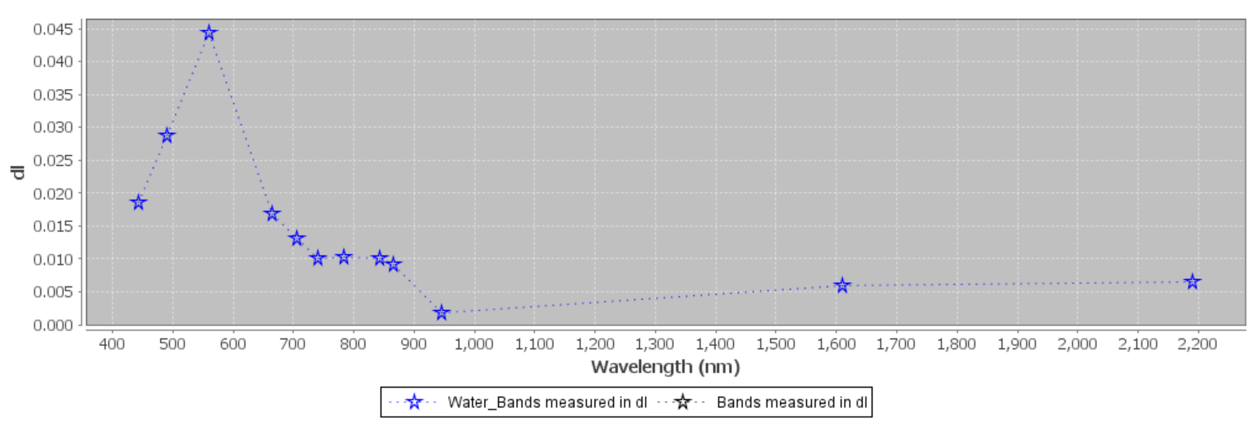

h- Dispersed vegetation

This class symbolizes the land where there are dispersed plants separated by a relatively large distance. Dispersed vegetation covers the land with low percentage of vegetation as we can see in the spectral response, we have lower reflectance near infrared range compared to other vegetation classes and also higher reflectance in SWIR range.

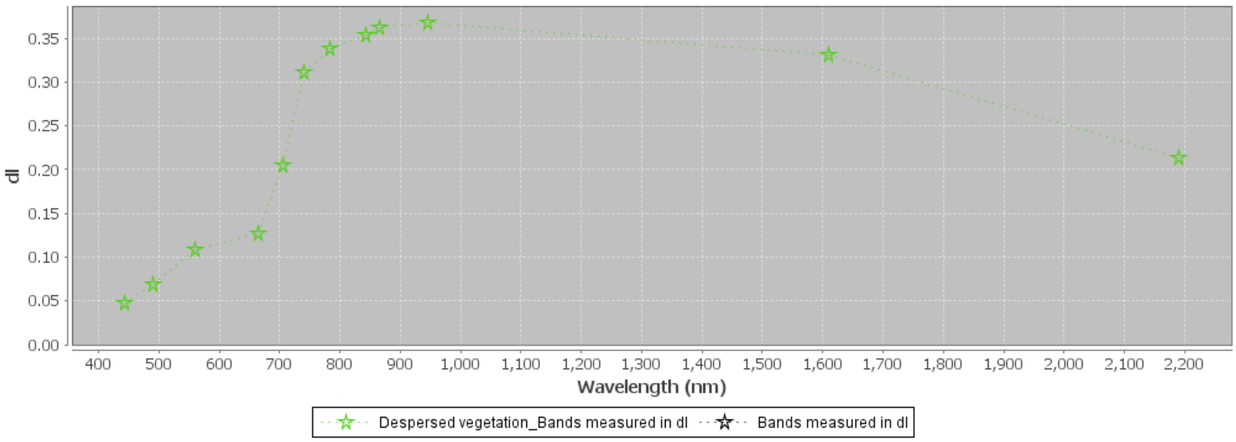

i- Agricultural plants :

This class regroups deferent types of agriculture plants and vegetation this type of vegetation characterized by low reflectance in the SWIR range that means high absorption of water and high reflectance in the near infra-red range which describes the good health of vegetation.

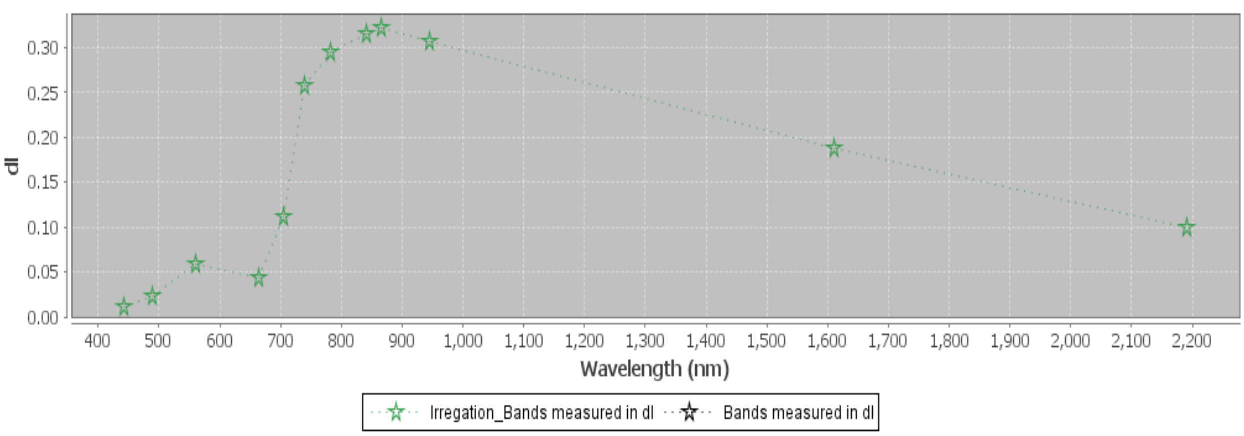

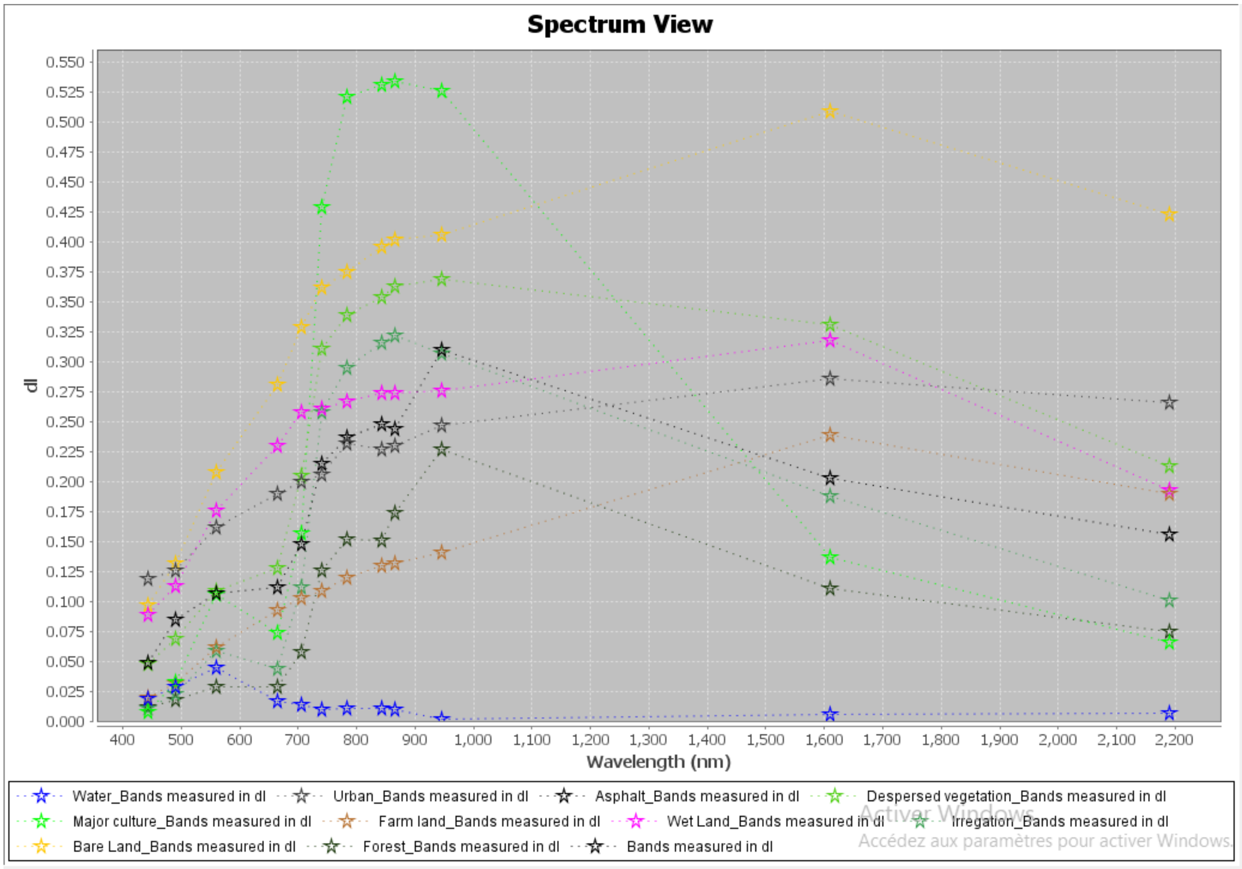

Figure 39: Spectrum Vue Showing the Spectral responds for different classes

V-4-2-2- Random forest classification (RF)

Before proceeding to classification, we had to take region of inters ROI as training data. The selection of the training samples is very important in this method and a biased selection can badly affect the accuracy of classification. We have used different source to precisely choose the training data such google earth pro and means of photo-interpretation. We took between 50 and 100 ROI in each class distributed all over the scene to assure the accuracy of our classification. Then we processed random forest classifier which spreads random seeds all over the scene to build a forest of decision trees that takes the input training data and associate each pixel to the correspondent class.

Figure 40: Region of interest selection (ROI)

.

V-4-2-2Results

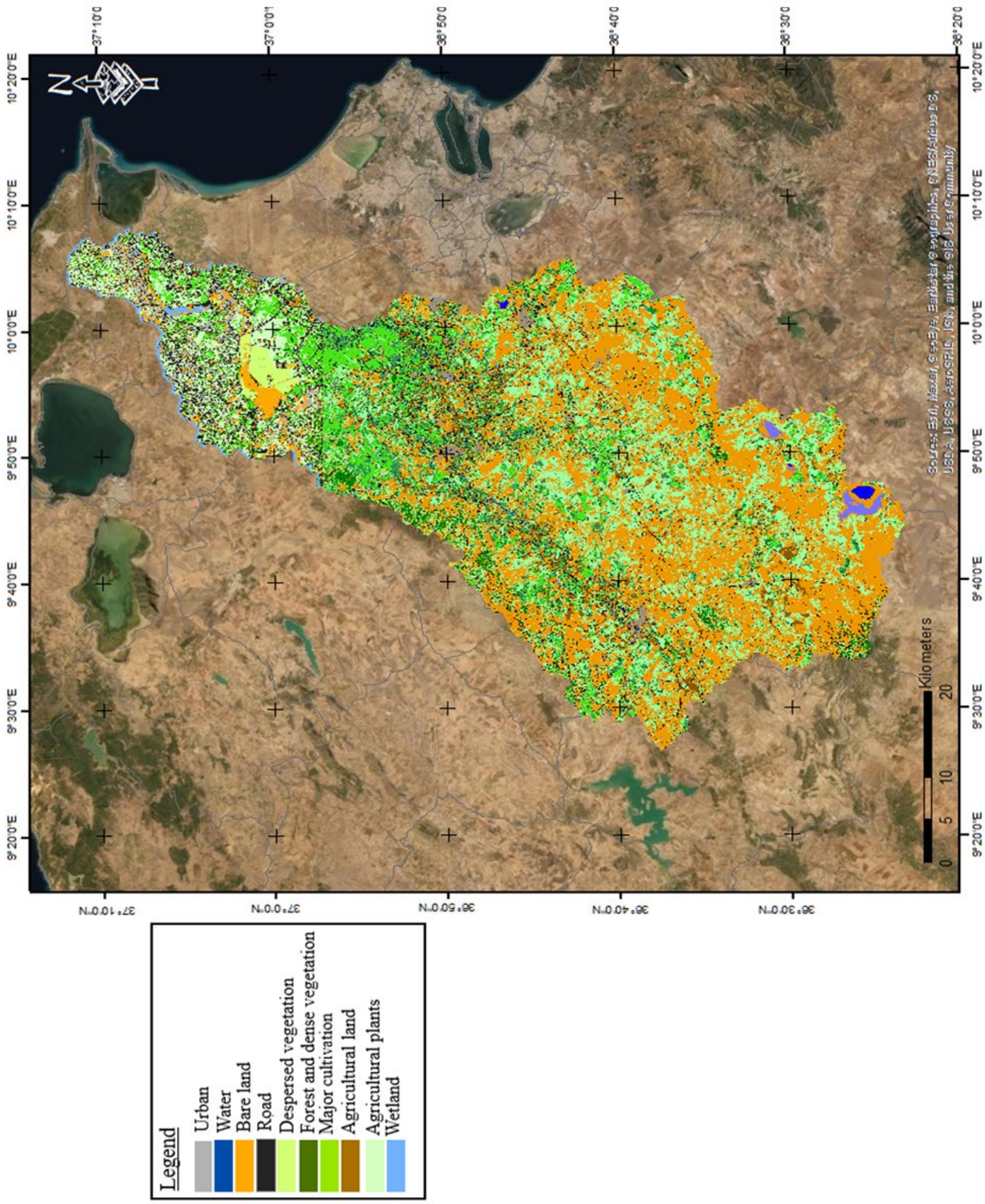

Figure 41:Land Use Map 2020

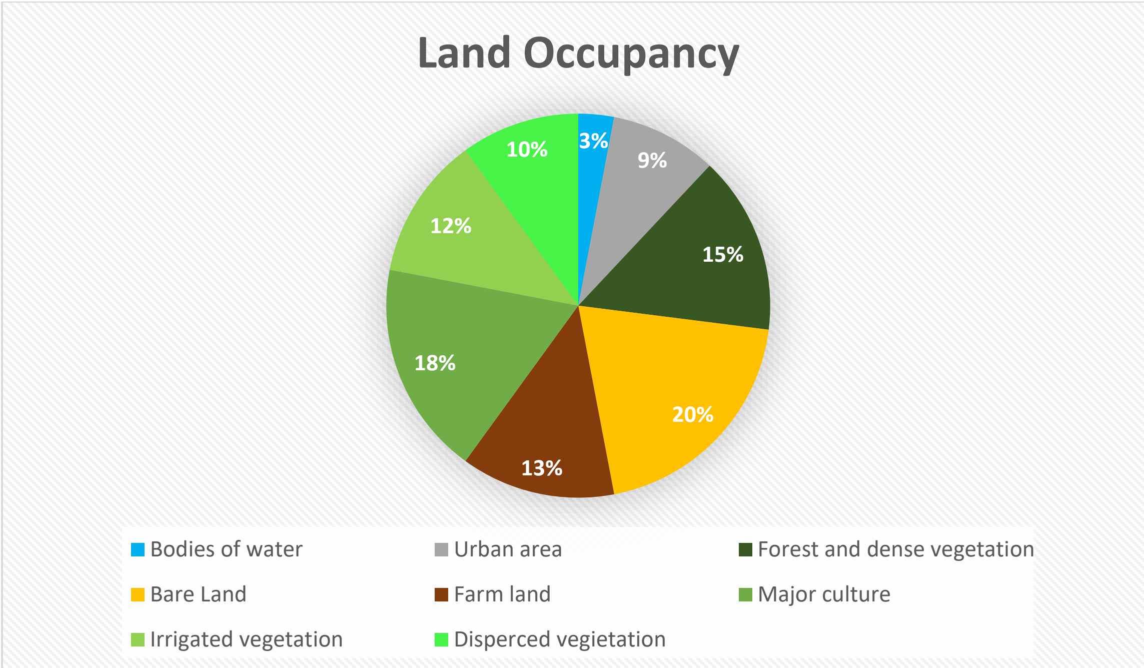

Figure 42: Graph of Land occupancy percentages

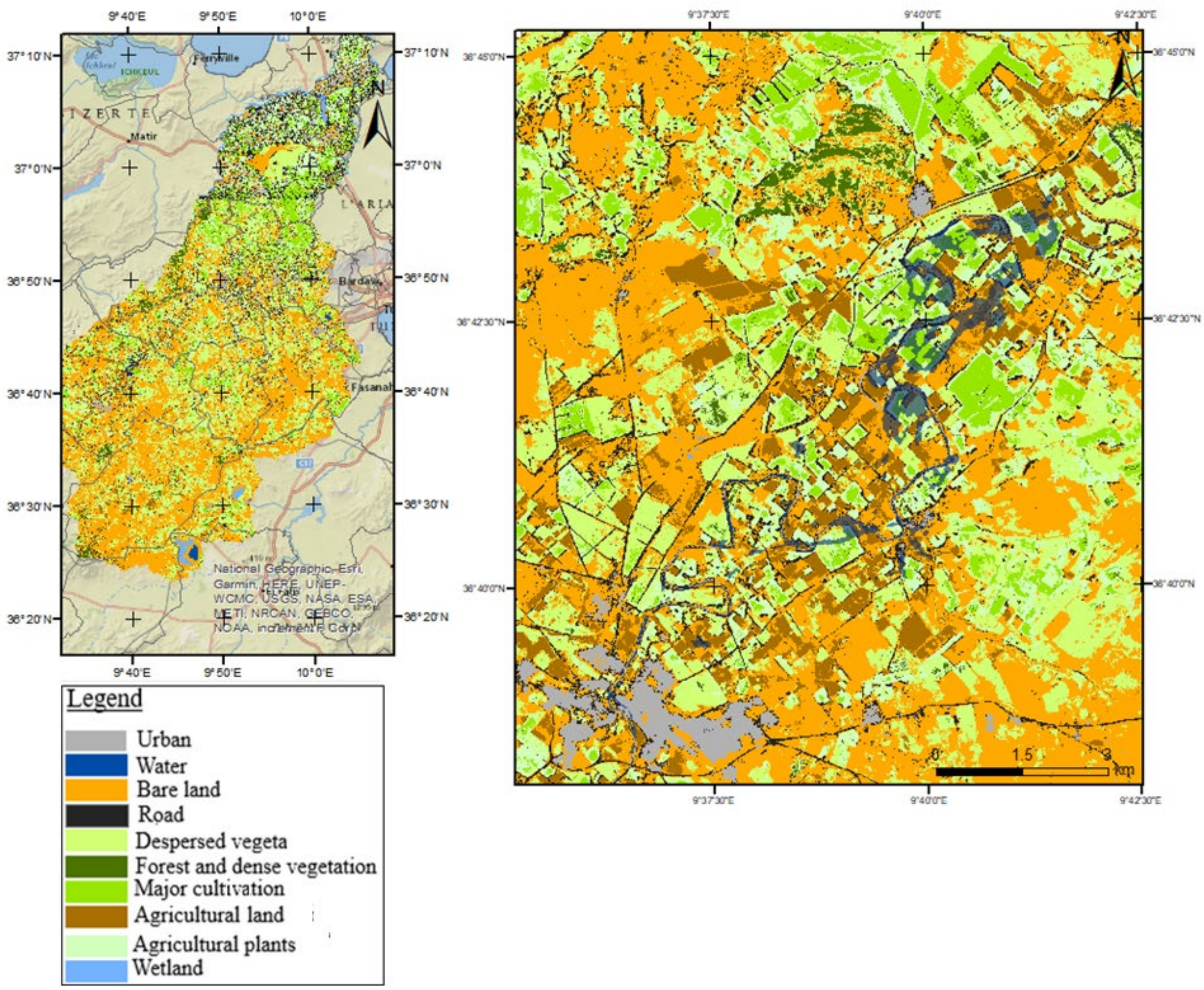

Figure 43: Map of flooded land cover

As shows (Figure 43) the majority of the flooded areas are agricultural land and the land of major cultivation, the flood covers 450 hectares of these types.

III-4.3. Validation

After the classification process, it is useful to assess the accuracy of land cover classification, in order to identify and measure map errors. Usually, accuracy assessment is performed with the calculation of an error matrix, which is a table that compares map information with reference data (i.e. ground truth data) for a number of sample areas (Congalton and Green, 2009).

For this purpose, we used **semi-automatic classification plugin** in Qgis to create random ROI's with the tool **Multiple ROI Creator** then we associated each ROI to the appropriate class finely we generated the confusion matrix (table 6).

Class	Urban	Bare Land	Forest and dense vegetation	Road	Major Culture	Dispersed vegetation	Agricultural land	Agricultural plants	Water	Wet land	Total
Urban	420	0	0	1	0	0	0	0	6	0	420
Bare Land	0	818	1	4	0	1	43	0	5	12	827
Forest and dense vegetation	0	0	626	0	107	1	0	13	0	0	703
Road	0	1	2	422	0	0	4	0	10	0	428
Major Culture	0	0	59	0	7116	0	0	36	0	0	7506
Dispersed vegetation	0	3	3	0	82	717	3	49	0	0	722
Agricultural land	0	5	0	1	0	0	2303	0	0	0	2353
Agricultural land	0	5	0	1	0	0	2303	0	0	0	2353
Agricultural plants	0	0	12	0	201	3	0	595	0	0	693
Water	0	0	0	0	0	0	0	0	2799	0	2820
Wet land	0	0	0	0	0	0	0	0	0	1236	1248
Total	420	827	703	428	7506	722	2353	693	2820	1248	17720

Table 6: Confusion matrix of 2020 Land Use Classification

a- Overall Accuracy

The overall accuracy is calculated by summing the number of correctly classified values and dividing by the total number of values. The correctly classified values are located along the upper-left to lower-right diagonal of the confusion matrix. The total number of values is the number of values in either the truth or predicted-value arrays.

Overall Accuracy: = 86.2302 %

b- Kappa Coefficient

The kappa coefficient measures the agreement between classification and truth values. A kappa value of 1 represents perfect agreement, while a value of 0 represents no agreement. The kappa coefficient is computed as follows:

$$\kappa = \frac{N \sum_{i=1}^{n} m_{i,i} - \sum_{i=1}^{n} (G_i \, C_i)}{N^2 - \sum_{i=1}^{n} (G_i \, C_i)}$$

Where:

- i is the class number
- N is the total number of classified values compared to truth values
- $m_{i,i}$ is the number of values belonging to the truth class i that have also been classified as class i (i.e., values found along the diagonal of the confusion matrix)
- C_i is the total number of predicted values belonging to class i
- G_i is the total number of truth values belonging to class i

Kappa Coefficient = 0.8511

c- Errors of Commission

Errors of commission represent the fraction of values that were predicted to be in a class but do not belong to that class. They are a measure of false positives. Errors of commission are shown in the rows of the confusion matrix, except for the values along the diagonal.

d- Errors of Omission

Errors of omission represent the fraction of values that belong to a class but were predicted to be in a different class. They are a measure of false negatives. Errors of omission are shown in the columns of the confusion matrix, except for the values along the main diagonal.

Class	Commission (percent)	Omission (percent)
Urban	1.64	0.0
Bare Land	7.47	1.09
Forest and dense vegetation	16.20	10.95
Road	3.87	1.40
Major cultivation	1.32	5.20
Dispersed vegetation	16.34	0.69
Agricultural land	0.26	2.12
Agricultural plants	26.63	14.14
Water	0.0	0.74
Wet land	0.0	0.96

III-5-Conclusion

Accurate land cover information is required for science, monitoring, and reporting. Land cover changes naturally over time, as well as a result of anthropogenic activities. Monitoring and mapping of land cover and land cover change in a consistent and robust manner over large areas is made possible with Earth Observation (EO) data. Land cover products satisfying a range of science and policy information needs are currently produced periodically at different spatial and temporal scales. The increased availability of EO data—particularly from the Landsat archive (and soon to be augmented with Sentinel-2 data)—coupled with improved computing and storage capacity with novel image compositing approaches, have resulted in the availability of annual, large-area, gap-free, surface reflectance data products.

.

Chapter 6: Interactive map development

VI-1-Introdction

The provision of maps via the Internet is a rapidly evolving area of development and investment. While classical cartographic concepts still apply in how geospatial information can best be presented, the interactive nature of the Internet has offered (and continues to offer) novel ways to capture and communicate geospatial information .Accordingly in this is the last part of this report we have developed an interactive web application to serve as a powerful tool in disaster and emergency management also as a new form to publish cartographies products on line .

So, this chapter first presents the choice of the work and development environment, then the explanation of the work methodology and finally, the implementation and presentation of the map and the publishing of the results.

VI-2-The work environment

VI-2-1 The software environment

a- StarUML

StarUML is a UML design and modeling software which enables computer processing and their associated databases to be modeled. It is intended for data architectures, information architectures and enterprise architectures. This software is intuitive and easy to install and use, consumes few system resources and allows to generate C, C ++, Java and PHP code from UML modeling, thanks to the various plugins that compose it.

b- Visual Studio 2019

Visual Studio Code is an open-source, free and multiplatform code editor, developed by Microsoft, supporting a very large number of languages thanks to extensions. It supports autocomplete, syntax highlighting, debugging, and git commands. In VS code it is possible to change the theme, keyboard shortcuts, preferences and install extensions that add additional functionality.

c- XAMPP 7.4.9

XAMPP is a set of software used to easily set up a Web server, an FTP server and an e-mail server, allowing PHP scripts to operate locally without connecting to an external server. It is a distribution of free software X Apache MySQL Perl PHP, offering a good flexibility of use, known for its simple and fast installation.

Thus, it is within the reach of most people since it does not require specific knowledge and works on the most common operating devices.

d- Apache 2.4.46

Apache is open-source web server software that powers many websites around the world. Its official name is Apache HTTP Server and it is maintained and developed by the Apache Software Foundation. This server allows clients to serve content on the web by acting as a virtual delivery person, it is able to interpret HTTP requests arriving on the port associated with the HTTP protocol and to provide a response with this same protocol.

VI-2-2-Languages and Framework

a- Open Layers

OpenLayers is free software released under the BSD license. It constitutes a library of JavaScript functions providing a core of functionalities oriented towards the implementation of fluid web cartographic client applications. OpenLayers can display tiled basemaps as well as markers from a wide variety of data sources. Part of this library also makes it possible to manage the ergonomics offered to the user, but this is not directly his role.

b- PHP 7

PHP is a free programming language, specially designed for the development of web applications including the production of dynamic web pages via an HTTP server, but which can also function as any language interpreted locally. In its version seven, PHP established itself as the reference object-oriented language, because of its simplicity, its free and its origin as free software.

c- HTML 5

HTML is the Hypertext Markup Language, denotes a type of descriptive computer language and is based on a markup system designed to represent web pages. HTML also makes it possible to semantically structure the page, to format the content, to create input forms, to include multimedia resources, such as images, videos and computer programs. It makes it possible to create interoperable documents with a wide variety of equipment in accordance with the requirements of web accessibility. It is often used in conjunction with the JavaScript programming language and CSS Cascading Style Sheets.

d- CSS 3

CSS is the acronym for Cascading Style Sheets which can be translated as Cascading Style Sheets. It is a computer language used on the Internet for formatting files and HTML pages. Cascading style sheets allow you to define rules applied to one or more HTML documents, these rules relate to the positioning of elements, alignment, fonts, colors, margins and spacing, borders, images background and quite a few other operations. CSS also makes it possible to separate the presentation of an HTML page and its structure, which offers more transparency at the source code level.

e- Bootstrap

Bootstrap is an open source front-end development framework made up of HTML, CSS and JavaScript code. It provides tools with styles already in place for themes, buttons, navigation interfaces and many more interactive elements. Bootstrap is designed to develop sites with a responsive design, which adapts to any type of screen, and primarily for smartphones. It is one of the most popular projects on the GitHub development management platform.

f- Geoson

GeoJSON is an open standard format designed for representing simple geographical features, along with their non-spatial attributes. It is based on the JSON format. The features include points (therefore addresses and locations), line strings (therefore streets, highways and boundaries), polygons (countries, provinces, tracts of land), and multi-part collections of these types. GeoJSON features need not represent entities of the physical world only; mobile routing and navigation apps, for example, might describe their service coverage using GeoJSON.The GeoJSON format differs from other GIS standards in that it was written and is maintained not by a formal standards organization, but by an Internet working group of developers.

VI-3- Methodology

For the development of an interactive web map we need four main elements as shown in the figure:

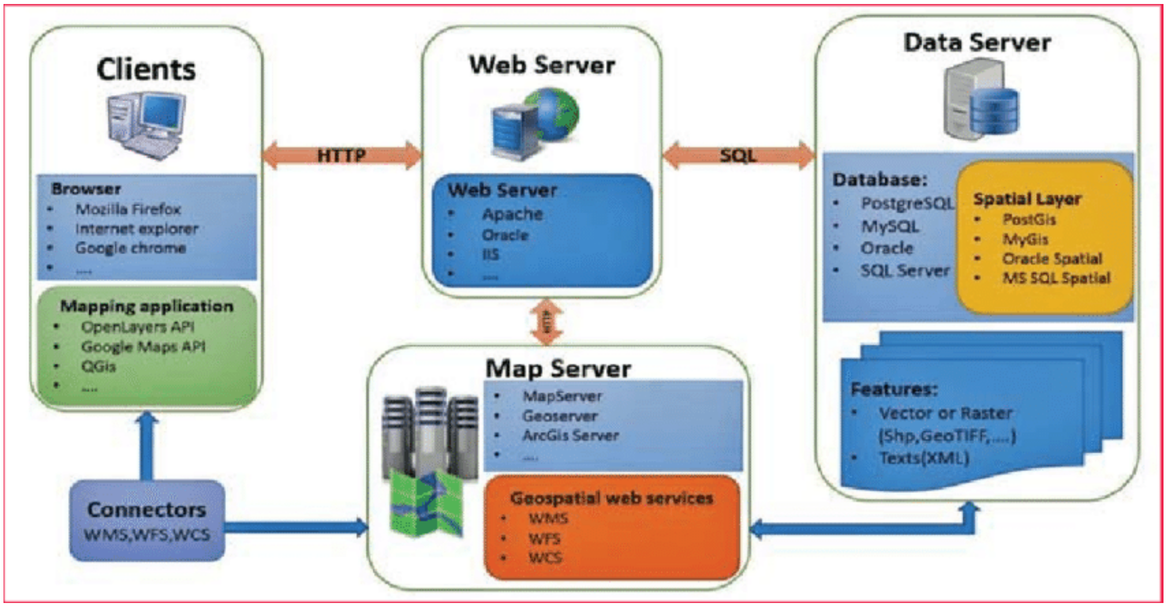

Figure 44: Application development methodology

1-Web Client

A client is a computer or a program that, as part of its operation, relies on sending a request to another program or a computer hardware or software that accesses a service made available by a server. As for our case the client is the web browser which connect the web servers and retrieve web pages for display .

2- Web Server

A web server is server software, or hardware dedicated to running this software, that can satisfy client requests on the World Wide Web. A web server can, in general, contain one or more websites. The primary function of a web server is to store, process and deliver web pages to clients. The communication between client and server takes place using the Hypertext Transfer Protocol (HTTP).

3- Database server

A database server is used to store, retrieve, and manage data in a database. It also allows you to manage the updating of data. It gives simultaneous access to this database to several Web servers and users. Finally, it ensures data security and integrity. And when we talk about data, we mean perhaps millions of items simultaneously accessible to thousands of users.

4-Geoserver

In computing, GeoServer is an open-source server written in Java that allows users to share, process and edit geospatial data. Designed for interoperability, it publishes data from any major spatial data source using open standards. GeoServer has evolved to become an easy method of connecting existing information to virtual globes such as Google Earth and NASA World Wind as well as to web-based maps such as OpenLayers, Leaflet, Google Maps and Bing Maps. GeoServer functions as the reference implementation of the Open Geospatial Consortium Web Feature Service standard, and also implements the Web Map Service, Web Coverage Service and Web Processing Service specifications.

VI-4-Analysis and design

The analysis and design phase are the initial phase of creation and implementation of this project and its success depends on their qualities. In fact, this chapter represents an important stage of reflection on the software development cycle through the identification of the actors who will interact with the future product and the specification of the needs, subsequently detailing the design of the project using of the UML formalism which will be translated by the use case diagrams, their textual descriptions and the class diagram.

VI-4-1- Analysis

Analysis is a review process that collects and presents data with an overview of all platforms and aims to grasp the details of the project by breaking it down into its constituents. It therefore first establishes criteria for identifying actors and specifying needs.

VI-4-1-1- Identification of actors

A- super-user

The super user is either the responsible authority for disaster management, response teams, or emergency services. This actor can take advantage of a cartographic interface through which he can do the following:

- Make analysis based on cartographic products shared on the map
- Launch alerts of any type of emergency
- View emergency calls in real-time
- Add cartographique featuers with representative symboles
  - Point : Point of distribution , Meeting point, shelter
  - Line : Emergency road , Evacuation road
  - Polygone : Danger Zone, Contamination zone, Restricted area

- Share emergency measures and instructions

The super user must authenticate using an ID and a password ,attributed by the administration ,to access the additional functionality like cartographies layers that we have produced earlier also he have more complicated interface .

B- User

All citizens can access the map to see emergency information , alert the authorities also to call for help with a simple click no login is required for this level of users .

C- Admin

The admin is an actor with privilege he have access to all the data and he is responsible for attributing login information to other services and he is meant to update and organize the data available .

VI-4-1-2- Requirements specification

The requirements specification step consists of defining the set of functionalities that the system must provide. These needs will be divided into two groups: functional and non-functional.

a- Functional needs

This application is a tool supposed to work in an emergency or disaster time. Therefore, the application must be accessible at all times from any device connected to the internet securely. It must be dynamic in every sense of the word and be easy to navigate while respecting best practices allowing users to easily find the information they are looking for as well as the essential elements that must be visible and accessible. The goal of this project is to implement a mapping tool open to several participants, as well as the possibility of sharing information and to facilitate the work of the services intervening in the field of civil protection by giving a view on local, regional and national the scale.

b- Non-functional needs

After determining the functional needs, we present below all the constraints to be observed to guarantee the performance of the system while meeting the needs of the manipulator. The future application should allow the following actions for each user.

Security: The application must meet a high level of security in order to secure user accounts, including their own data.

Portability: The application must be cross-platform, so that it works on all operating systems and in any medium where there is a web browser.

The availability: The application should be available on the web at all times, with the exception of the maintenance period which should not be too long.

The performance: The application must ensure minimum response time while meeting the requirements of the operator optimally.

The simplicity: Every user will be able to use this application in an easy and clear way.

The ergonomics of the interface: Interfaces must be simple, responsive or adaptive and user-friendly.

The modularity of the application: Have a simple code that is easy to maintain and understand when needed.

The analysis part made it possible to identify the actors of the application, to deliver a complete specification of the needs and to structure them in a form which facilitates understanding and which drafts towards the design activity.

VI-4-2-Design

The fundamental motivation of modeling is to provide an earlier approach in order to reduce the complexity of the system studied during the design and to organize the realization of the project by defining the modules and the stages of the implementation. Several modeling approaches are used. In this work, we adopt an object approach based on the UML modeling tool. In fact, UML Unified Modeling Language is an open standard that specifically facilitates the interoperability of object-oriented systems. It is the result of the unification of many graphic modeling languages, notations and object-oriented concepts.

VI-4-2-1- Use case diagram

Design begins with the preparation of use case diagrams which are UML diagrams used to provide a holistic view of the functional behavior of the system and absolutely not a computer view. These diagrams are not exhaustive inventories of all the functions of the system, they only list essential and main general functions without going into detail. A use case represents a discrete unit of interaction between the user and the system.

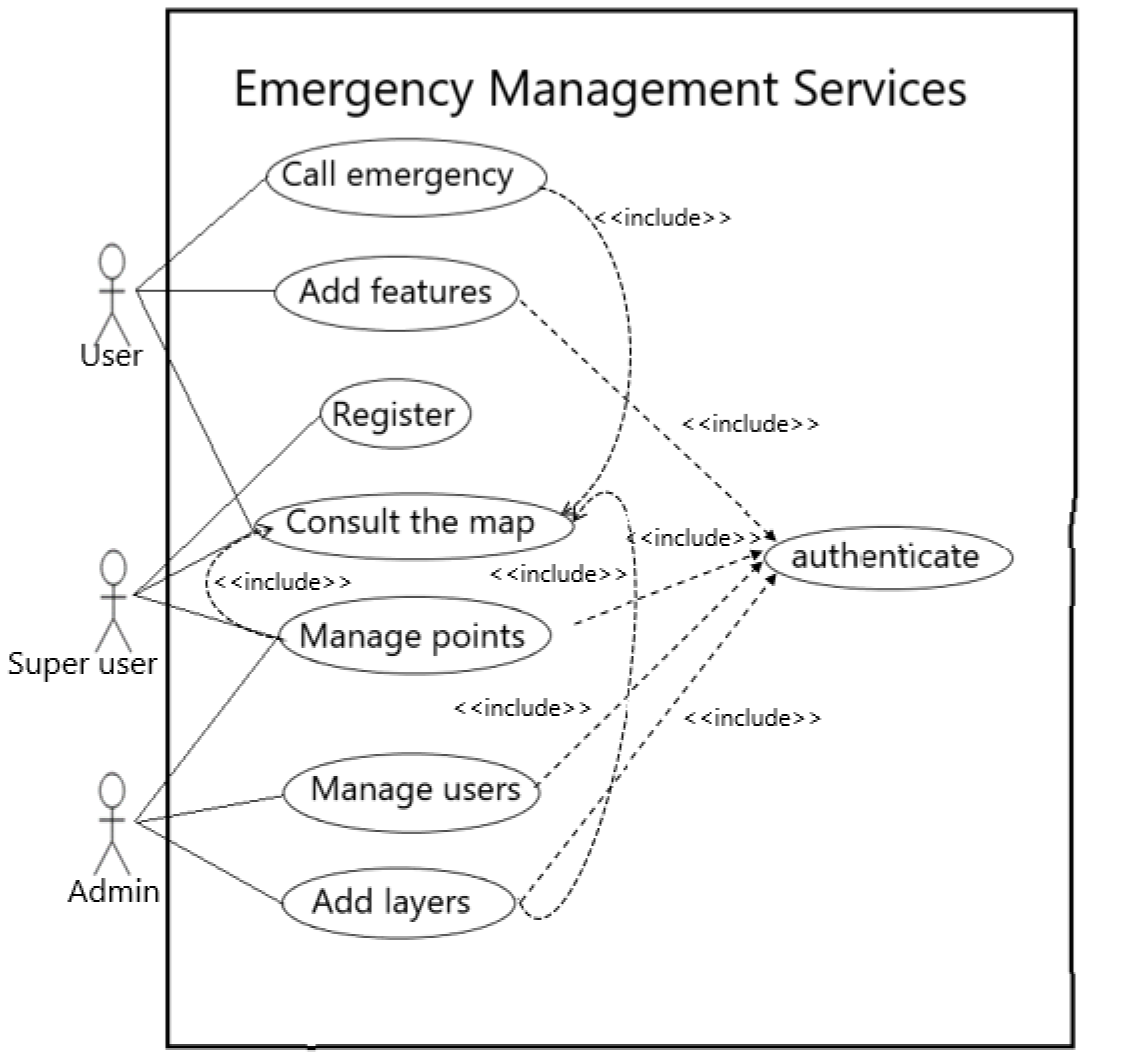

Figure 45:General use case of the application

VI-4-2-2- The database

The DBMS used to create the database is PostgreSQL, as mentioned earlier. Our database called EMSdatabase,

a- User Table

The user table stores the list of all users subscribed to the application this table is made up of 5 attributes:

- a primary key user-id of integer and auto increment type,
- a name and a first name of type varchar and of size 25 characters maximum,
- an e-mail address of the varchar type and size 50 characters,
- a password, date of birth and a varchar service of 25 characters,
- a gender of varchar type and size 5 characters,

b- Emergency table

This table stores all the emergency call made of 3 attributes

- a name and a first name of type varchar and of size 25 characters maximum,
- Type attribute with varchar type size 20 characters
- Coordinates attribute with type geometry

c- Alert table

This table reserved to store the alert events lunched by the emergency services composed of 5 attributes

- a primary key event-id of integer and auto increment type
- Type attribute with varchar type size 20 characters
- Date attribute type date
- Coordinates type geometry
- Description varchar type

VI-5- Application interfaces

Web interfaces make the application suitable, user-friendly and pleasant to navigate, so this standard can differentiate between applications despite their functional similarities. We relied on the bootstrap framework for the development of the front-end part, it allowed us to create and make dynamic changes in terms of interface appearance more particularly given the size of the screen and the orientation of the devices used. We've placed a lot of emphasis on content, search engine visibility and performance on all types of devices, ensuring our app is user-friendly as a virtual desktop.

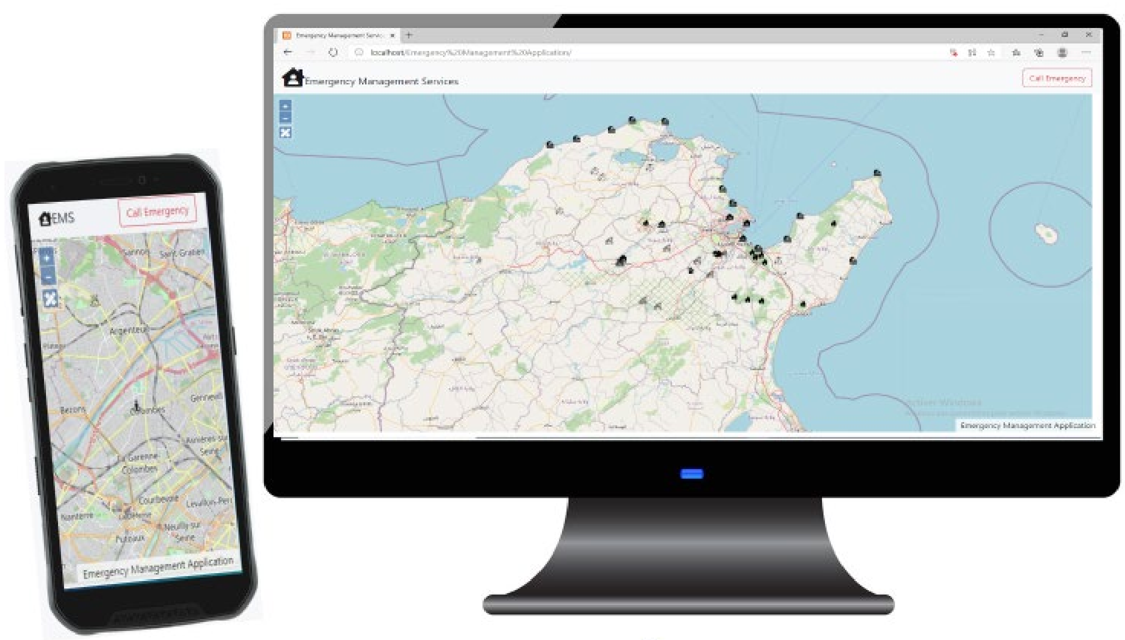

We have tried as much as possible to create interfaces similar to those of the most popular social networks, due to the fact that the user has become accustomed to consulting them. Thanks to this, the subscriber will have no difficulty in using our product. This section contains all application interfaces accompanied by a brief description.

1. **Standard interface :**

   This the main interface that you will see the first thing if you open our web site you can see on the map all the emergency alerts on your layer extent and you will find on the upper right corner a big red button with label "Call Emergency" on click you a pop up will appear (next figure) , and you can chose your emergency type and submit in the same moment without refreshing the page your emergency will appear and the authorities will be notified in real time .

   On the same corner you can find login button if you are a super user you can

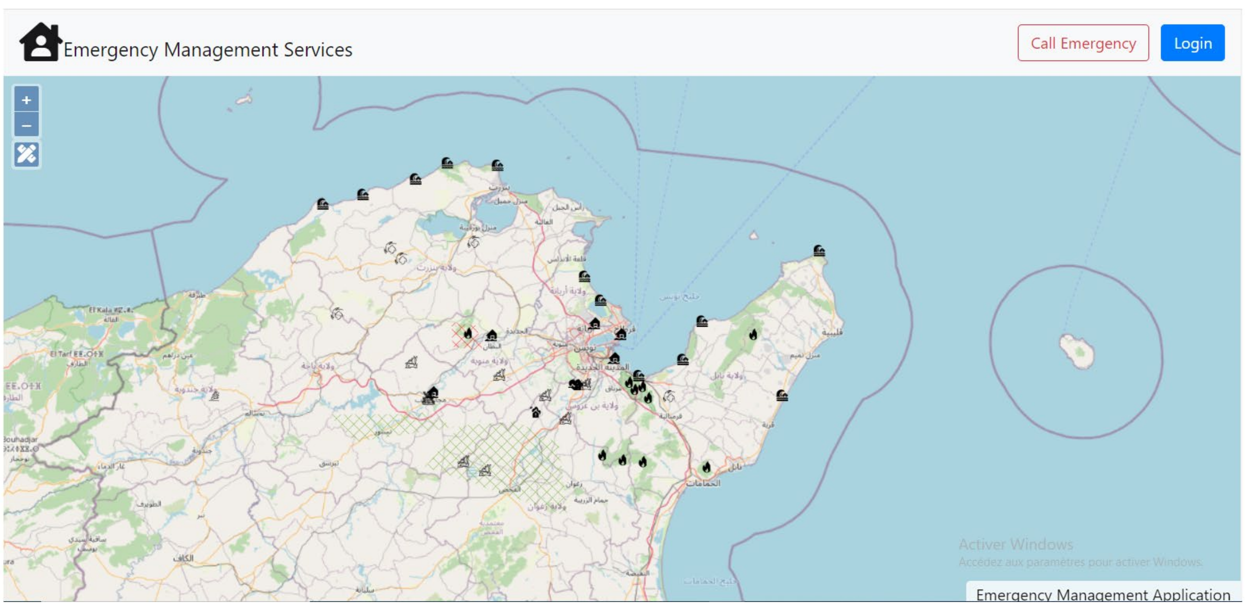

Figure 46:Welcome page

2. **Emergency form**

   After calling the call emergency function this form will appear where you can fill your name and the type of emergency by choosing your case from the list then you submit.

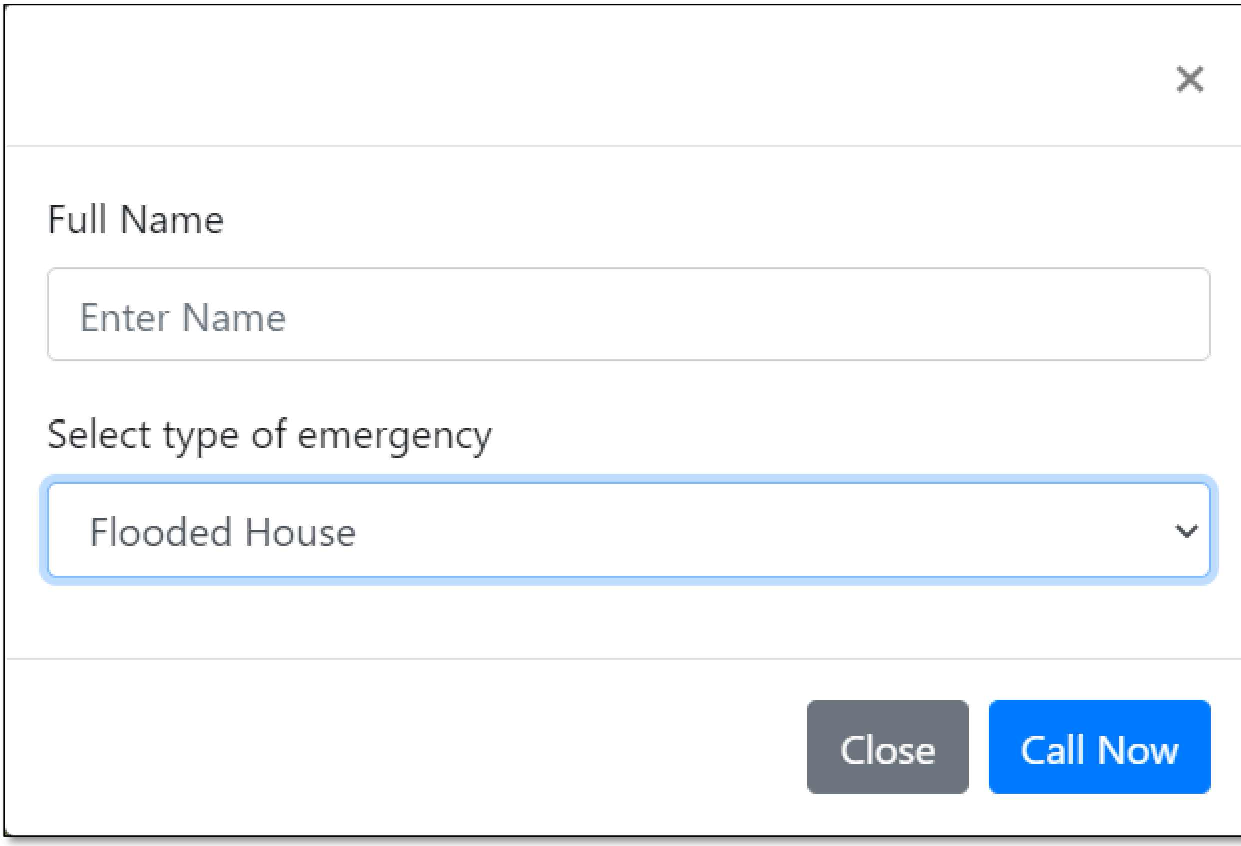

Figure 47:Emergency form

3. Super user interface

If you are a super user after having authentication you can access this interface:

Interface legend

- Button 1: zoom in and out controls.
- Button 2: adding feature and alerts.
- Button 3: layer switcher.
- Button 4: log out.

As you can see ,in figure 46 and figure 47, the flood mask and the land use classification Map produced in this study are published you can access them to do analyses based on this layer to evaluate emergency events and start alert accordingly if necessary by calling button 2 and start adding alerts with representative symbols that will appear on all the active screens.

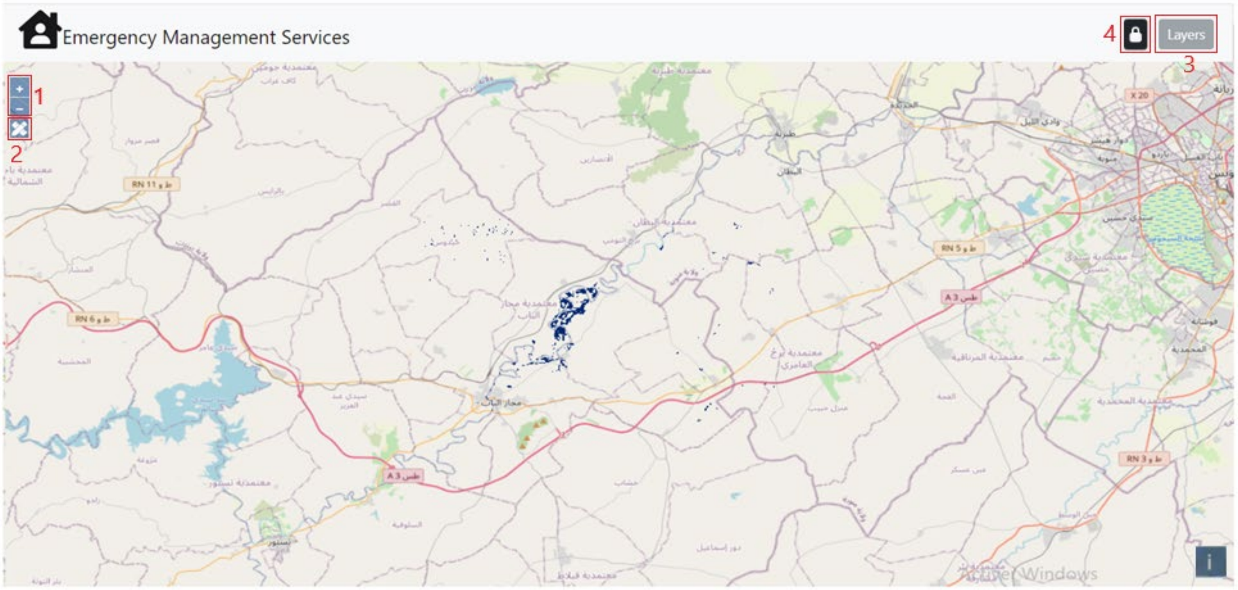

Figure 48: Publishing the result of the flooded area Mars 2015

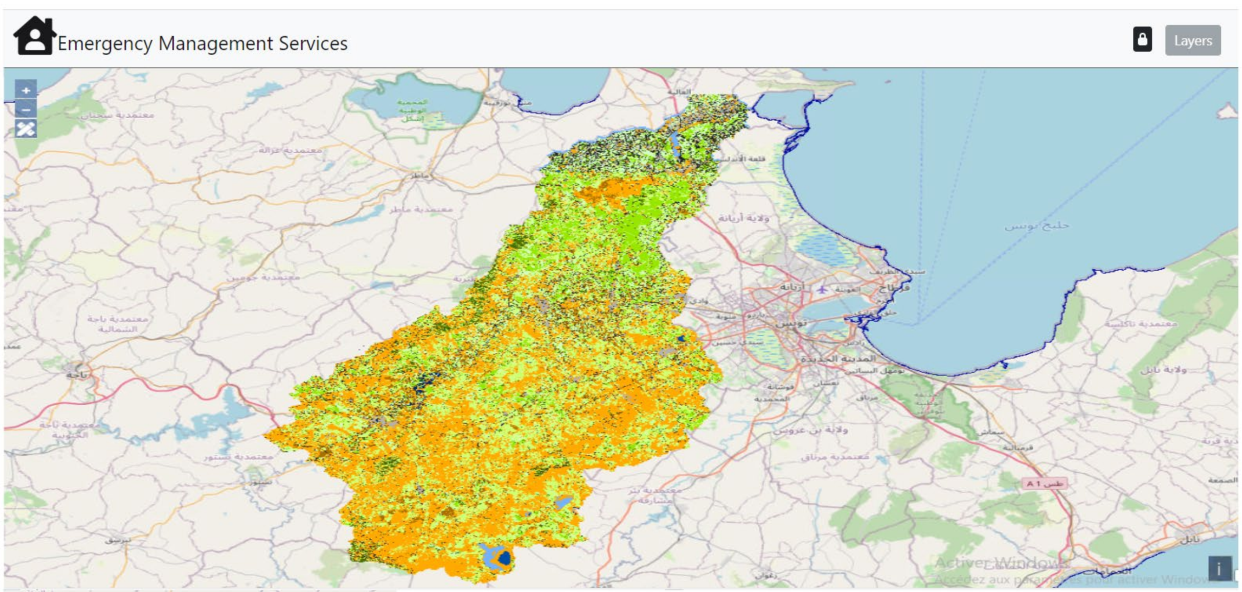

Figure 49: Land Use Map of Low valley Majerda online

VI-6 Conclusion

Web mapping is conceptually fairly straightforward, but the myriad techniques for actually implementing maps on the web can become quite detailed and technical, which reflects the actual complexity hidden underneath the deceptively simple interactions we have with web maps on a daily basis. Beyond the simplest maps, computer programming skills are needed to develop and support web maps, with the most complex maps requiring teams of programmers and designers, each with specialized skills and duties. Nevertheless, having some general understanding of how web maps are implemented is vital to anyone working with geospatial technology. This simplified introduction is provided with the caveat that since there are a large number of technologies that are evolving on a daily basis, this overview is outdated and incomplete. However, this page can be a starting point for further investigation of contemporary web mapping practices.

Conclusion

Synthetic Aperture RADAR (Radio Detection and Ranging) is a powerful active remote sensing technology used for several applications, including flood monitoring. RADAR are active systems that illuminate the Earth's surface and therefore, images can be acquired by day during any lighting conditions, or at night, in the total absence of sunlight. In addition, these images are not affected by cloud cover, fog, or smoke because the RADAR signals have the ability to penetrate these covers (Cunjian, Y 2001, Martínez 2007).

Under the weather conditions in which floods occur, these types of images are the most suitable for study. Active radar systems incorporate an antenna that generates and transmits electromagnetic pulses (between 0.3 and 300 cm) to the Earth's surface, and after interacting with the objects, the echoes of the backscattered signal are collected and amplified by a receiver at certain frequencies and polarization modes. Currently, there is a wide variety of SAR missions that have improved spatial resolution, bands, revisiting times, and polarization modes that have increased the monitoring potential (Argenti 2013).

The current and potential uses of Space Remote Sensing make it an effective and low-cost means of identifying, prospecting and assessing natural hazards. The main exploitation of satellite images of floods to date is flood mapping. In particular, under the Space and Catastrophe Majeures charter, satellite images of floods are processed, in an operational context, to provide flood maps useful for flood management in the context of a crisis. The study showed that Remote Sensing could be a robust way to track urban footprint and flood mapping also this technology makes a decisive contribution to the various issues of land use, environment, health and the prevention of natural disasters. Despite the results that this technology enables us to extract, it remains limited by the lack of free data with the necessary accuracy so we can process more advanced treatments which aims to provide more information that can be integrated in a hydrographic model.

Bibliographical references

Berz G., 2000, Flood disasters: lessons from the past - worries for the future, Actes de colloque, Water and Maritime Engineering, Proceedings of the institution of Civil Engineers, Vol. 142.

Gresillon J. M., 2004, Inondations, Aléa et enjeux au regard du changement climatique, Actes de colloque, Colloque ONERC, Collectivités locales et changement climatique : quelles stratégies d'adaptation ? Paris.

Ancey C., 2005, Une introduction à la Dynamique des Avalanches et des Écoulements Torrentiels, Cours, Ecole Polytechnique Fédérale de Lausanne

Beschaouch A., 1986. De l'Africa latino-chrétienne à l'Ifriqiya arabo-musulmane : questions de toponymie. CRAI, vol. 130, n°3, 1986, pp. 530-549.

Oueslati A., Charfi F., et Baccar F., 2006. La basse vallée de l'Oued Majerda et la lagune de Ghar El Melh. Projet WADI, 5ème rencontre internationale, Tunis, 6-9 décembre 2006.

Poncet J., 1956. La mise en valeur de la basse vallée de la Majerda et ses perspectives humaines, Annales de géographie, vol. 65, n°349, 1956, pp. 199-222.

Polidori L., 1997, Cartographie radar, Livre, Gordon and Breach science publishers, 289 p.

Small D., Holecz F., Meier E., Nüech D. & Barmettler A., 1997, Geometric and Radiometric calibration of RADARSAT images, Actes de colloque, Geomatics in the ERA of RADARSAT, Ottawa Canada.

Yésou H., Chastanet P., Fellah K., Jeanblanc Y., De Fraipont P. & Bequignon J., 2000, Contribution of ERS SAR images and ERS coherence data to a flood information system on the Meuse basin - France, European Space Agency, (Special Publication) ESA SP, pp. 597-605.

Saad A. & El Assad S., 1985, Filtrage d'ordre vectoriel adaptatif du speckle dans les images ROS polarimétriques, I-REVUE INIST.

Comblet F., 2005, Détection, localisation et identification de cibles radar par imagerie électromagnétique bistatique, Thèse de doctorat, spécialité Science de la Matière, de l'Information et de la Santé, Univertsité de Bretagne Occidentale.

Ulaby F. T., Moore R. K. & Fung A. K., 1982, Microwawe remote sensing active and passive : vol.II : Radar remote sensing and surface scattering and emission theory, Livre, Artech House (GBR).

Jingfeng X., Jing L. & Moody A., 2003, A detail-preserving and flexible adaptive filter for speckle suppression in SAR imagery, International Journal of Remote Sensing, Vol. 24 (12), pp. 2451- 2465.

Lee J., 1980, Digital image enhancement and noise filtering by use of local statistics, IEEE Transactions on Pattern Analysis and Machine Intelligence.

Frost V., Stiles J. & Holtzman J., 1982, A model for RADAR images and its application to adaptative digital filtering of multiplicative noise, IEEE Transactions on Pattern Analysis and Machine Intelligence, Vol. 4 (2), pp. 156-166.

Lopes A., Touzy R. & Nezry E., 1990, Adaptative speckle filters and scene heterogeneity, IEEE Transactions on Geosciences and Remote Sensing, Vol. 28 (6), pp. 992 - 1000. Lopes A., Nezry E., Touzy R. & Laur H., 1993, Structure detection and statistical adaptative speckle filtering in SAR images, International Journal Of Remote Sensing, Vol. 14 (9), pp. 535 - 544.

Mansourpour M., Rajabi M. A. & Blais J. A. R., 2006, Effects and Performance of Speckle Noise Reduction Filters on SAR Imageries, Actes de colloque, Topographic Mapping from Space, ISPRS Ankara Workshop, Ankara, Turkey.

Ulaby F. T., Moore R. K. & Fung A. K., 1986, Microwawe remote sensing active and passive : vol.III : From theory to applications, Livre, Artech House (GBR).

Ulaby F. T. & Dobson M. C., 1989, Handbook of radar scattering statistics for terrain, Livre, 357 p.

Ulaby F. T., Dubois P. C. & van Zyl J., 1996, Radar mapping of surface soil moisture, Journal of Hydrology, Vol. 184 (1-2), pp. 57-84.

Polidori L., 1997, Cartographie radar, Livre, Gordon and Breach science publishers, 289 p.

Bioresita, F.; Puissant, A.; Stumpf, A.; Malet, J.F. Fusion of Sentinel-1 and Sentinel-2 image time series for permanent and temporary surface water mapping. Int. J. Remote Sens. 2019, 40, 9026–9049.$

McFeeters, S.K. The Use of the Normalized Difference Water Index (NDWI) in the Delineation of Open Water Features. Int. J. Remote Sens. 1996, 17, 1425–1432.

Ji, L.; Zhang, L.; Wylie, B. Analysis of Dynamic Thresholds for the Normalized Difference Water Index. Photogramm. Eng. Remote Sens. 2009, 75, 1307–1317.

Shen, X.; Wang, D.; Mao, K.; Anagnostou, E.; Hong, Y. Inundation Extent Mapping by Synthetic Aperture Radar: A Review. Remote Sens. 2019, 11, 879.

Tomer, S.T.; Al Bitar, A.; Sekhar, M.; Zribi, M.; Bandyopadhyay, S.; Sreelash, K.; Sharma, A.K.; Corgne, S.; Kerr, Y. Retrieval and Multi-scale Validation of Soil Moisture from Multi-temporal SAR Data in a Semi-Arid Tropical Region. Remote Sens. 2015, 7, 8128–8153.

Filion, R.; Bernier, M.; Paniconi, C.; Chokmani, K.; Melis, M.; Soddu, A.; Talazac, M.; Lafortune, F.-X. Remote sensing for mapping soil moisture and drainage potential in semi-arid regions: Applications to the Campidano plain of Sardinia, Italy. Sci. Total Environ. 2016, 573, 862–876.

Ulaby, F.T.; Moore, R.K.; Fung, A.K. Microwave Remote Sensing: Active and Passive, Volume 2, Radar Remote Sensing and Surface Scattering and Emission Theory; Addison-Wesley: Reading, MA, USA, 1983; pp. 1840–1852. [Google Scholar]

Kelly, R.; Davie, T.; Atkinson, P. Explaining temporal and spatial variation in soil moisture in a bare field using SAR imagery. Int. J. Remote. Sens. 2003, 24, 3059–3074.

Smith, L. Satellite remote sensing of river inundation area, stage, and discharge: A review. Hydrol. Process. 1997, 11, 1427–1439.

European Exchange Circle on Flood Mapping (EXCIMAP). Handbook on Good Practices for Flood Mapping in Europe. Available online: https://ec.europa.eu/environment/water/flood_risk/flood_atlas/pdf/handbook_goodpractice.pdf (accessed on 10 September 2019).

Martínez, J.M.; Toan, T. Mapping of flood dynamics and vegetation spatial distribution in the Amazon floodplain using multitemporal SAR data. Remote Sens. Environ. 2007, 108, 209–223.

Cunjian, Y.; Yiming, W.; Siyuan, W.; Zengxiang, Z.; Shifeng, H. Extracting the flood extent from satellite SAR image with thesupport of topographic data. In Proceedings of the International Conferences on Info-Tech and Info-Net. Networks (ICII 2001), Beijing, China, 29 October–1 November 2001; IEEE: Piscataway, NJ, USA, 2001; Volume 1, pp. 87–92. [Google Scholar]

Argenti, F.; Lapini, A.; Alparone, L. A tutorial on speckle reduction in synthetic aperture radar images, IEEE Geosci. *Remote Sens. Mag.* **2013**, *1*, 6–35

European Space Agency (ESA). Copernicus Open Access Hub. Available online: https://scihub.copernicus.eu/dhus/#/home (accessed on 2 May 2019).

Klemas, V. Remote sensing of floods and flood-prone areas: An overview. *J. Coast. Res.* **2015**, *31*, 1005–1013.

Tavus, B.; Kocaman, S.; Gokceoglu, C.; Nefeslioglu, H.A. Considerations on the use of Sentinel-1 data in flood mapping in urban areas: Ankara (Turkey) 2018 floods. *Int. Arch. Photogramm. Remote Sens. Spat. Inf. Sci.* **2018**, *XLII-5*, 575–581.

Martinis, S.; Twele, A.; Voigt, S. Unsupervised extraction of flood-induced backscatter changes in SAR data using Markov image modeling on irregular graphs. *IEEE Trans. Geosci. Remote Sens.* **2011**, *49*, 251–263.

Borah, S.B.; Sivasankar, T.; Ramya, M.N.S.; Raju, P.L.N. Flood inundation mapping and monitoring in Kaziranga National Park, Assam using Sentinel-1 SAR data. *Environ. Monit. Assess.* **2018**, *190*, 520.

Martinis, S.; Twele, A.; Voigt, S. Unsupervised extraction of flood-induced backscatter changes in SAR data using Markov image modeling on irregular graphs. *IEEE Trans. Geosci. Remote Sens.* **2011**, *49*, 251–263.

Psomiadis, E. Flash flood area mapping utilising Sentinel-1 radar data. In Proceedings of the SPIE 10005, Earth Resources and Environmental Remote Sensing/GIS Applications, Dresden, Germany, 11 November 2013; VII 100051G. SPIE: Edimburgh, UK, 2016. [Google Scholar]

Dumitrascu, N.; Oniga, E.; Florian, S.; Marcu, C. Floods damage estimation using sentinel-1 satellite images. Case study: Galati County, Romania. RevCAD. J. Geod. Cadas. 2017, 22, 115–122. [Google Scholar]

Pham-Duc, B.; Prigent, C.; Aires, F. Surface Water Monitoring within Cambodia and the Vietnamese Mekong Delta over a Year, with Sentinel-1 SAR Observations. Water 2017, 9, 366.

Zhang, B.; Wdowinski, S.; Oliver-Cabrera, T.; Koirala, R.; Jo, M.J.; Osmanoglu, B. Mapping the extent and magnitude of severe flooding induced by hurricane Irma with multi-temporal Sentinel-1 SAR and InSAR observations. Int. Arch. Photogramm. Remote Sens. Spat. Inf. Sci. 2018, XLII-3, 2237–2244.

Amitrano, D.; Guida, R.; Ruello, G. Multitemporal SAR RGB Processing for Sentinel-1 GRD Products: Methodology and Applications. IEEE J. Select. Top. Appl. Earth Obs. Remote Sens. 2019, 12, 1497–1507.

Amitrano, D.; Guida, R.; Ruello, G. Multitemporal SAR RGB Processing for Sentinel-1 GRD Products: Methodology and Applications. *IEEE J. Select. Top. Appl. Earth Obs. Remote Sens.* **2019**, *12*, 1497–1507.

Matgen, P.; Schumann, G.; Henry, J.-B.; Hoffmann, L.; Pfister, L. Integration of SAR-derived river inundation areas, high-precision topographic data and a river flow model toward near real-time flood management. *Int. J. Appl. Earth Obs. Geoinf.* **2007**, *9*, 247–263.

Lambin, E.F.; Geist, H.J. Global land-use and land-cover change: What have we learned so far? Glob. Chang. News 2001, 46, 27–30.

Donnay, J.P.; Barnsley, M.J.; Longley, P.A. Remote Sensing and Urban Analysis; Taylor and Francis: London,UK, 2001.

10. Herold, M.; Goldstein, N.C.; Clarke, K.C. The spatiotemporal form of urban growth: Measurement, analysisand modeling. Remote Sens. Environ. 2003, 86, 286–302. [CrossRef]

Taubenböck, H.; Wegmann, M.; Berger, C.; Breunig, M.; Roth, A.; Mehl, H. Spatiotemporal analysis of Indian megacities. In Proceedings of the International Archives of the Photogrammetry, Remote Sensing and Spatial Information Sciences, Beijing, China, 3–11 July 2008; Volume 10, pp. 75–82.

Xu, H. A new index for delineating built-up land features in satellite imagery. Int. J. Remote Sens. 2008,29, 4269–4276

Small, C.; Okujeni, A.; van der Linden, S.; Waske, B. Remote Sensing of Urban Environments. Compr. Remote Sens. 2018, 96–127

Zha, Y.; Gao, J.; Ni, S. Use of normalized difference built-up index in automatically mapping urban areas from TM imagery. Int. J. Remote Sens. 2003, 24, 583–594.

Gamba, P.; Aldrighi, M.; Stasolla, M. Robust Extraction of Urban Area Extents in HR and VHR SAR Images. IEEE J. Sel. Top. Appl. Earth Obs. Remote Sens. 2011, 4, 27–34.

Valdiviezo-N, J.C.; Téllez-Quiñones, A.; Salazar-Garibay, A.; López-Caloca, A.A. Built-up index methods and their applications for urban extraction from Sentinel 2A satellite data: discussion. J. Opt. Soc. Am. A 2018, 35, 35.

Weng, Q. Thermal infrared remote sensing for urban climate and environmental studies: Methods,

applications, and trends. ISPRS J. Photogramm. Remote Sens. 2009, 64, 335–344. [CrossRef]

35 Zhan, W.; Chen, Y.; Zhou, J.; Wang, J.; Liu, W.; Voogt, J.; Zhu, X.; Quan, J.; Li, J. Disaggregation of remotely

sensed land surface temperature: Literature survey, taxonomy, issues, and caveats. Remote Sens. Environ.

2013, 131, 119–139

Yu, B.; Shu, S.; Liu, H.; Song, W.; Wu, J.; Wang, L.; Chen, Z. Object-based spatial cluster analysis of urban landscape pattern using nighttime light satellite images: A case study of China. Int. J. Geogr. Inf. Sci. 2014, 28, 2328–2355

De Zan, F.; Guarnieri, A.M. TOPSAR: Terrain observation by progressive scans. IEEE Trans. Geosci. Remote Sens. 2006, 44, 2352–2360.